Eddy Current Probes Design for Defect Detection in Metallic Parts Made by Additive Manufacturing Processes

by

Heba ElSayed Mahmoud Ahmed Farag

A thesis
presented to the University of Waterloo
in fulfillment of the
thesis requirement for the degree of
Doctor of Philosophy
in
Mechanical and Mechatronics Engineering

Waterloo, Ontario, Canada, 2022

© Heba ElSayed Mahmoud Ahmed Farag 2022

Examining Committee Membership

The following served on the Examining Committee for this thesis. The decision of the Examining Committee is by majority vote.

External Examiner:	Simon Yang Professor, School of Engineering , University of Guelph
Supervisor(s):	Behrad Khamesee Professor, Dept. of Mechanical and Mechatronics Engineering, University of Waterloo Ehsan Toyserkani Professor, Dept. of Mechanical and Mechatronics Engineering, University of Waterloo
Internal Member:	Mihaela Vlasea Professor, Dept. of Mechanical and Mechatronics Engineering, University of Waterloo
Internal Member:	Kevin Musselman Professor, Dept. of Mechanical and Mechatronics Engineering, University of Waterloo
Internal-External Member: ,	Omar M. Ramahi Professor, Dept. of Electrical and Computer Engineering University of Waterloo

Author's Declaration

I hereby declare that I am the sole author of this thesis. This is a true copy of the thesis, including any required final revisions, as accepted by my examiners.

I understand that my thesis may be made electronically available to the public.

Abstract

Non-destructive testing (NDT) is the method where an object or materials are being tested for any type of damage or features without harming the object during the process. There are different NDT techniques; in this thesis the main focus is to explore the feasibility of using eddy current (EC) non-destructive testing technique to detect different types of flaws in metallic parts. One of the contributions in this project is to develop different models to design an EC probe that is sensitive to detect small flaw sizes in parts made by additive manufacturing. Additive manufacturing (AM) is the process where an object is created by layering materials based on three dimensional (3D) Computer-Aided Design (CAD) data. In this thesis, the main focus are the products created by laser powder bed fusion process (LPBF) which is one of the metal AM technologies. Defects such as pores and cracks will be created within the parts because of, but not limited to the un-melted powder or the excessive material vaporization during laser-material interaction. The existence of these defects will affect the quality of parts therefore, NDT should be done on these parts for early detection of defects. Eddy current probes have been designed based on modelling developed to detect subsurface defects in parts made by the LPBF technology. Several samples made of stainless steel (316L) and titanium (Ti64) were considered for the detection process to explore the probe response while testing different materials with different conductivity and permeability. Artificial defects were embedded inside the parts at different depths, with different geometries and sizes as well. The probes operate at a wide frequency range for the purpose of increasing the standard depth of penetration of the eddy currents inside the material which, increase the probes, sensitivity to detect subsurface flaws. Experiments were carried out to further test the performance of the designed probes to detect flaws embedded inside parts made by AM.

Some of the challenges in testing parts made by AM are the surface roughness and the effect of edges. The problem of edge effect phenomena is a major problem when it comes to testing small samples. The edge of the small sample will create a signal that is similar to the one obtained from a crack. The small diameter of the probe coil and the tip added to it helps distinguishing between the actual defect signal and the signal produced by the test piece edge. Another contribution is that the EC probe is designed in a way that can overcome the problem of surface roughness and the unwanted resultant signal produced by rough surface by adding a coating layer made of thin paper to the bottom of the probe; some of the experimental findings and contributions are listed below:

Subsurface notches that simulate subsurface cracks with different sizes in the range of (0.07 mm-0.4 mm) and subsurface blind holes with different diameters in the range of (0.2 mm-0.5 mm) embedded inside plates made of stainless steel and titanium materials have

been detected successfully. The plates sizes are 50 mm×50 mm. FEM models with the same parameters were created in ANSYS Maxwell to validate the experimental results.

Multiple probes with different parameters such as number of turns, length, inner and outer diameter were designed to investigate the effect of each parameter on the sensitivity of the probe to detect small size defects. Core tip analysis for focusing the magnetic field were done. Different tip shapes of the core with different geometries were considered to increase the detectability of the probe to subsurface defects. Optimization for the designed probe was conducted to determine the optimal probe parameters such as length, inner and outer diameter that gives the best values for the magnetic field. Shields with different thickness were added around the coils to increase and focus the eddy current distribution under the probes coils. Amplification circuits were attached to the probe coil winding to amplify the detected defect signal since the measured detected signals are in millivolts. In conclusion, it is clear that the eddy current testing technique has a potential to be used to inspect parts made by AM.

Acknowledgements

Thanks to Allah that I have reached this point where I can see the results of sleepless nights and hard work during these past four years. I would like to thank all the people who made this thesis possible. Special thanks to my parents and my brothers Moataz and Islam for their continuous support and prayers. I also appreciate the support of my family and friends specially the support of my friends Dr. Ali Ibrahim, Jasmine Mahmoud, Dr. Mohamed Said, Dr. Heba Alzaban, Dr. Mohamed Mashagbeh, Kyle, Andrew, Grace, Alyson, Mony, YoYo, Zyzy, Soso, mom Debbie, Pitty, Garcelyn, Razan, and many other friends.

I would like to thank my supervisors Prof. Behrad Khamesee, Prof. Ehsan Toyserkani, HI-AM and NSERC organizations for their guidance and funding the project during the four years of my PhD.

I also would like to thank all the students that I interacted with specially those who nominated me to receive the Mechanical and Mechatronics Teaching Assistant Excellence award.

To all of my lab-mates who became like family to me, it was such and honor and pleasure working with you in the lab for the past few years, Azeem, Dan, Saksham, Chaupon, Pari and Pooryia !!!

This is not the end, this is just the beginning!!, so excited and ready for my next giant leap!!

Dedication

This is dedicated to the people I love the most in this life, my parents and my brothers.

Table of Contents

List of Figures xii

List of Tables xvii

Nomenclature xviii

1 Introduction 1

1.1 Motivation 1

1.2 Basic principle of Eddy Current (EC) testing and background 2

1.2.1 Standard depth of penetration calculations 4

1.2.2 Eddy current testing applications 6

1.3 Advantages and disadvantages of eddy current testing 7

1.4 Eddy current testing technologies 11

1.5 Eddy current instruments 12

1.5.1 Probes types and their application in industry 12

1.5.2 Data acquisition system 14

1.6 Additive manufacturing technology 16

1.7 Problem statement, objective and contribution 18

1.8 Thesis outline 19

2 Literature review **20**

2.1 History of non-destructive testing(NDT) 20

2.1.1 Examples of NDT applications in industry 21

2.2 Examples and considerations for EC testing in additive manufacturing . . . 23

2.3 The usage of EC in inspection in AM and other fields compared to other NDT techniques 25

2.4 Defect types created in additively manufactured parts 28

2.5 Summary 29

3 Probe design and analytical modelling of the probe impedance **30**

3.1 Introduction 30

3.1.1 Solenoid coil design for eddy current detection 30

3.2 Probe design and coil dimension determination 31

3.3 Analytical modelling of the coil impedance change 38

3.4 One layer structure 42

3.5 Multi-layer structure 43

3.6 Conclusion 44

4 Finite element modelling of the probe impedance **45**

4.1 Finite element analysis and software tools 45

4.1.1 Limitation with simulation modelling of the probe impedance change 45

4.2 Model design and simulation in ANSYS Maxwell 46

4.2.1 Tip analysis and B_max measurements 47

4.2.2 Evaluation of designed probe in basic defect detection 49

4.3 Simulation for notches and voids 51

4.4 Methods for modeling sensitivity analysis simulations 52

4.4.1 Testing close to an edge 53

4.4.2 Effect of lift-off distance 54

4.4.3 Multiple defects in the same region . . . 61
4.4.4 Effect of temperature . . . 68
4.5 Sensitivity analysis for new designs . . . 71
4.5.1 Shield effect . . . 78
4.6 Summary . . . 81

5 Characterisation and experiments **83**
5.1 Introduction . . . 83
5.2 Methods, materials, and instrumentation . . . 83
5.2.1 Limitation with eddy current in experiment . . . 85
5.2.2 Testing done on machined parts using absolute probe . . . 85
5.2.3 Three notches same width different lengths . . . 87
5.2.4 Three notches same length different width . . . 89
5.2.5 Blind holes with different diameters . . . 91
5.3 Testing done on parts made by AM using absolute and reflection probes . . . 93
5.3.1 Samples used for experiment . . . 94
5.3.2 Intermittent measurements, sensing and circuitry . . . 97
5.3.3 The experimental setup used during the detection process. . . . 100
5.3.4 Detecting defects in stainless steel samples . . . 100
5.3.5 Detecting defects in titanium samples made by AM . . . 102
5.3.6 Material conductivity comparison for both probes . . . 103
5.4 Methods for sensitivity analysis experiments . . . 105
5.4.1 Testing close to an edge . . . 106
5.4.2 Effect of lift-off distance . . . 106
5.4.3 Multiple defects in the same region . . . 108
5.5 Summary . . . 110

6 Conclusions and Future work **113**

6.1 Conclusions 113

6.2 Future work 115

References **117**

APPENDICES **124**

A Matlab codes **125**

List of Figures

1.1 Solenoid coil geometry. 3

1.2 Schematic eddy currents distribution under a coil on top of a stainless steel plate; (a) shows the distribution of eddy currents in case of no defect, (b) shows the perturbation of eddy currents due to an artificial surface crack in the plate. 4

1.3 Probe signal representation of defects at different depths; (A) shows the probe on top of material with different defect types, (B) shows EC signal representation of each defect from an absolute probe, (C) shows EC signal representation from a differential probe. 6

1.4 Defects orientation with respect to eddy current flow direction under a surface probe [21]. 9

1.5 Absolute and reflection probe geometry differences; (a) shows an absolute probe that has only one coil, (b) shows a reflection probe that has two coils. 14

1.6 Available eddy current instruments in the market. 15

1.7 The powder bed fusion system schematic diagram to the left and the directed-energy deposition system schematic diagram to the right [34]. 17

3.1 Sweep over the inner radius of the coil, the data exported from ANSYS Maxwell and the best B_max value is at inner radius 3.5 mm. 31

3.2 Sweep over position of the coil at 200 KHz. 32

3.3 Standard depth of penetration at 200 KHz. 33

3.4 Sweep over position of the coil at 28 KHz. 34

3.5 Skin depth based type mesh 34

3.6 Sweep over position of the coil at 2 mm mesh size. 35
3.7 Sweep over position of the coil at 0.2 mm mesh size. 35
3.8 Cross-section of the coil geometry. 36
3.9 Probe on top of a plate with defect. 41
3.10 Probe on top of one layer plate. 42
3.11 Probe on top of multi-layer plate. 43

4.1 ANSYS eddy current simulation of the designed probe, where (a) shows the magnetic field distribution and (b) shows the eddy current distribution under the coil. 47
4.2 Different tip geometry, where (a) is a cone tip shape, (b) cylindrical tip shape, (c) polygon tip shape, and (d) square tip shape. 48
4.3 Graphical abstract of the simulation procedures. 49
4.4 The magnitude of the eddy currents distribution, where (a) shows eddy current distribution in case there is no defect, (b) shows eddy current distribution if the defect is aligned with the center of the coil, and (c) shows eddy current distribution if the defect is aligned with the coil winding. . . 50
4.5 Shows simulation results of the probe impedance change on top of a plate with a defect at 10 mm, where (a) defect type is a sphere, (b) defect type is a notch. 52
4.6 Subsurface notch close to an edge. 53
4.7 Subsurface void close to an edge. 54
4.8 No lift-off distance. 55
4.9 No lift-off distance current density. 56
4.10 1 mm lift-off distance. 57
4.11 1 mm lift-off distance current density. 58
4.12 2 mm lift-off distance. 59
4.13 2 mm lift-off distance current density. 60
4.14 Sweep over the position on top of a plate with one void defect type. 62
4.15 Current density under a probe on top of a plate with one void defect type. 63

4.16 Sweep over the position on top of a plate with two voids besides each others in the same region. 64
4.17 Current density under a probe on top of a plate with two parallel voids in the same region. 65
4.18 Sweep over the position on top of a plate with two voids above each others in the same region. 66
4.19 Current density under a probe on top of a plate with two voids above each others in the same region. 67
4.20 Sweep over position on top of a plate with one void defect type at high temperature for conductivity analysis. 68
4.21 Sweep over the position on top of a plate with one void defect type at room temperature for permeability analysis. 69
4.22 Sweep over the position on top of a plate with one void defect type at high temperature for permeability analysis. 70
4.23 Sweep over the outer radius(4.5mm-7mm) and position on top of a plate with a 0.1 mm notch width. 72
4.24 Sweep over the outer radius(4.5 mm-7 mm) and position on top of a plate with a 0.2 mm blind hole radius. 73
4.25 Transmit/receive probe sweep over the outer radius of the transmitter 3 mm to 5 mm. 74
4.26 Transmit/receive probe sweep over the outer radius of the receiver 4.5 mm to 7 mm. 75
4.27 Different coil geometry for new probes designs. 76
4.28 A shield surrounding the coil of the absolute probe 78
4.29 Top view of the shield effect on the distribution of the eddy currents under the coil where(a) is eddy current distribution under the coil in case of a shield around the coil and (b) is eddy current distribution under the coil in case there is no shield. 79
4.30 Eddy current density and impedance change in case of a shield around the coil. 79
4.31 Sweep over shield thickness. 80

5.1 Plate with three notches same width and different length. 87
5.2 The average and standard deviation values of the defect for each length. . . 88
5.3 Comparison between the experimental, analytical, and simulation results for the three notches same width different length case. 89
5.4 Plate with three notches same length and different width. 90
5.5 The average and standard deviation values of the defect for each width. . . 90
5.6 Comparison between the experimental, analytical, and simulation results for the three notches same length different width. 91
5.7 Plate with blind holes with different diameters. 92
5.8 The average and standard deviation values of the defect for each void radius. 92
5.9 Comparison between the experimental, analytical, and simulation results for each subsurface void. 93
5.10 CT results of a stainless steel sample. 95
5.11 The measured surface roughness size of the samples where (a) stainless steel (SS316L) sample, (b) Titanium sample (TI-64). 96
5.12 Schematic diagram of a proposed intermittent defect detection. 98
5.13 Circuit attached to the absolute probe. 99
5.14 An illustration of the reflection probe circuit. 100
5.15 Experimental setup showing both probes used to test titanium and stainless steel samples. 101
5.16 Normalized values of the measured voltage for both probes on top of plates made of stainless steel with notches with different widths made by AM. . . 102
5.17 Normalized values of the measured voltage for both probes on top of machined plates made of stainless steel with different radius blind holes. . . . 103
5.18 Normalized values of the measured voltage for both probes on top of plates made of titanium with notches with different widths. 104
5.19 Measured Vpp values using absolute eddy current sensor on top of titanium and stainless steel samples with notches. 105
5.20 Measured Vpp values using reflection eddy current sensor on top of titanium and stainless steel samples with notches. 105

5.21 Notches close to edges in stainless steel samples. 107
5.22 Two voids separated by a very small distance in a stainless steel sample . . 108
5.23 Three voids separated by a very small distance in a stainless steel sample. . 109

List of Tables

1.1 Specs of some of the available EC instrumentation in the market. 16

2.1 A comparison between different inspection techniques in additive manufacturing. 27

3.1 Different values for Fabry factor (G) at different coil lengths for fixed inner and outer diameters of 7 mm and 16 mm, respectively. 37

3.2 Parameters used for one layer plate structure. 43

3.3 Parameters used for multi-layer layer plate structure. 44

4.1 B_max value for each tip shape at 0.2 mm distance under the coil. 48

4.2 Parameters used for both simulation cases. 52

4.3 Specs of the new designed absolute probes. 77

4.4 Specs of the new designed reflection probes. 77

5.1 Coil and core parameters of the absolute probe. 86

5.2 Measured voltage of the probe at different lift-off distances. 108

5.3 Measured voltage of the probe for cases of multiple defects in the same region. 110

Nomenclature

List of Symbols

J	Current density
σ	Electrical conductivity
μ	Magnetic permeability
f	Frequency
δ	Standard depth of penetration
β	Phase lag
$\bigtriangledown$	Curl
L	Coil length
r	Coil radius
D	Coil diameter
d	Wire diameter
N	Number of turns
$\mu_e ff$	Effective permeability
H	Magnetic field intensity
E	Electric field intensity
ϵ	Permittivity
ϕ	Electric scalar potential
A	Magnetic vector potential
ω	Angular frequency
ΔZ	Impedance change

List of Acronyms and Abbreviations

AMP	Ampere
AM	Additive Manufacturing
AWG	American Wire gauge
CAD	Computer-Aided Design
EC	Eddy current
FEM	Finite element modelling
LPBF	Laser powder bed fusion process
PT	Penetrate testing
MT	Magnetic particle testing
NDT	Non-destructive testing
UT	Ultrasonic testing
IR	Infrared testing
MF	Magnetic field
SDP	Standard depth of penetration
TREE	Truncated Region Eigenfunction Expansion method
3D	Three dimensional
PEC	Pulsed eddy current
RFT	Remote-field testing
PECT	Pulsed Eddy Current Thermography
LWIR	Long-wave infrared
Vpp	Peak-to-peak voltage
RMS	Root mean square

Chapter 1

Introduction

1.1 Motivation

One of the necessary stages of the product production process in any field is to test the product to ensure its quality and reliability for years to come. There are two different testing categories of the quality control operation to evaluate the products quality and reliability. The two categories are destructive testing and non-destructive testing. Destructive testing determines the component quality by applying continuous stresses and pressure until it fails. Non-destructive testing (NDT) is also used to evaluate the quality of the product without damaging it as the name implies. Both destructive testing and NDT are valid methods for product inspection. NDT methods have more advantages over destructive testing methods such as significant cost savings and reduced material waste because NDT preserves the part under test without damage.

There are two categories of NDT. The first category requires a good contact between the sensor and the surface of the part under test. Examples are ultrasonic testing (UT) which involves hitting the test piece by ultrasound waves to locate the defects and eddy Current testing (EC) that involves inducing eddy currents inside the material and measuring the changes of these eddy currents in case of a defect. Other examples of NDT are liquid penetrate testing (PT) which involves injecting the test piece by a red liquid to locate the flaw region, magnetic particle testing (MT) which involves magnetizing the test piece, and electromagnetic testing. The second category does not require physical contact between the sensor and the part under test such as radiography testing, thermal/ infrared testing (IR), and visual inspection.

NDT techniques are used for product testing and evaluation in many technologies. One of the technologies that require inspection and using NDT to test the product quality is additive manufacturing. The way parts are made by additive manufacturing (AM) technology, materials are laid layer-by-layer, they exhibit different types of defects such as cracks and porosities. There are many physical phenomena such as keyhole, solidification cracking, oxidization, lack of fusions, etc., during AM processes that cause porosities and cracks to form; the existence of these defects will affect the quality of AM-made products. To ensure the parts quality, integrity and reliability, non-destructive testing (NDT) should be carried out on these parts for early detection of defects. There is a wide range of NDT techniques that can be used in testing of AM-made parts. For example, acoustic emission testing, thermography and photo-diode signal can be used for in-situ inspection in AM [1,2]; some other non-destructive imaging techniques such as infrared thermography and laser reflection technique were investigated in [3].

Each of these NDT techniques has its pros, cons, and challenges during the testing process. In addition, techniques such as Eddy current testing, X-ray, laser ultrasonic testing, and visual inspection can be used for the post process NDT inspection. There are different classes of AM processes. The focus of this thesis is the powder bed fusion (PBF) process. In PBF, powder is sintered either by an electron or a laser beam. The types of materials used in PBF are ferrous alloys, nylon, titanium alloys, aluminum, etc. Non-destructive testing techniques such as eddy current testing, radiography and ultrasonic testing are all suitable for in-situ and post process inspection of parts made by PBF. The focus in this paper is using eddy current technique to detect subsurface defects in parts made by PBF technology. There are different challenges with using eddy current technique for defect detection in PBF [4] such as detecting unwanted signal which sometimes makes it difficult to interpret the measured signal.

1.2 Basic principle of Eddy Current (EC) testing and background

Eddy current (EC) follows the electromagnetic induction law (Faraday's law of induction). Once a conductive material is subjected to a changing electromagnetic field which is originally created by passing an alternating current through a coil, eddy currents will start to flow in this part in a circular path or a loop. The intensity of the original magnetic field created within the coil depends on input current source value, the number of turns in the coil and the coil geometry. An additional secondary magnetic field (MF) is produced by the eddy currents induced inside the material. The secondary magnetic field will oppose

the primary magnetic field created in the coil of the testing probe (Lenz's law) [5,6], and the total effect is a reduced magnetic flux linking the coil. A sensor is used to measure total MF near the part under test [5]. The existence of any crack or defects will perturb the distribution of the eddy currents field causing variations in the phase and the magnitude of it. These variations can be measured using another receiver coil [5]. An example of the solenoid coil geometry of an eddy current probe that works in the absolute mode is shown in Fig. 1.1. An illustration of the induced eddy currents inside the material and their perturbation due to the existence of a defect is shown in Fig. 1.2.

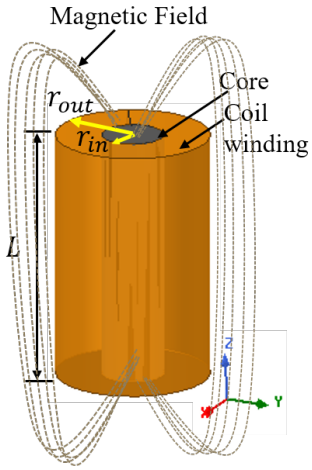
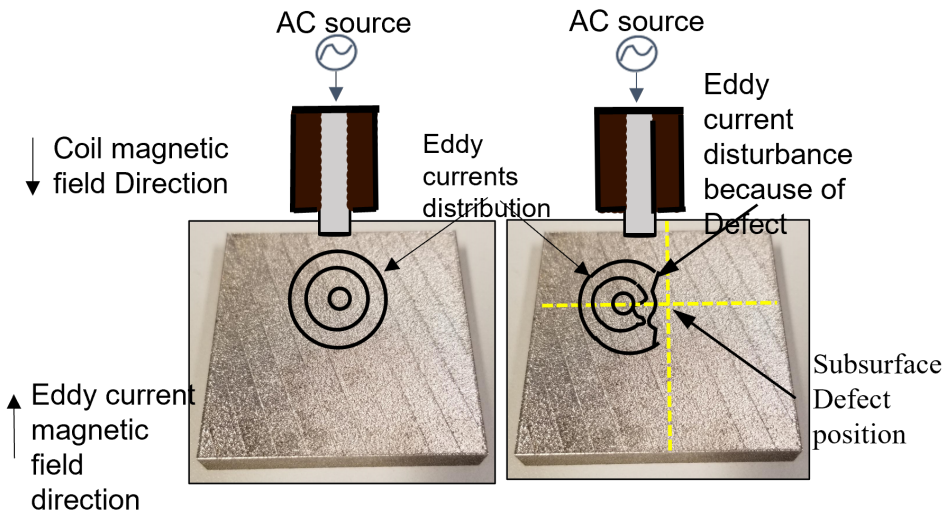


Figure 1.1: Solenoid coil geometry.



(a) (b)

Figure 1.2: Schematic eddy currents distribution under a coil on top of a stainless steel plate; (a) shows the distribution of eddy currents in case of no defect, (b) shows the perturbation of eddy currents due to an artificial surface crack in the plate.

Eddy current formula can be expressed in a form of the diffusion equation. The derivation of a useful equation for modelling the effect of eddy currents in a material starts with the differential, magnetostatic form of Ampere's Law providing an expression for the magnetizing field (**H**) surrounding a current density (**J**) as shown in equation (1.1). Both (**H**) and (**J**) are vectors.

$$\bigtriangledown \times H = J \tag{1.1}$$

1.2.1 Standard depth of penetration calculations

To determine how deep the eddy currents can go through the material, the depth of penetration formula given in equation (1.2) can be used. It depends on the material conductivity and permeability of the test piece and also the frequency used for the alternating current source.

$$\delta = \frac{1}{\sqrt{\pi f \mu \sigma}} \tag{1.2}$$

Where, δ is the standard depth of penetration (SDP) (mm), f is the frequency (Hz) during the test process, σ is the material electrical conductivity (Siemens/m) and, μ is the material magnetic permeability of the part under test. Usually, for a high depth of penetration, low frequencies are preferred in case of subsurface defects. In case of surface defects, high frequency is suitable to be used since there is no need for a high depth of penetration. The frequency selection will be fine-tuned to detect flaws at different depths depending on the type of probe being used during the testing process, because of the skin depth effect, the density of the eddy currents decreases with the inside the material. Phase lag β , given in equation (1.3) means that the subsurface eddy currents are not in phase but lag the ones at the surface, it is measured in radian.

$$\beta = \frac{x}{\delta} \tag{1.3}$$

Where, x is depth under the surface (mm) and δ is the SDP(mm) shown in equation (1.2). Phase lag varies with the test frequency since it is a function of the standard depth of penetration, it allows distinguishing between which signals represent an actual defect and which one are irrelevant indications. Fig. 1.3 shows that the phase angle representation of the sub-surface void is higher than the ones obtained from the deep crack signal on a plate made of aluminum, although the crack goes deeper inside the plate. This is because of the exponential attenuation in EC density under the surface, which causes the contribution of the crack top half to the integrated signal higher than the contribution of the bottom one. The absolute probe has only one coil meanwhile the differential probe has two coils. To detect surface defects in materials, high frequencies should be used since eddy currents will be concentrated close to the surface and the standard depth of penetration will be low. To detect subsurface defects in materials, low frequencies should be used since eddy currents will flow deeper inside the material and the standard depth of penetration will be high. There are different types of sub-surface defects in parts made by LPBF such as voids and cracks. The subsurface defects are located from 0.5 mm to 3 mm beneath the surface.

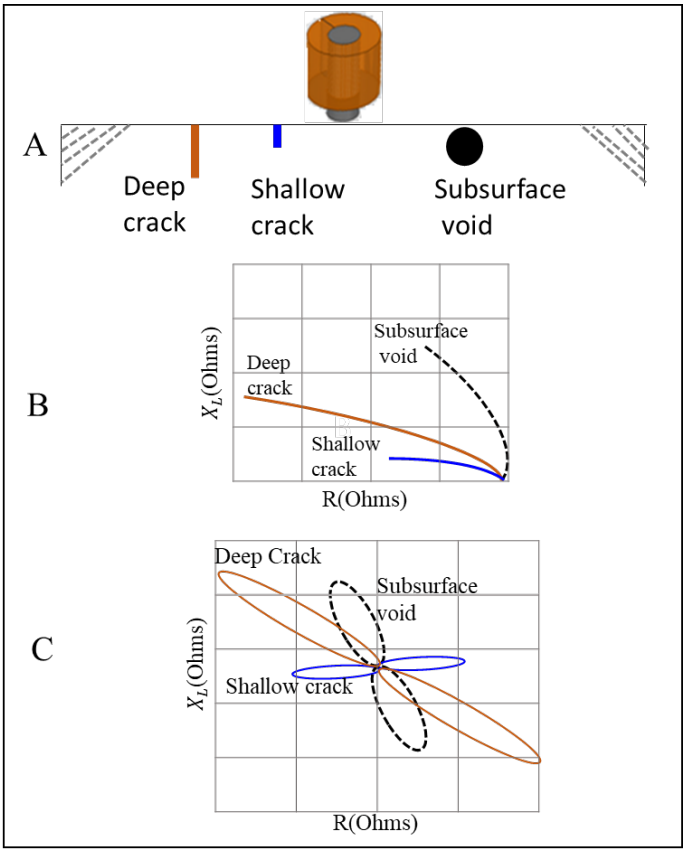


Figure 1.3: Probe signal representation of defects at different depths; (A) shows the probe on top of material with different defect types, (B) shows EC signal representation of each defect from an absolute probe, (C) shows EC signal representation from a differential probe.

1.2.2 Eddy current testing applications

Eddy current technique is used for inspection in the nuclear [7], inspection of the heat exchanger, bolt holes inspection, pipe inspection, testing of materials in aircraft energy, transportation, aerospace industries [8-10], and in high-speed rails. Eddy current testing is applicable for any conductive material developed by any conventional or AM technologies. The potential applications of eddy current non-destructive testing are [7-17]:

- Conductivity testing, the ability of EC testing to measure conductivity can be used to identify and sort ferrous and nonferrous alloys [11,12].

- Surface inspection, EC can easily detect surface cracks in machined parts and metal stock. Inspection of the area around fasteners in aircraft and other critical applications falls under this category[13].
- Tubing inspection, common EC applications include in-line inspection of tubing during the manufacturing process as well as field inspection of tubing such as heat exchangers [7,13].
- Detection of corrosion, EC instruments can detect and quantify corrosion on the inside of thin metals such as aluminium aircraft skin [8].
- Bolt hole inspection, cracking inside bolt holes can be detected using bolt hole probes, which are frequently used in conjunction with automated rotary scanners[14].

1.3 Advantages and disadvantages of eddy current testing

There are some advantages and disadvantages for using the EC testing method, it can be used to test parts with complex geometries where Eddy currents can go through surface coating and allows detection for subsurface defects. Advantages of this study, compared to other NDT methods are listed in [17–21]. The designed probe and the testing devices are portable because of the way it designed which allows for outdoor inspection. It is suited to detect all type of volumetric flaws such as corrosion, wear, cracks, and porosities. It may provide good sensitivity to small flaws at or near the surface of the sample. The part under inspection doesn't require much preparation while testing using the eddy current technique. As any other non-destructive techniques, there are some disadvantages associated with eddy current technology.

- Automation potential since the probe can be attached a robot arm while the manufacturing process is going on.
- Capability for quantitative flaw sizing based on the design of the probe itself. Some probes can rotate with different angles on top of the defect that helps defining the defect size.
- Provides a faster scanning speed than conventional ultrasonic testing (UT) since the probe does not have to be in contact with the object under test and the magnetic

field interacts directly with its surroundings. However, to use ultrasound as a testing technique, the sample under test has to be prepared by adding either gel coupling to link the sound waves into the material, which will take longer time to do the testing.

- Physically complex geometries investigated since the probe size and shape optimized and designed in a way that fits any type of geometry no matter how complex it is.
- The testing devices are portable because of the way it designed, as the body of the testing devices have reasonable sizes in hard cases and contain rechargeable batteries.
- It is suited to detect all type of volumetric flaws such as corrosion, wear, cracks and large porosities.
- Can detect through several layers. Good sensitivity to small flaws at or near the surface of the sample; also it can detect through material coatings.

Some disadvantages that associated with using EC as a testing technique:

- This technique is very susceptible to any changes in the magnetic permeability or electrical conductivity in case of a change in the temperature of the part under test; any type of changes shown as a false defect signal because of the disturbance of the eddy currents distribution, especially in ferromagnetic materials that makes the inspection of welds and ferromagnetic materials difficult. Proper probe designs and modern flaw detectors of course can solve this issue.
- Another constraint is that it won't be able to detect defects that are parallel to the surface since the flow of the eddy currents are always parallel to the surface, if there is a planar defect that does not interface with the eddy current then the defect won't be detected. Since eddy currents flow parallel to the coil winding, not all of the defects can be detected, some types of defects can only be detected with certain probe designs. In Figure 1.4 a schematic diagram shows how the eddy current flows with surface coils. Figure 1.4 Also shown are defects that cannot be detected with coil configurations because they do not obstruct eddy current flow, such as laminar defects in plates and defects at the centre of solid bars or wire. A horseshoe probe design can theoretically detect laminar defects. Similarly, a surface probe could be used to induce eddy currents in the centre of a bar or wire. The types of defects that will be detected are those that are perpendicular to the eddy current flow [21].
- Sometimes it is not suitable for large areas or complex geometries that makes the technique not flexible enough for inspection in certain industries.

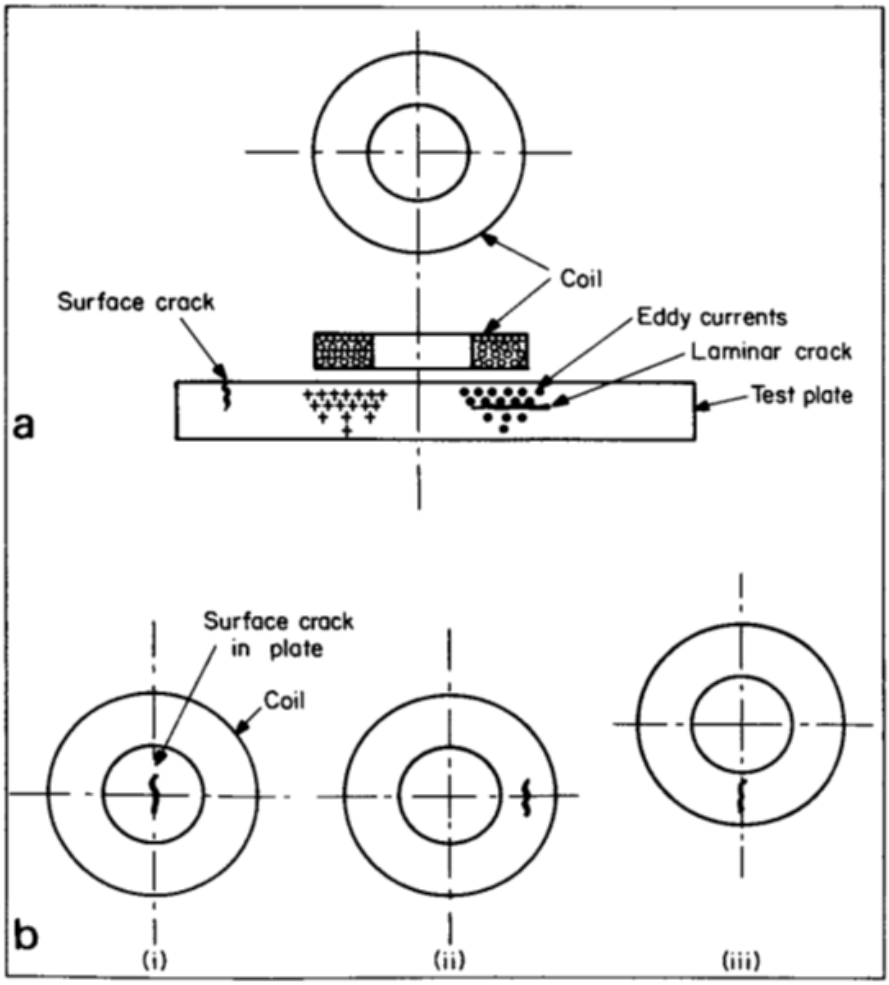


Figure 1.4: Defects orientation with respect to eddy current flow direction under a surface probe [21].

- The main limitation of eddy current testing is that only electrically conductive materials can be tested, the material has to be able to support a flow of electrical current. This constraint makes it difficult to test fiber-reinforced plastics [22,23]. The probe used in eddy current testing can detect the desired material characteristics such as discontinuities and conductivity and it can detect unwanted signals related to conductivity and magnetic permeability, leading to increased complexity in results interpretation.

- One of the challenges that faces eddy current detection is the surface roughness, it will result in producing a signal that is similar to the flaw signal and it will be hard to distinguish between a flaw and non-flaw signal.
- The size of the part under test is also a concern, if the part under test is too small, it will be hard to move the probe over it without causing what's called an edge effect. Edge effect means that the edges of the part under test will produce a similar signal as a defect signal since the eddy currents will be disturbed because of the parts edge.
- The lift-off distance which is the distance between the probe and the part under test might be a challenge as well if not kept constant. In eddy current testing, it is important not to leave an air gap between the probe and the part under test for the defects to be detected successfully.

1.4 Eddy current testing technologies

There are different eddy current testing technologies that are developed with time. Choosing the suitable technology depends on the type of application. Some of these techniques are suitable for remote field detection, some are suitable for defect detection in fields where a high temperature exists, and some techniques are suitable for detecting defects in large areas [22-29].

- Pulsed eddy current (PEC) is an effective method to detect defects in multi-layer structures because of it's rich information in both time and frequency domain. It is used in many different applications such as inspection of defects in oil/gas pipeline, air crafts, high-speed rail and nuclear steam pipes. It is made up of a frequency spectrum, which means that each pulse signal contains information from a variety of depths within a given test object. The pulse signals are extremely low-frequency rich, allowing for excellent depth penetration [22,23].

- Array Scanning technique is a series of single elements arranged in a row to allow the user to cover large areas in single pass. The way this technique works could lead to suboptimal results, so multiplexing is necessary to get accurate results. Multiplexing done by activating and deactivating coils in a sequence to leverage the probes width [24,25,26].

- Remote-field testing is where the transmitter coils of RFT probes are spaced two tube diameters away from the reception coil. The magnetic field produced by the transmitter coil moves radially and axially in the direction of the receiver through and out of the tube wall. To get to the receiver, the magnetic field must go through the tube wall once more. RFT is known as through-transmission, and this is what it means. Through-transmission makes it possible to detect flaws both internal and external with same sensitivity this technique is used in the petroleum industry to detect corrosion in the installations since 1960s. It is a highly sensitive technique to the variations in the wall thickness [26].

- Lorentz force eddy current enables detecting the defects that are laying deep inside a moving non-magnetic conducting material [11]. In this technique, the relative motion of an object under test with respect to the static/primary magnetic field can be used to obtain induced EC. If the material has a flaw, the perturbation of the induced currents or its secondary magnetic field is detected by a change in the Lorentz force acting on the permanent magnet [27].

- Pulsed eddy current thermography (PECT) is a hybrid of pulsed eddy current and thermography. This technique is classified into two types: induction and heat diffusion [15, 12]. A short burst of electromagnetic excitation is used to induce the material under test. the area with increasing current density experiences higher levels of Joule heating, and the defect is identified using an infrared camera during the heating and cooling period. The flash thermography is used in the heat diffusion PECT. The interaction between heat and defect occurs via EC diversion and heat dissipation [28].

- Multi-frequency technique involves collecting data at various frequencies, this method is used to inspect heat exchanger tubes. The signal from the mounting bracket is frequently problematic when attempting to inspect the full wall thickness of the tubing, the effects of the bracket could be reduced by collecting a signal at the frequency required to inspect the entire thickness of the tube and subtracting it from a second signal collected at a lower frequency [29].

1.5 Eddy current instruments

There are different tools used in eddy current techniques, the main important tool is the probe, which is responsible for inducing the eddy currents in the material under test and sensing the resulted signal to detect the defects within the layers of the material. There are different probe types used in eddy current inspection, the probes are classified into two different categories, which are configuration and mode of operation of the test coil. Some examples of these probes for both configurations are, the absolute probe that includes only a single coil which works as a transmitter and receiver in the same time, and the differential probe which uses two coils and responds only to the sharper changes such as cracks, and the donut probe which is used to inspect aircraft fastener holes and the surface probe which is used to scan wide areas for surface and sub-surface cracks [29].

1.5.1 Probes types and their application in industry

Depending on the type of probe used, eddy current instruments can perform a wide range of tests, and careful probe selection will help optimise performance. The following are some examples of common probe types:

- Surface probes are used to detect flaws on and beneath metal surfaces, they are typically large in diameter to accommodate lower frequencies for deeper penetration or scanning larger areas.
- Pencil probes which have smaller diameter with high-frequency coils for high resolution of near-surface flaws.
- Bolt hole probes are used to inspect the inside of a bolt hole, these probes can be rotated manually or automatically with the aid of a rotary scanner.
- Donut probes - Used to inspect aircraft fastener holes while the fasteners are still in place.
- Sliding probes - These probes are used to test aircraft fastener holes and have a higher scan rate than donut probes.
- ID probes - Available in a variety of sizes, these are used to inspect heat exchangers and similar metal tubing from the inside.
- OD probes - Used for outside inspection of metal tubing and bars, with the test piece passing through the coil.

Modes of operation of probes

The main tool used in eddy current testing is the probe used for detection. Eddy current probes are responsible for inducing the eddy current inside the material and in the meantime detecting the defect signal. Eddy current probes operate in different modes and the probes designs can be customized to be used in different applications. Most of the available probes either have one coil which works in the absolute mode or two coils which works in the reflection or differential mode.

- Absolute probe has only a single coil, the coil induces the eddy currents inside the material and senses the defect signal. Absolute probes are commonly used for thickness, conductivity, lift-off measurements and flaw detection. A schematic diagram of the absolute probe is shown in Fig. 1.5.
- Reflection probe has two coils, one of the coils induces the eddy currents inside the material and the other one senses the defect signal. Sometimes it is referred to the reflection probes as driver/pickup probes. A schematic diagram of the reflection probe is shown in Fig. 1.5.

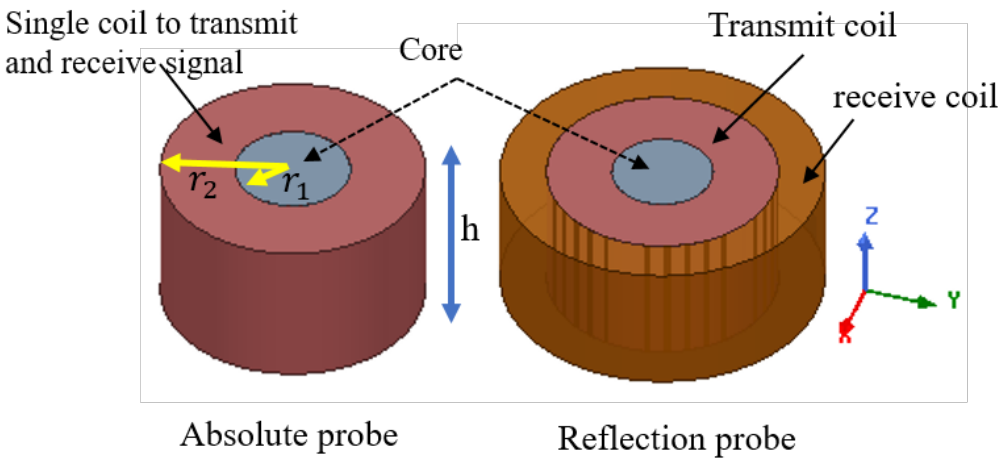


Figure 1.5: Absolute and reflection probe geometry differences; (a) shows an absolute probe that has only one coil, (b) shows a reflection probe that has two coils.

- Differential probe also has two coils, the coils could be wounded in an opposition or in addition way; both winding ways will give the same results. In case of a defect a differential signal will be created between both coils since one of the coils will be on top of a defect and the other coil will be on top of a good material.
- Hybrid probe which can operate in a differential or a reflection mode. Hybrid probes are very sensitive to surface defects.

1.5.2 Data acquisition system

Many eddy current inspection instruments are available in the market. An overview of the most important ones and a comparison between their specs listed in table 1.1. It is a comparison between the range of frequency used, the size of defect and the depth of the defects detected from the surface.

There are four existing categories of eddy currents devices, which sorted as (1) Handheld eddy current devices, (2) High end performance eddy current devices but mobile, (3) Fixed installation eddy current equipment for quality control of objects in production and (4) specialized equipment for military equipment detection.

In the first category considers eddy current devices such as Nortec 600 from Olympus or the Phasec 3 from GE. This kind of equipment operates in specific mode and gives relatively limited flexibility in terms of data access. Typically these instruments are used on parts, which are manually scanned.

Regarding the second category of eddy current instruments, the equipment are also transportable but often heavy. In this category you will find the Zetec MIZ-21C , the Apollo from GE and Ectane from Eddyfi, such devices often used to inspect heat exchanger and steam generators in power plants.

The third category specially developed for in-production quality control. The two famous leaders for this kind of dedicated devices are Dr. Förster and Rohmann. The online control unit can for example detects a specific conductivity of a material and activates an alarm in case the conductivity is not anymore within the set parameters. For example the Eloscan PL500Q from Rohman can be used with a robotic guidance for in production or quality control inspections. A picture of some of the available EC instruments are shown in Fig. 1.6.



Figure 1.6: Available eddy current instruments in the market.

Product name	Frequency range	Defect depth	Defect length
NORTEC 600	10 Hz-12 MHz	0.254mm to 0.762mm	0.254 mm-2.54 mm
Olympus-MS 5800 ER	40 KHz per channel	0.508mm to 1.27mm	2.54 mm-5.08 mm
ELOTEST IS 500	10 Hz-12 MHz	0.05mm to 0.75mm	0.25 mm-1.5 mm
Zetec MIZ 21C	5 Hz to 10 MHz	up to 4.0 mm	0.2 mm-5 mm

Table 1.1: Specs of some of the available EC instrumentation in the market.

To be able to choose the right eddy current instrument for the experimental set up, two different data acquisition systems have been tested and a comparison between them added in the measurements and validation chapter.

In the following section will talk about additive manufacturing (AM) technology which is one of the new promising technologies that is being used in many industries. Eddy current (EC) testing has been around and while AM is relatively new. Many researches have been reported on AM, however, there are very little work on integrating these two subjects, and this thesis will investigate application of EC in AM.

1.6 Additive manufacturing technology

Additive manufacturing (AM) is the process where objects are being created from a three-dimensional computer aided design data, the parts are created by laying materials layer by layer [30], Fig. 1.7. There are seven categories of technologies for AM. The categories are powder bed fusion, material jetting, material extrusion, binder jetting, vat photo-polymerisation and directed energy deposition [31-34].

AM is used in a broad range of fields and applications, it is used to fabricate a replacement for damaged human tissues in biomedical field, transportation, and used in aerospace industry, because of the wide range of applications for the additive manufactured produced parts, NDT techniques are required for inspecting these parts. Different NDT techniques are used to detect defects, porosities and cracks created within the layers of LAM- made parts [30].

The laser additive manufacturing process (LAM) specifically laser powder bed fusion process (LPBF) involves many parameters which affects the quality of the produced parts,

this why a good inspection technique is necessary to ensure having a good quality parts. The testing process in additive manufacturing is necessary to ensure product's integrity, quality and reliability.

There is a wide range of NDT techniques that are used as post-process inspection methods such as liquid penetrant testing, ultrasonic testing, visual inspection, magnetic particle testing, radiography and eddy current testing. Each one of these techniques has its advantages and disadvantages. In this thesis, the focus will be on the eddy current NDT technique.

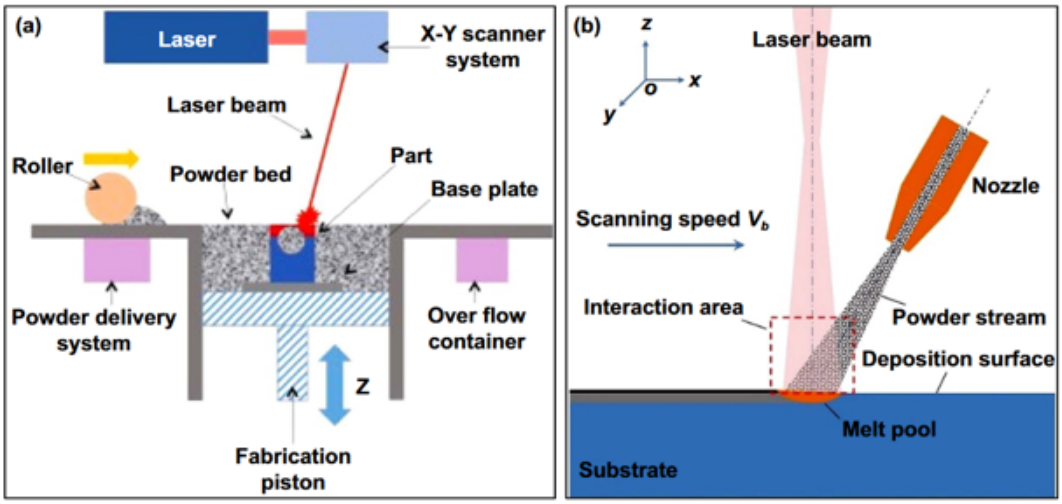


Figure 1.7: The powder bed fusion system schematic diagram to the left and the directed-energy deposition system schematic diagram to the right [34].

The way parts made by additive manufacturing technology where materials are laid layer-by-layer creates different types of defects like cracks and porosities between those layers. Porosities and cracks are formed by the gas evolution which is caused by the moisture in the powder during melting. The existence of these defects will affect the quality of the products made by additive manufacturing (AM) technology. Different non-destructive testing techniques can be used for inspecting these parts. These techniques can be used for in-situ and post-process inspection. Acoustic emission testing, thermography and photodiode signal can be used for in-situ inspection in AM [30]. In addition, techniques such as eddy current testing, x-ray, laser ultrasonic testing, and visual inspection can be used for post process NDT inspection.

1.7 Problem statement, objective and contribution

The main objective in this thesis is to design an eddy current probe that can detect small size sub-surface cracks and voids in parts made by laser powder bed fusion process. Locating the defect and getting an estimation about its type and size is considered as well. The probe is the main tool since it determines the amount of eddy currents that are induced in the material and how sensitive it is to detect small defects. This is achieved by optimizing and designing a probe that is sensitive to very small defects in parts with a rough surface. Several factors affect the sensitivity of the probe such as coil dimensions and number of turns, some of these factors are discussed later on. A model is designed in ANSYS Maxwell simulation tool to control the factors that affects the sensitivity of the probe. several cases are considered for sensitivity analysis in both simulation and during experiment. The cases are shown below:

- Testing samples with defects close to the edge of it to find out the best way to detect those defects without getting a false signal produced by the samples edges that represents a crack. Experimental results are shown in section 5.12.1 and simulation results are shown in section 4.4.1.
- Second case is to explore the effect of different lift-off distances on the accuracy of defect detection. Experimental results are shown in section 5.12.2 and simulation results are shown in section 4.4.2.
- Third case is to explore detecting multiple defects that exist in the same region or defects that are separated by small distance in between. Experimental results are shown in section 5.12.3 and simulation results are shown in section 4.4.3.

- The major contribution is investigating using eddy current NDT technique for defect detection in additive manufacturing.
- A second contribution in this project is designing a proper probe suitable for additive manufacturing based on proposed analytical model verified by finite element and experiment.
- The third contribution is proposing a method to reduce the sensitivity to surface roughness and edge effect for better detection of flaws inside material.

1.8 Thesis outline

Chapter one gives an introduction about additive manufacturing technology and non-destructive testing techniques specifically the eddy current testing technique. The theory behind eddy current testing and its application are explained in more details.

Chapter two gives an overview about the history of non-destructive testing and the history of using eddy current testing in additive manufacturing. The limitations associated with using eddy current testing technique in additive manufacturing and the types of defects created within the parts made by additive manufacturing are also included.

Chapter three includes different analytical models to calculate the probe impedance change on top of material with defect and without defect. It also shows the steps to design an eddy current probe that works in the absolute mode.

Chapter four includes finite element analysis and different simulation models of the probe to detect subsurface notches and subsurface blind holes. The notches have different widths in the range of 0.07 mm to 0.5 mm and different lengths of 5 mm, 15 mm, and 25 mm. The blind holes have different diameters in the range of 300 micron to 600 micron.

Chapter five shows the experimental setup that is used for the detection process. The different tools including the eddy current probes and the measurements taken during the experiment.

Chapter six includes a discussion about the outcomes of using eddy current testing in additive manufacturing and a comparison between different eddy current probes and different materials that are used during experiment.

Chapter 2

Literature review

Many non-destructive testing techniques are reliable and helpful to detect defects in parts produced using additive manufacturing. Using each one of these techniques might face some challenges and limitations, sometimes combining different techniques together can give better and more accurate results. Eddy current technique considered as a reliable non-destructive technique to be used in additive manufacturing, working on providing solutions for the challenges that faces this technique will make it more reliable.

2.1 History of non-destructive testing(NDT)

The evolution and the development of the NDT techniques have been changing fast over the past years. There are several technologies that use non-destructive techniques as a way to evaluate flaws and the properties of materials since 1850. The modern NDT began mostly in the medical field around 1885, and that is when Wilhelm Conrad Rontgen produced and investigated electromagnetic radiation, which he named later as (X-rays) [30]. In the year 1915 the French physicist Paul Langevin filed a patent [25], he developed a technique based on ultrasound to find icebergs in the sea after the Titanic accident. This is one of the first developments, which used subsequently to identify objects in materials.

Dr. Lester in 1920s was the first person that used X-ray to test casting and weld structure to find inclusions [30-34]. Eddy currents were discovered in 1851 by the French scientist Leon Foucault which was a long time before using it for NDT. David Hughes, the English scientist found out in 1879 , how the inductance and resistance of a coil changes when placed in contact with materials that have different permeability and conductivity

levels [11, 12], that was the beginning of using eddy currents testing for material sorting. In 1933, Friedrich Forster worked for the Kaiser-Wilhelm institute in Germany; he did a lot of intensive research on eddy currents. In 1948, he bought the license for eddy current testing and developed further instruments. Many other countries after that got involved in the development of the eddy current instruments such as Olympus, GE, Zetec, etc.

In 1950 and 1960, EC inspection advanced mainly with the needs of high reliability in the nuclear and aircraft industries because of the necessity for high safety, which achieved only by non-destructive testing. Many recent developments in eddy current testing emerged, especially sensors development, configurations or electronic performances. Analytical modeling and simulation helped to understand the eddy current signal better for engineers and inspectors.

2.1.1 Examples of NDT applications in industry

There are many examples for NDT and applications in the industry. The improvement of the devices or machines are very important and depends on the application itself. The machine improvement done in many aspects such as the weight and the size or the structure of the design and the sensitivity to detect the smallest defects [35-41].

This demonstrated by taking an example from the aerospace industry where regular check-ups are strictly regulated. Regular check-ups and inspections done with several different types of non-destructive testing method, for example regular passenger airplane. A plane has to be regularly checked and disassembled. The regulations for commercial turbine powered aircrafts follow a continuous inspection program, which approved by airworthiness institutions such as the "Luftfahrt-Bundesamt" in Germany or the "Bundesamt fur Zivilluftfahrt" in Switzerland. The maintenances are divided in four main intervals and depending on the type of airplane and several other parameters divided in subintervals. Below is an example of intervals taken from the Minor Project of Michael Bseliss.

In the aerospace industry where regular check-ups are regulated and guarantees the reliability. Inspections and regular check-ups done in so many different ways using different NDT techniques; for example the regular inspection done to turbines of the aircrafts. In Switzerland, the airworthiness institutions such as "Bundesamt fur Zivilluftfahrt" or "Luftfahrt-Bundesamt" in Germany give the approval to the regular inspection for the turbine-powered air-crafts, the inspection and the maintenance divided in four different intervals and based on the type of the airplane and other parameters. An example of these intervals taken from the project of Bseliss shown in [37]:

The A-check interval takes place for approximately every 250-700 flight hours which needs around 20-50 person-hours of work and that means an overnight check-up. For B-check interval, that happens approximately every 1000h. This happens every 3 to 5 months, usually it needs around 150 person-hour of work overnight or at least the plane has to be on the ground for minimum 12 hours. In the C-check interval, inspection takes place every 15 to 18 and that depends on the type of the airplane, this interval may take up to 5000 man hours of work, which means that the airplane may stay on the ground for inspection for almost two weeks. During this check, some of the main parts like seats removed from the aircraft. For D-Check interval, it done every 6 to 10 years and that might need up to 50000 man hours of work which will take from 4 to 6 weeks on the ground.

As shown in the previous paragraph some of the inspection procedures taken in the aerospace industry require a tremendous amount of work and effort to ensure safety, this applies to aerospace industry and other industries such as the nuclear power industry which follows similar strategies [18].

Eddy currents were discovered in 1851 by French physicist Léon Foucault, and the phenomenon is sometimes referred to as Foucault currents. To demonstrate that eddy currents (magnetic fields) are generated when a material moves within an applied magnetic field, Foucault built a device that used a copper disc moving in a strong magnetic field.

Eddy current testing began in large part as a result of the 1831 discovery of electromagnetic induction by the English scientist Michael Faraday. When a magnetic field passes through a conductor (a material in which electrons move easily)—or when a conductor passes through a magnetic field—an electric current will flow through the conductor if there is a closed path through which the current can circulate.

Another breakthrough was made in 1879 when another English scientist, David Hughes, demonstrated how the properties of a coil change when it comes into contact with metals of varying conductivity and permeability. However, it was not until the Second World War that advances in electromagnetic wave transmission and reception were put to practical use for materials testing.

Professor Friedrich Förster began adapting eddy current technology to industrial use in 1933, while working for the Kaiser-Wilhelm-Institute in Germany, developing instruments for measuring conductivity and sorting mixed-up ferrous components. Förster founded his own company in Reutlingen in 1948, a business based on eddy current testing that still exists today. Other businesses quickly followed. Throughout the 1950s and 1960s, many advances were made, particularly in the aircraft and nuclear industries. Many recent advancements in eddy current testing have resulted in improved performance and the development of new applications, eddy current testing is now a well-known and widely used

inspection technique for flaw detection as well as thickness and conductivity measurements.

2.2 Examples and considerations for EC testing in additive manufacturing

In additive manufacturing, there are many challenges to choose the best and applicable non-destructive-testing technique suitable for inspecting the (WAAM) parts [30]. For the Wire and Arc additive manufacturing industry, there is a potential for the production of large-scale structures. This technique involves designing component and subsequent welding deposition of multi-layer structure to produce the parts that allows producing customized large parts at lower cost. With the view of qualifying WAAM for applications such as structural components, an applicable non-destructive inspection technique developed to detect porosities and lack of fusion between layers.

Non-destructive testing is required at various stages of fabrication to ensure the quality of the products. Real-time layer-by-layer monitoring of the AM fabrication process while the component was being built was required to reduce or eliminate reliance on post-process inspection. Array Eddy current NDT technique developed to detect discontinuities and surface irregularities in parts without physical contact with the powder and fused layer surface inside an LPBF chamber at elevated temperature [38,39].

A multi-frequency eddy current method for electrical conductivity measurements of lattice structure investigated and compared to other NDT techniques to select the better NDT technique of inspecting the parts produced using the AM technology [29].

The main limitation of eddy current testing is that it can only test electrically conductive materials [18,19,20]. The probe used in Eddy current testing can detect desired material properties such as discontinuities and conductivity, as well as unwanted signals related to conductivity and magnetic permeability, resulting in increased complexity in results interpretation.

AM techniques can print a wide variety of materials, including metallic and non-metallic materials [32]. Because eddy current testing is designed to be used on electrically conductive materials, parts made of bio-materials, polymeric materials, and ceramic materials are not suitable for this NDT technique. Surface roughness is typically described in parts produced using AM technology [30]. Eddy currents, in addition to other inspection techniques, are used to obtain more accurate results, particularly with manufactured parts with high surface roughness [36,37,38].

Parts made by additive manufacturing require inspection to insure its quality. Eddy current testing technique is a reliable technique to be used for defect detection in parts made by AM technology. Like any other NDT techniques, there are limitations that are associated with using EC for defect detection in AM.

First, eddy current could be used only for inspecting parts that are made of conductive material. Some of the parts made by additive manufacturing has small size or a complicated geometry which will disturb the eddy currents and cause what's called edge effect.

Parts made by additive manufacturing have rough surface which could be challenging to test these parts using eddy current technique. Material factors such as surface roughness and alloy uniformity can affect eddy current results and sensitivity to detect subsurface defects. Surface condition is of concern when testing metallic components because it limits surface defect detectability. Rough surfaces produce signals that are very similar to signals produced by shallow flaws in the surface adjacent to the test coil, resulting in poor sensitivity to actual shallow surface defects. In new wrought materials, alloy uniformity is usually unimportant. Wrought alloys, on the other hand, can change during service, either in composition (i.e., oxygen contamination of reactive metals such as titanium) or in heat treat condition (i.e. over ageing of aluminium alloys). Such mechanisms can cause variations in resistivity, which can affect eddy current response. Alloy segregation in castings and welds can cause variations in resistivity and magnetic permeability. Eddy current response is greatly influenced by changes in magnetic or electrical properties [8]. At best, such variations reduce signal-to-noise, resulting in lower defect sensitivity that could be misinterpreted as serious flaws. A rough surface will produce a signal that appears to be noise, requiring filtering to distinguish between the flaw and the signal produced by the roughness of the surface.

It is challenging to use eddy current testing while the manufacturing process is happening since the eddy current probe would give reliable results in a solidified region compared to a melt pool region, for example while manufacturing parts using Laser Powder bed fusion (LPBF) technology its challenging to detect defects or move the EC probe over the test piece due to the heat produced by the laser while the manufacturing process is happening. This heat may have a big effect on the impedance of the coil and may lead to inaccurate results. If there are a lot of variations in the temperature either in the melt pool or the distance between the probe and the test samples, that will cause the appearance of false signals that could be interpreted as a defect[35-41].

2.3 The usage of EC in inspection in AM and other fields compared to other NDT techniques

All types of non-destructive techniques including eddy currents help industries to reduce any risk of having accident or failure because of material degradation or aging. There are some NDT techniques that are compatible with each other and can be combined together to get better inspection results and gives more information about the structure and the health state. For example, eddy current technique can be used with another technique such as ultrasound because the procedure of the testing process are the same, later in the chapter results will show a comparison between eddy current technique and ultrasound technique for defect detection of a defect of the same size. One of the main features eddy current testing technique is that it doesn't need contact between the testing probe and the sample under test, meanwhile ultrasound techniques requires some preparation such as adding water or gel coupling to link the sound waves into the material. In addition, one other advantage of using eddy current inspection technique is that the signal acquisition is fast because the magnetic field reacts immediately to any material close to it.

However, ultrasound might take longer time because it limited to the speed of sound in the material. There are other non-destructive techniques that are even slower in reaction such as dye penetrating testing because the speed limited by the chemical reaction. Since speed is very important feature when it comes real time inspection, eddy current testing techniques considered as one of the fastest testing techniques when it comes to achieving accurate and time efficient inspection. A comparison between the different testing techniques and their applicability to additive manufacturing process shown in table 2.1 [38]:

NDT technique	**Inspection type**	**Sensitivity to defects**	**Applicable additive manufacturing process**	**Challenges**
Eddy current	surface and subsurface	It depends on material conductivity and permeability, orientation and type of defect, and surface quality of the material and the used frequency.	• Direct energy deposition. • Powder bed fusion.	• Any surface roughness of the part under test will cause unwanted signal. • Post processing is necessary.
Liquid penetrate testing	Surface	Using visible dye penetrant, a 5 micrometer can be detected and using fluorescent penetrate a 2 micrometer crack can be detected.	• Vat photopolymerisation. • Powder bed fusion.	• Smooth surface required before examination. • Polishing for the parts and post processing required.
Visual inspection	Surface	0.25 inches is the minimum discontinuity size a human can detect.	• Direct energy deposition, Powder bed fusion, Material Jetting, Sheet lamination. • Binder jetting, Material extrusion.	Using optical aids required for the monitoring process.
Magnetic particle testing	Surface	Only defects that lie up to +45 degrees to the direction of the magnetic flux can be detected.	• Direct energy deposition. • Powder bed fusion.	• Can be used only with ferromagnetic materials. • Only applicable for AM material such as Nickel and Cobalt.

Ultrasonic	Surface and subsurface	Detected defect size range will be of the order of half the wavelength with the use of the particular frequency.	• Direct energy deposition, Powder bed fusion, Material Jetting. • Sheet lamination, Binder jetting, Vat photopolymerisation.	Surface roughness may cause unwanted noise in the defect signal.
Radiography	Surface and subsurface	Selected exposure penetrating through the material is a crucial factor and should produce X-rays that is sufficient to penetrate the material.	• Direct energy deposition, Powder bed fusion, Material Jetting. • Sheet lamination, Binder jetting, Vat photopolymerisation, Material extrusion.	Inspection for specimens with high atomic numbers might not be accurate or give good results.
Acoustic emission testing	Surface	Can detect crack growth of the order 25 micrometer.	• Direct energy deposition, Powder bed fusion, Material Jetting. • Binder jetting, Material extrusion.	It might be hard to identify the source that is causing change in sound signature.
Thermography	Surface	It is suitable for identification of defects from the surface to a depth of 10 cm.	• Direct energy deposition, Powder bed fusion, Material Jetting. • Sheet lamination, Binder jetting, Vat photopolymerisation, Material extrusion.	The broad temperature range of the melt pool of the powder bed fusion process might cause calibration problem of the infrared camera.

Table 2.1: A comparison between different inspection techniques in additive manufacturing.

2.4 Defect types created in additively manufactured parts

Laser powder bed fusion is one of the most important additive manufacturing technologies for producing metallic components. One of the most difficult aspects of AM is quality control. The layer-wise nature of Laser powder bed fusion (LBPF) allows for process monitoring while also being a potential source of defect detection. The laser powder bed fusion manufacturing process consists of three stages that are iteratively repeated until the part is completed [9]:

- Powder recoating.
- Lowering of the base plate.
- Laser melting or exposing.

First, a metallic powder is uniformly distributed over a metallic base plate with a defined layer thickness of (25-50) micron. During the exposing phase, laser radiation selectively melts the powder based on the 2D geometrical information, which is referred to as slicing of a 3D volumetric model. Because of the small melt pools, the molten powder solidifies quickly, resulting in material cohesion. The base plate is then lowered by the layer thickness, and the next iterative loop begins. Porosity; cracking and delamination; balling; geometric defects; surface defects; microstructural inhomogeneities and impurities are the defect categories compiled for L-PBF. An example of the types of defects is shown in Fig. 1.4.

L-PBF is known as a process with numerous influencing factors that can result in defects and affect part quality. As a result, various in-situ monitoring approaches have been developed to observe specific process parameters and objects such as laser power, powder recoating and powder bed surface, powder bed compaction, plume and spatter behaviour, particle gas emissions, and part distortion. Monitoring the spatial and temporal temperature conditions within or near the laser-material interaction zone has also been studied and widely applied by many authors.

Bartlett et al. used a long-wave infrared (LWIR) camera to track the production of L-PBF in aluminium specimens. They were able to detect 82 percent of lack-of-fusion pores by signal deviations and 50 percent of defects smaller than 50m using their method. Mitchell et al. placed an off-axis two-color pyrometer with two CMOS cameras directly within an L-PBF machine's build chamber. They concentrated on the melt pool and its temperatures, deriving process irregularities from differences in melt pool peak tempera-

tures and melt pool shapes. They were able to associate pyrometric data deviations with cavities with a cross section length of 120 µm.

2.5 Summary

In This chapter several topics has been discussed. The history of non- destructive testing and the history of using eddy current as a non-destructive testing are shown. Also a comparison between using eddy current testing and other non-destructive testing techniques in additive manufacturing is done. The types of defects that are created in parts made by additive manufacturing and limitation with using eddy current testing in additive manufacturing are explored.

Chapter 3

Probe design and analytical modelling of the probe impedance

3.1 Introduction

In this chapter, the main procedures to design an eddy current probe are explained. Different analytical modelling of the coil impedance change on top parts made of conductive material are provided. The analytical modelling solves the eddy current problem of finding the impedance of the coil on top material with defect and without defect.

3.1.1 Solenoid coil design for eddy current detection

One of the important factors that affect the probe sensitivity to small size defects, is the coil dimension. The diameter of the coil becomes wider as its operating frequency lowers (i.e., a 1 mm diameter, the coil will not work at 1 KHz). Therefore, for eddy current probe to find a flaw in a 2 mm plate thickness made of aluminum, the test frequency needs to be low, hence, a larger coil diameter should be used. The minimal detectable flaw size is proportional to the diameter of the coil. As the diameter of the coil increases, the minimum detectable flaw also increases. For notches, the rule of thumb is a quarter of a coil diameter. No matter what, the smaller the coil diameter, the smaller that defect size that can be detected. There are different parameters that are considered to optimize the design of the coil, such as coil geometry, shielding, use of ferrite cores, shields, number of turns, and diameter of the wire.

3.2 Probe design and coil dimension determination

To be able to determine the best dimensions for the coil design such as inner diameter, outer diameter, and length of the coil, the maximum input current should be specified as a first step. The maximum current input to the coil is chosen to be 0.457 Amps. The copper wire gauge that satisfies the requirement is the American wire gauge (AWG) AWG-25. The standard value of the AWG-25 wire diameter (d) is 0.45466 mm, which can be used to determine the number of turns for the coil.

Next step is to specify the inner radius, outer radius and the length of the coil. Based on the size of the parts made by AM, The outer radius value was fixed at 8 mm since the eddy currents distribution under the coil will be almost twice the size of the coil's diameter. Another reason is to leave enough room for the coil to move without disturbing the distribution of the eddy currents under the coil because of the edge effect. A parametric sweep is done using ANSYS Maxwell over the inner radius of the coil for values in the range of 0.5 mm - 5 mm to get the best value of the magnetic field under the coil. In Fig. 3.1 the best value of B_max is at the inner radius value (Rin), equal to 3.5 mm.

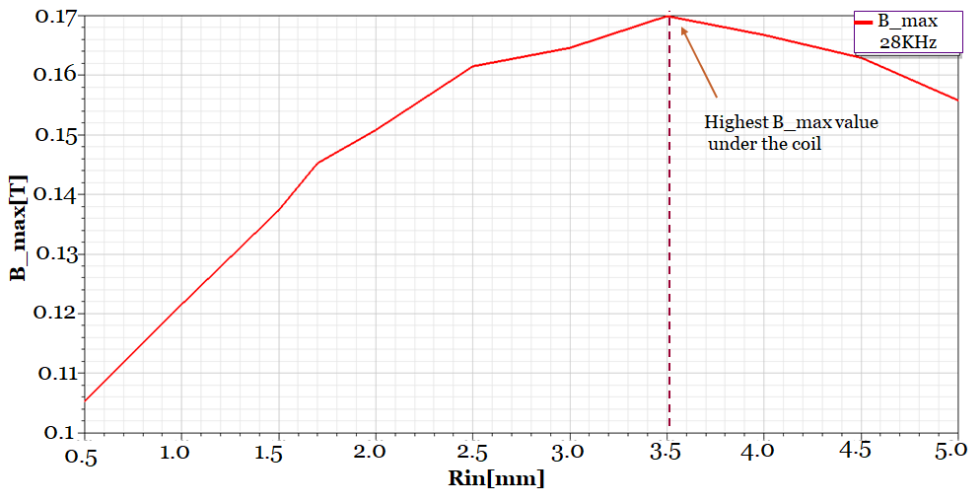


Figure 3.1: Sweep over the inner radius of the coil, the data exported from ANSYS Maxwell and the best B_max value is at inner radius 3.5 mm.

The input voltage that is supplied to the coil is 5 V. A plate made of stainless steel (316L) with a spherical shape defect that has a 0.5 mm radius were created in ANSYS Maxwell to chose the suitable frequency for the probe. The finite element model was run

at different frequencies in the range of 28 KHz - 200 KHz. The reason for running the model at 28 KHz, 100 KHz, and 200 KHz is to evaluate the performance of the probe at low frequency, medium frequency, and high frequency values. The impedance change of the coil was evaluated in case of 200 KHz and 28 KHz as shown in Fig. 3.2 and Fig. 3.4. Running the finite element model at 200 KHz didn't show any results for the impedance of the coil since the standard depth of penetration of the eddy currents inside the material is very small with a value of 0.9 mm as shown in Fig 3.3. The frequency range higher than 50 KHz is suitable for surface defects. The best detection results were obtained at 28 KHz frequency value which is chosen as the operating frequency for the probe. The standard depth of penetration for 28 KHz is shown in Fig. 3.5.

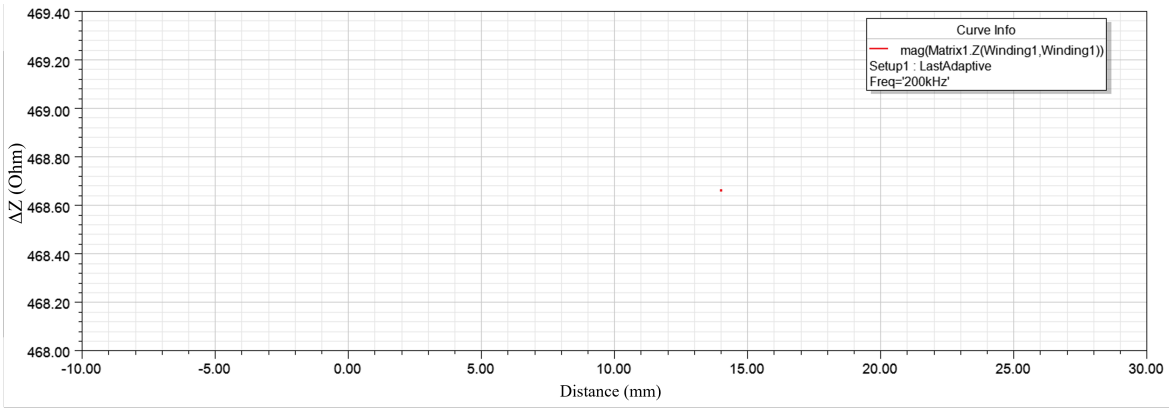


Figure 3.2: Sweep over position of the coil at 200 KHz.

The mesh type used for simulation is on selection, skin depth type. The surface triangle length specified for the mesh was selected at different values in the range of 0.2 mm to 2 mm for mesh dependency analysis as shown in Fig. 3.5. The depth of penetration can be calculated through the skin based mesh selection window. As shown in Fig. 3.5, the depth of penetration inside the stainless steel plate is around 2.6 mm. The smallest mesh size that gives accurate results for this model is 0.2 mm. In case of choosing mesh size smaller than 0.2 mm, the simulation will stop and can't be completed. Choosing a smaller size mesh gives more accurate results but it takes more execution time and requires more computational resources. An example of the impedance value of the coil in case of choosing 2 mm and 0.2 mm mesh sizes is shown in Fig. 3.6 and Fig. 3.7. The best detection results were obtained at 0.2 mesh size since it is small enough compared to the defect size. The results obtained in case of running the model at 2 mm mesh size are not accurate since the mesh size is big compared to the defect size.

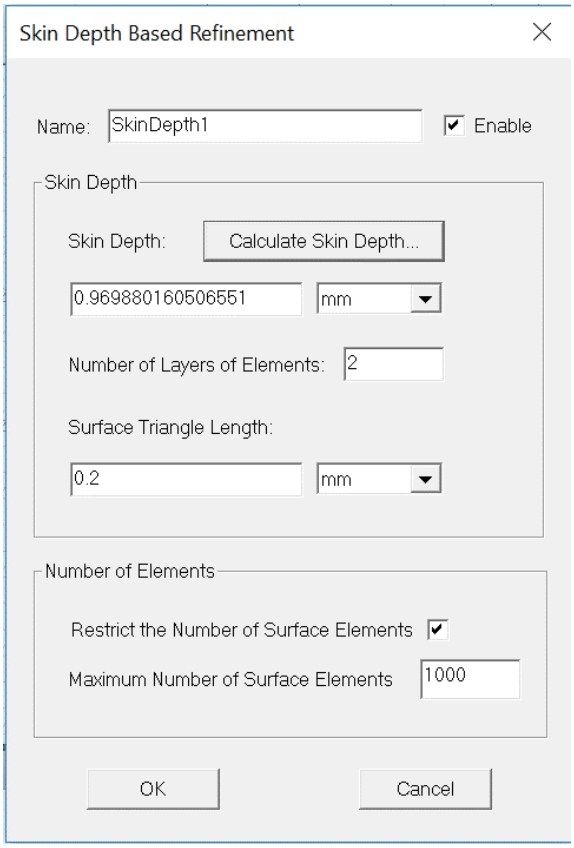


Figure 3.3: Standard depth of penetration at 200 KHz.

After determining the inner and outer diameter of the coil, the next step is to determine the length of the coil. Using the Fabry factor formula shown in equation (3.1), to get the best coil length which gives the highest value of the B_max, will help determine the last important coil dimensions for the probe design.

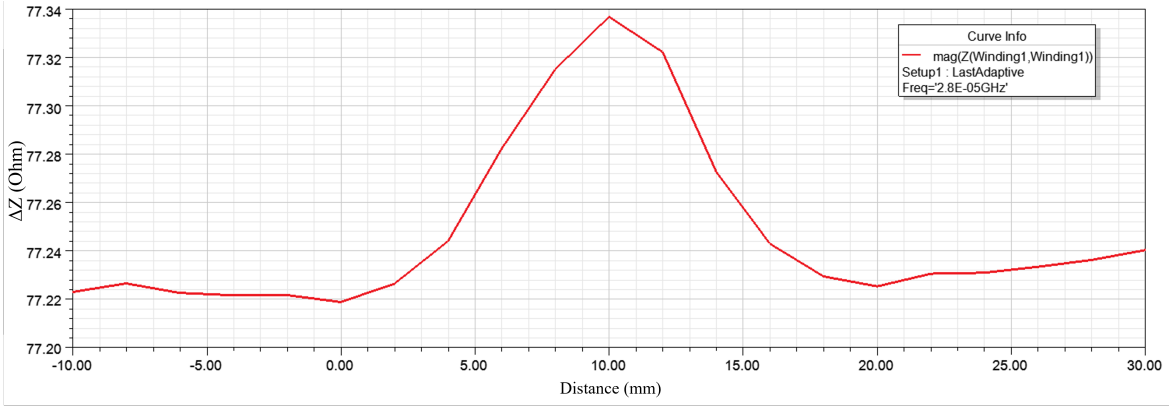


Figure 3.4: Sweep over position of the coil at 28 KHz.

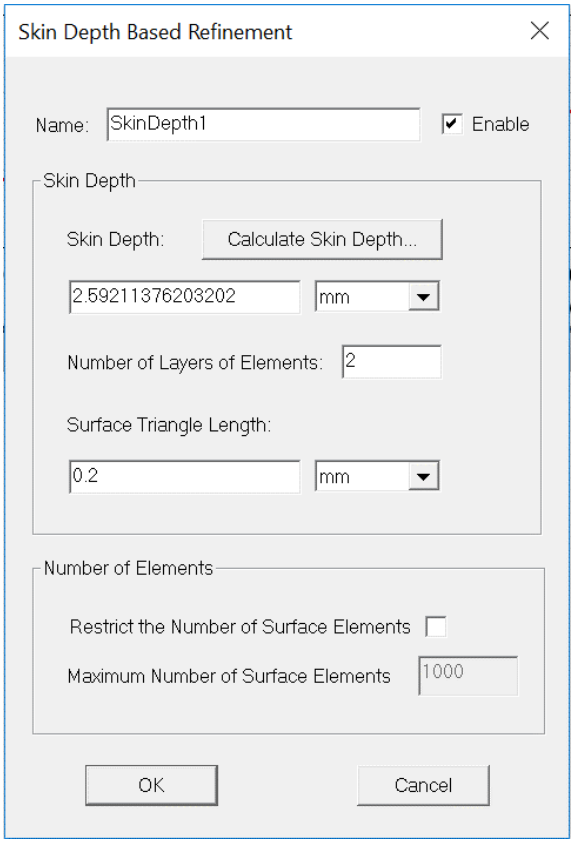


Figure 3.5: Skin depth based type mesh

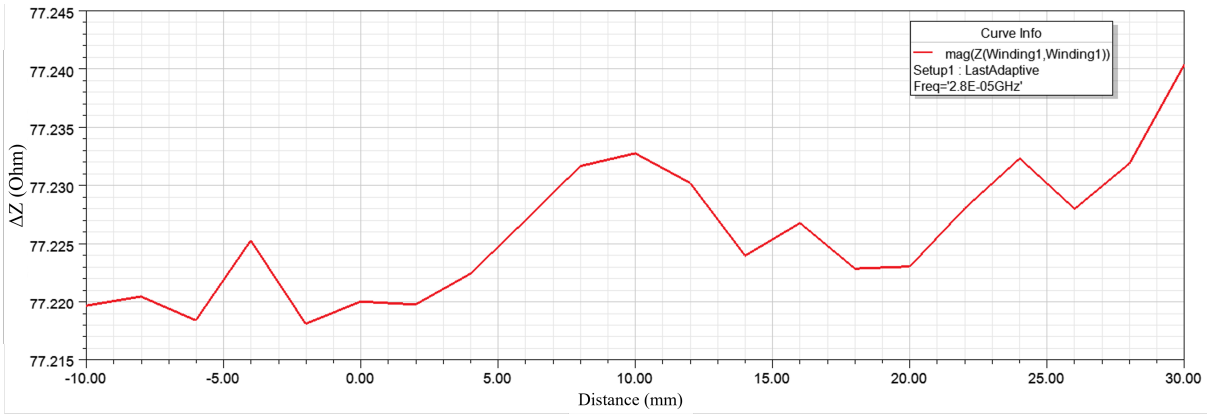


Figure 3.6: Sweep over position of the coil at 2 mm mesh size.

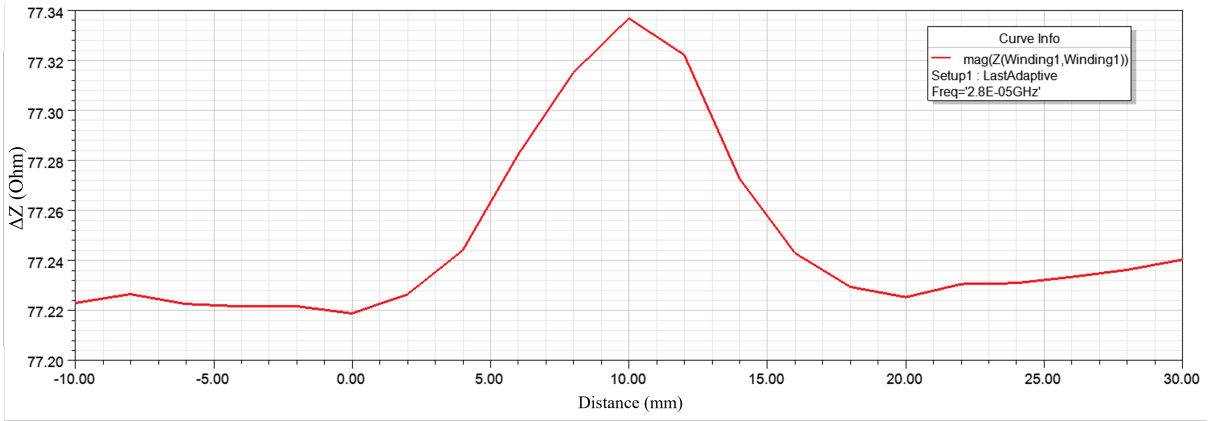


Figure 3.7: Sweep over position of the coil at 0.2 mm mesh size.

Fabry factor and inductance calculations

Some of the basics to design magnetic coils are defined by the work done by Fabry, Bitter, and Cockcroft. They created a formula called by Fabry Factor for power efficiency (G) which is dimensionless. The standard value of the G factor is 0.179 and the best power efficiency of any designed coil should be close to this value. The formula is shown in equation (3.1).

$$G(\alpha,\beta)=\frac{\sqrt{2\pi}}{5}\sqrt{\frac{\beta}{\alpha^2-1}}\ln\frac{\alpha+\sqrt{\alpha^2+\beta^2}}{1+\sqrt{1+\beta^2}} \tag{3.1}$$

where, $\alpha=\frac{D}{D_i}$, $\beta=\frac{L}{D_i}$, coil length is L, D is coil outer diameter, D_i coil inner diameter. When G = 0.179, α = 3.095, and β = 1.862 or close [12]. An illustration of the coil is shown in Fig. 3.8.

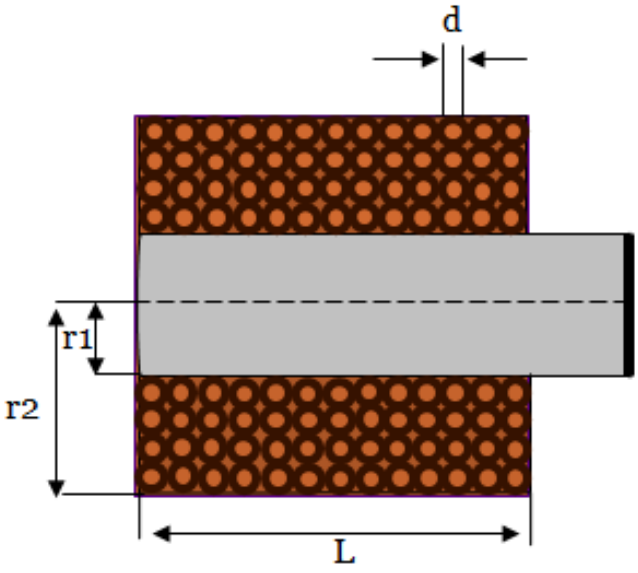


Figure 3.8: Cross-section of the coil geometry.

Table 3.1 shows different values for the coil lengths and the result of the Fabry factor. The best value of the length that gives a proper (G) value equals 0.17324 is at length 9.435 mm.

Length (mm)	Alpha	Beta	G
5	2.28	0.71429	0.1529
9.435	2.28	1.3479	**0.17324**
20.76	2.28	2.9657	0.15885
31.14	2.28	4.4486	0.13905
41.52	2.28	5.9314	0.12376
51.9	2.28	7.4143	0.1121
62.28	2.28	8.8971	0.10318

Table 3.1: Different values for Fabry factor (G) at different coil lengths for fixed inner and outer diameters of 7 mm and 16 mm, respectively.

After determining the geometry of the coil, the next step is to determine the number of turns of the coil. The core type used in the design is the ferrite core to focus the magnetic field, which increases the sensitivity of the coil to detect small size defects. Using equation (3.2), the number of turns of the coil can be calculated.

$$Numberofturns = \frac{L}{d}\frac{r_2 - r_1}{d} \times 0.8 \tag{3.2}$$

Where d is the diameter of the wire. Taking the fill factor into consideration that is 0.8. After considering fabrication, the approximate number of turns =164 turns. An illustration of the coil geometry is shown in Fig. 3.8. Equation (3.3) can be used to calculate the number of turns per layer.

$$Turns/layer = \frac{L}{d} \tag{3.3}$$

Number of turns per layer equals approximately 20 turns per layer. The number of layers can be calculated by dividing the number of turns by number of turns per layer which equals approximately 8 layers. The total inductance calculated for the coil is 444.94 µH using (3.4) where, $\mu_e ff$ is the effective permeability of the core [13]. The measured inductance value using the RLC meter is 518 µH.

$$Inductance = \frac{\mu_e ff \times (Numberofturns(r_2 + r_1))^2}{127(13r_2 + 9l - 7r_1)} \tag{3.4}$$

By following the past few steps, the main parameters to design the absolute probe and to determine its coil dimensions are done. Tip analysis and several cases were considered to

test the designed absolute probe through FEM modelling which are shown later in chapter 4. The same cases were considered for experiments to validate the simulation results which are shown in chapter 5.

3.3 Analytical modelling of the coil impedance change

To determine the existence of a defect inside the part under test, it is important to evaluate the impedance of the probe used for inspection. The evaluation of the impedance change of the probe should be done fast and in a reliable way. Most of the available analytical models solve the partial differential equation arising when the Maxwell equations are applied to the problem geometry. In Dodd's model it gives a closed integral form for solving the eddy current problem for different cases and conditions. The solution for the eddy current problem applied in the cylindrical coordinates since the eddy currents are usually produced by a cylindrical shape coil. The well-known Dodd's model applied to one layer of material and extended to multi-layer using the matrix method of Cheng and co-workers. Other scenarios of calculating the probe impedance were considered for different cases where a change is done either in the conductivity or the magnetic permeability of a multi-layered plate for different coil geometries [41-44].

The boundaries of the eddy current problem in Dodd and Deeds models were set to infinity, which results in providing Fourier-Bessel integral form solutions. Other models used the concept of truncating the solution region by imposing insulation boundaries at a reasonable distance from the source coil. The resulting electromagnetic field expressions and the impedance are in the series form not the integral one. Many advantages in terms of computation speed and accuracy control comes with the replacement of the integral solution with the series expansion one.

The solution domain of the eddy current problem were set to infinity in the Dodd and Deeds model. All the analytical models built in this chapter follows a different mathematical path, this is done by truncating the solution domain and by imposing magnetic solution boundaries at an appropriate distance from the source coil. Because of truncating the solution domain, the expression of the magnetic field and the impedance will change into a series instead of integral form. In case of no defect inside the material of the part under test, the series expansion will cause the existence of discrete eigenvalues. In case of the existence of a defect inside the material, these discrete eigenvalues will become complex eigenvalues. To compute these complex eigenvalues, it is important to find the roots of a complex function that satisfies the electromagnetic interface conditions between the mate-

rial and the defect. These complex eigenvalues can be calculated either using Mathematica, Newton Rapson method, or Cauchy argument principle.

The eddy current equation:

The general equation that governs the time varying field in a conductive material with magnetic permeability is originally driven from the famous Maxwell equations which is briefly shown below:

$$\bigtriangledown \times H = \sigma E + \frac{\partial(\epsilon E)}{\partial t} \tag{3.5}$$

$$\bigtriangledown \times E = -\frac{\partial B}{\partial t} \tag{3.6}$$

$$\bigtriangledown \cdot (\mu H) = 0 \tag{3.7}$$

$$\bigtriangledown \cdot E = \frac{\rho}{\epsilon} \tag{3.8}$$

Where E is the electric field intensity and H is the magnetic field intensity, and ρ is the electric charge , σ material conductivity, ϵ is the permittivity, μ is the medium permeability.

$$B = \bigtriangledown \times A \tag{3.9}$$

$$E = - \bigtriangledown \phi - \frac{\partial A}{\partial t} \tag{3.10}$$

$$B = \mu H \tag{3.11}$$

Where A is called the magnetic vector potential and ϕ is the electric scalar potential. Next step is substituting (3.9), (3.10), (3.11) in (3.5), (3.6), (3.7), and (3.8). After doing simplification to the curl-curl relationship and using the coulomb gauge ($\bigtriangledown \cdot A = 0$), then equation (3.5) becomes:

$$- \bigtriangledown^2 A + \mu\sigma(\frac{\partial A}{\partial t}) = \mu\epsilon(\frac{\partial(- \bigtriangledown \phi - \frac{\partial A}{\partial t})}{\partial t}) \tag{3.12}$$

$$\bigtriangledown^2 A = \mu\sigma(\frac{\partial A}{\partial t}) - \mu J_s \tag{3.13}$$

The final formula for the eddy current equation is shown in (3.14):

$$\bigtriangledown^2 A + k^2 A = -\mu J_s \tag{3.14}$$

Where, J is the current density of the source excitation coil, A is the vector potential and $\bigtriangledown^2$ is the Laplace operator, σ is the material conductivity, ϵ is the permittivity, μ is the medium permeability. k^2= -$\omega\mu(j\sigma + \omega\epsilon)$ where, ω is the angular frequency. Solving the eddy current equation depends on solving the Vector potential A.

Dodd and dodes model:

The probe impedance value on top of a conductive plate with a flow, some models use the integral form that is based on the Dodd and Deeds model which solves the vector potential using the integral form in equation (3.15) [42].

$$Z = [\frac{3}{2}\sigma\omega^2(\frac{A}{I})^2]Vol_\alpha \tag{3.15}$$

This part $[\frac{3}{2}\sigma\omega^2(\frac{A}{I})^2]$ depends only on the coil size and shape, frequency and conductivity parameters. The second part, which is, Vol_α depend on the defect geometry and the orientation of the defect.

Truncated region eigenfunction expansion method:

There are different analytical models that can be used to calculate the coil impedance change on top of plate with a defect. Some of these models uses the integral form and others uses the truncated region eigenfunction expansion (TREE) method. The impedance value of the probe on top of a plate made of stainless steel and titanium materials without a defect is calculated using equation (3.16) as mentioned in [43]. The coil impedance magnitude value calculated analytically on top of a stainless steel plate with 8 mm thickness at 28 KHz is 81.8 ohm. The coil impedance magnitude value calculated analytically on top of a titanium plate with 8 mm thickness at 28KHz is 83.9 ohm. The Matlab code is shown in the Appendix.

$$\Delta Z = -j2\omega\pi\mu_0 b^5 \sum l_N m(c_m)^2 exp(-2x_m l) \tag{3.16}$$

where *(Cm)* can only be determined by inner radius (r1), outer radius (r2), number of turns (w) and the height of the coil (h). Lift-off distance *(l)* and the complex function *(LNm)* that is determined by the plate thickness, conductivity, and relative permeability. The truncated field region (b). Some of the values are shown in table 5.1.

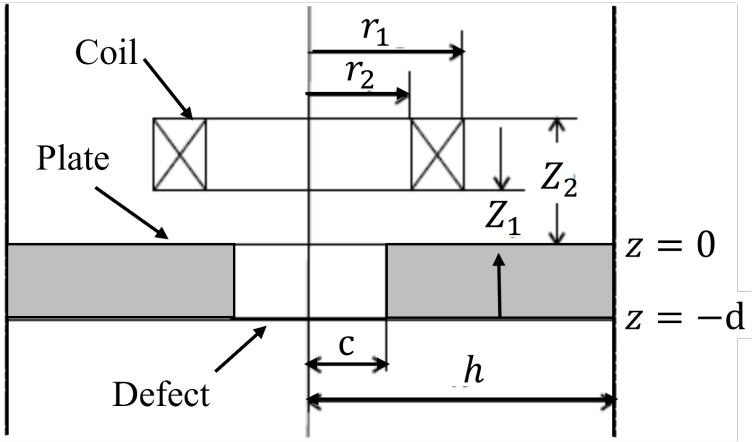


Figure 3.9: Probe on top of a plate with defect.

The formula used to calculate the impedance change of a probe on top of a plate with a defect using the truncated region eigenfunction expansion method is shown in equation (3.17) [44].

$$\Delta Z = \frac{j2\omega\pi\mu_0 N^2}{(r_2 - r_1)^2(z_2 - z_1)^2 h^2} C^T \times U \times J_0(uh)^{-2} \times W \times C \tag{3.17}$$

Where M, W, and T are matrices. r_1, and r_2 are the coil's inner radius and outer radius. The defect width is C and h is the width of the truncated region. Z_1 is the lift-off distance and Z_2 is the distance from the top edge of the coil to the surface of the plate. The thickness of the plate is d. $p^2 i = q^2 i + j\omega\mu_0\sigma$. For computing zeros of Bessel functions u=BesselJZeros[1, Ns]/h using Mathematica. J_0 is the zero order bessel function. A cross section view of the coil on top of a plate is shown in Fig. 3.9.

$$C = (e^{-u_1^z} - e^{-u_2^z}) x(Ur_1, Ur_2) U^{-4} \tag{3.18}$$

$$W = [M(I+T) - u^{-1}Mp(I-T)][M(I+T) + u^{-1}Mp(I-T)]^{-1} \tag{3.19}$$

$$T = e^{-pd}(u^{-1}Mp + M)^{-1}(u^{-1}Mp - M)e^{-pd} \tag{3.20}$$

3.4 One layer structure

In section (3.3) an introduction about different analytical models that are used to calculate the impedance change on top of a conductive material are discussed. Equation (3.16) is used to calculate the impedance change on top of stainless steel plate without defect. The reason behind choosing stainless steel 316L is because it is one of the common materials used in building parts by LPBF process. The model calculates the impedance change of the coil on top of stainless steel plate by selecting the conductivity values for all the layers to be the same for one layer structure. In case of calculating the impedance value of the coil over a multi-layer structure made of different materials, different conductivity values will be chosen for each layer. The model parameters are shown in table 3.2. An illustration of the model is shown in Fig. 3.10.

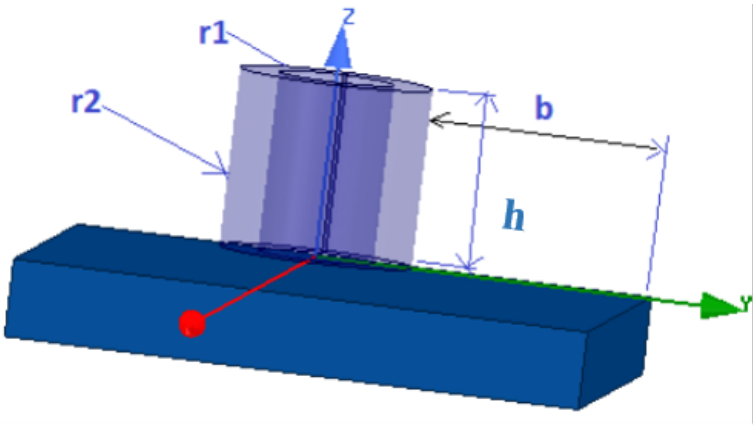


Figure 3.10: Probe on top of one layer plate.

At 18 KHz, Δ Z = 1.649923743746590 - 2.097178533703875i

At 28 KHz, Δ Z = 2.437320128899824 - 4.154976934204931i

The impedance of the coil is calculated at two different frequencies to show that the higher the frequency used for the input source the higher the impedance value of the coil. The impedance of the coil were calculated at 28 KHz frequency value since it is the same frequency chosen for the designed absolute probe.

Plate thickness	3.0mm
Truncated region (b)	40mm
Number of turns	164
Coil outer radius (r2)	8.0mm
Coil inner radius (r1)	3.5mm
Coil height (h)	9.435mm
Frequency	18KHz , 28KHz
Conductivity	1.35×10^6 siemens/m
Relative permeability	1
lift-off distance	0.2 mm
Summation term	300

Table 3.2: Parameters used for one layer plate structure.

3.5 Multi-layer structure

The impedance of the coil is evaluated in case of moving the coil on top of a multi-layer structure made of different materials. Equation (3.16) is used to calculate the impedance change on to of multi-layer plate without defect. The model calculates the impedance change of the coil on top of a plate made of one stainless steel layer and another titanium layer added to it by selecting the conductivity values for each layer to be different. The model parameters shown table 3.3. An illustration of the model is shown in Fig. 3.11.

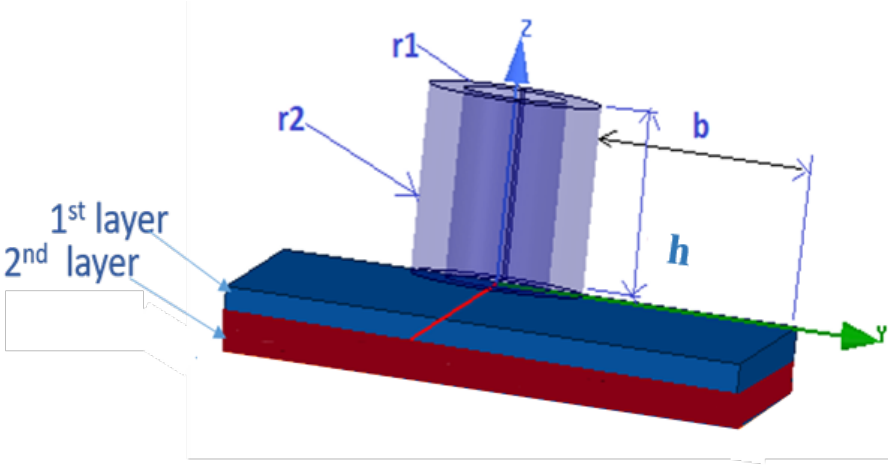


Figure 3.11: Probe on top of multi-layer plate.

Plate thickness	3.0mm, 1st layer 2mm, 2nd layer 1mm thickness
Truncated region (b)	40mm
Number of turns	164
Coil outer radius (r2)	8.0mm
Coil inner radius (r1)	3.5mm
Coil height (h)	9.435mm
Frequency	18KHz , 28KHz
Conductivity	1st layer 1.35×10^6 siemens/m, 2nd layer 0.56×10^6 siemens/m
Relative permeability	1
lift-off distance	0.2 mm
Summation term	300

Table 3.3: Parameters used for multi-layer layer plate structure.

Δ Z is the calculated value of the impedance of the coil at 18 KHz and 28 KHz.

At 18 KHz, Δ Z = 1.740973389415891 - 1.941462805480219i

At 28 KHz, Δ Z = 2.649791988098945 - 4.026699803746408i

The impedance of the coil is calculated at two different frequencies to show that impedance value of the coil increases in case of increasing the frequency of the input source. The impedance of the coil was calculated at 28 KHz frequency value since it is the same frequency chosen for the designed absolute probe. The same analytical modelling will be used later in chapter 5 to evaluate the impedance change of the coil on top of a plate made of stainless steel and titanium with different defects. The results obtained from the analytical modelling will be compared to the ones obtained from simulation and experiment for different defect types and sizes that are located at different depths.

3.6 Conclusion

In this chapter the main steps to design and eddy current probe are shown analytically. Several analytical models that are used to calculate the probe impedance change of the probe on top of conductive materials are explored. The probe impedance change of top of one layer material and multi-layer material is calculated.

Chapter 4

Finite element modelling of the probe impedance

4.1 Finite element analysis and software tools

There are different advantages of using finite element methods such as visualization, accuracy, and adaptability. It allows modelling of complex shapes and geometries to find solutions for different problems. There are different finite element modelling (FEM) software that are used for different purposes. The FEM software used for this work are ANSYS Maxwell, ANSYS circuit, ANSYS simplorer, and Solidworks. Different models were created in ANSYS Maxwell for different cases which will be shown later in this chapter. Different FEM models were created to detect subsurface notches that simulates subsurface cracks in parts made by AM. Different FEM models were created to detect subsurface blind holes that simulates subsurface voids in parts made by AM. Defects are embedded inside plates made of different materials such as titanium with conductivity 0.56×10^6 siemens/m and relative permeability 1.02 or stainless steel with conductivity 1.35×10^6 siemens/m and relative permeability 1.005. Each model was run at different mesh sizes for mesh dependency analysis.

4.1.1 Limitation with simulation modelling of the probe impedance change

To be able to measure the probe impedance change in case of a flaw inside the material, many factors such as the mesh size and frequency should be chosen carefully to avoid

increasing execution time and using more computational resources. Running simulation at high frequencies in the range between 50 KHz to 500 KHz affects the simulation time and increases it which may takes days to get results. Running simulation at higher frequencies is necessary in case the defect is located at the surface of the plate or close to it since the eddy currents will flow close to the surface with a small skin depth in case of high frequencies.

Another factor is the mesh size, the finer mesh size the longer it takes to get the results. The mesh size chosen for all the simulation cases has to be in the range of 0.3 mm to 5 mm depending on the size of the defect that needs to be detected. Choosing a smaller size mesh gives more accurate results but it takes more execution time and more computational resources. For example to detect a defect with a spherical shape that has a 0.5 mm radius, the mesh size should be around 0.2 mm to get accurate results.

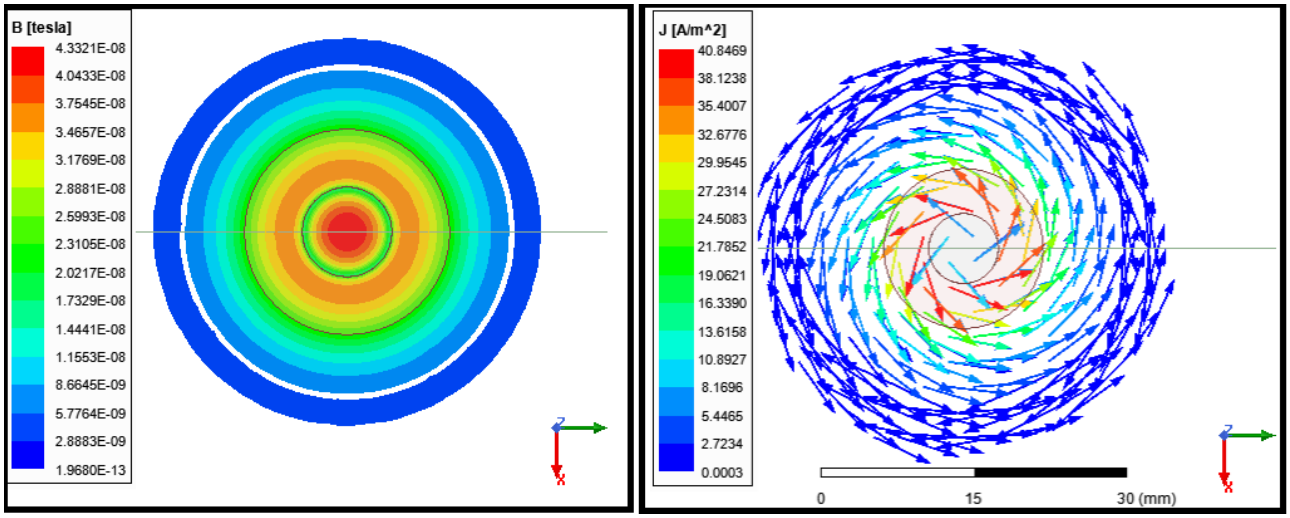
In case of doing a sweep over position of the probe across the plate, the step size has a big effect on the results and the simulation time. Choosing a small step size will give more accurate results meanwhile it will increase the simulation time. The mesh size, step size, frequency used should be chosen in a way that keeps the balance between computing resource usage and the accuracy of the results.

4.2 Model design and simulation in ANSYS Maxwell

The proposed model for designing a probe that is suitable for defect detection in parts made by AM is shown in chapter three. Some of the procedures to specify the designed eddy current probe dimensions is done using ANSYS Maxwell software tool. The designed eddy current probe that is shown in chapter three involves adding a core and a tip to the center of the probe to focus the magnetic field in the center of the probe's coil.

The core is made of ferrite material which has a high permeability. As seen in Fig. 4.1.a, the highest B_max under the probe is around the center of the coil. As shown on the scale bar in Fig.4.1.b, the eddy current distribution under the coil is almost double the size of the probe diameter. The probe diameter is 16 mm, meanwhile, the distribution of the eddy currents is around 30 mm. This will be one of the constraints of testing small size parts because of what is called the edge effect which is solved later by adding a tip to the coil's core. Edge effect means that the edges of the part under test will give a false signal similar to a defect signal [14, 15]. The probe used for the simulation model in Fig.4.1 is the designed absolute probe. The probe has only one cylindrical coil with 8 mm outer radius, 3.5 mm inner radius and a length of 9.345 mm. The frequency used is 28 KHz. The plate

made of stainless steel 316L material. The mesh size used for the model is 0.2 mm. The mesh type used for the model is on selection, skin depth based.



(a) (b)

Figure 4.1: ANSYS eddy current simulation of the designed probe, where (a) shows the magnetic field distribution and (b) shows the eddy current distribution under the coil.

4.2.1 Tip analysis and B_max measurements

As mentioned earlier in chapter three, the designed probe works in the absolute mode, which means that only one coil is used to induce the eddy currents inside the material and sense the defect signal. The probe has a core made of ferrite, which has a higher permeability compared to cores made of iron. The core length is 13.435 mm, where 9.435 mm is the same length as the length of the coil and 4 mm is considered for the core tip. The probe used for the simulation model in Fig.4.2 is the designed absolute probe. The probe has only one cylindrical coil with 8 mm outer radius, 3.5 mm inner radius and a length of 9.345 mm. The frequency used is 28 KHz. The plate made of stainless steel 316L material. The mesh size used for the model is 0.2 mm. The mesh type used for the model is on selection, skin depth based.

Adding a tip to the designed coil helps focus the magnetic field and makes it more confined. Another reason is to make it possible to detect very small defect sizes since there

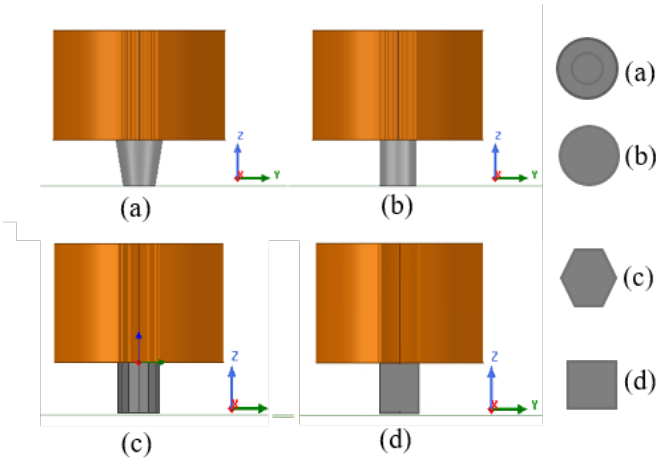


Figure 4.2: Different tip geometry, where (a) is a cone tip shape, (b) cylindrical tip shape, (c) polygon tip shape, and (d) square tip shape.

Tip Shape	**No plate under the coil**	**In case of a plate under the coil**
Cylindrical	B_max= 1.45 e^{-}8 T	B_max= 4.3 e^{-}8 T
Cone	B_max= 1.23 e^{-}8 T	B_max= 3.81 e^{-}8 T
Polygon	B_max= 1.39 e^{-}8 T	B_max= 4.01 e^{-}8 T
Rectangular	B_max= 1.201 e^{-}8 T	B_max= 3.78 e^{-}8 T

Table 4.1: B_max value for each tip shape at 0.2 mm distance under the coil.

is a relationship between the defect size and the probe diameter. Different tip geometries shown in Fig. 4.2 were considered for the probe design, and the magnetic field (B_max) was calculated for each case. The distance between the surface of the tip and the substrate was fixed in all cases for consistency since any changes in the distance between the tip surface and the substrate will create variations in the measured defect signal.

The value of the magnetic field (B_max) is measured at 0.2 mm distance under the coil in case of having substrate under the coil and in case of no substrate shown in table 4.1. The material considered in all cases is stainless steel (S3316L). Simulation is done using ANSYS Maxwell. Tip shapes considered for comparison are cylindrical, square, polygon and cone shapes. The volume of all tips is kept constant for consistency. The volume of all the tips is around 153.9 mm^3. The cylindrical tip shape showed a better (B_max) value under the probe, and it is selected for the probe design.

4.2.2 Evaluation of designed probe in basic defect detection

A finite element model has been created in ANSYS Maxwell to verify and evaluate the performance of the designed absolute probe. A graphical abstract of the simulation procedures shown in Fig. 4.3.

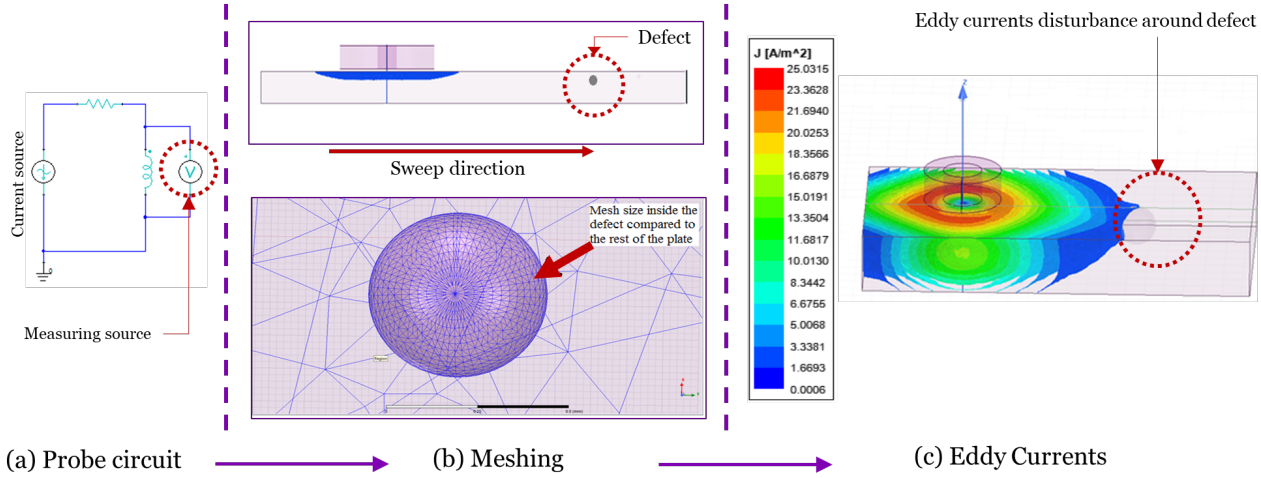
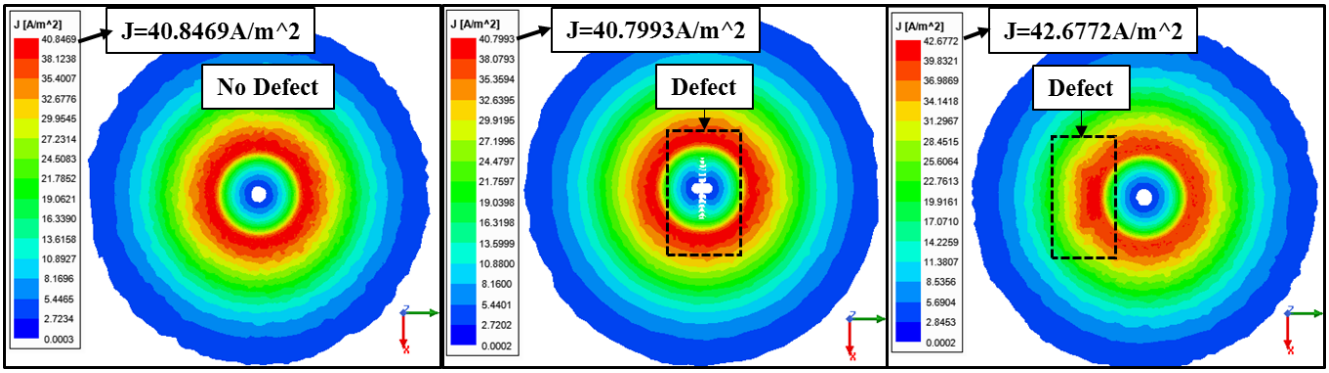


Figure 4.3: Graphical abstract of the simulation procedures.

The solution type used in the ANSYS Maxwell software tool is the eddy current solution type. For all types of designs and simulations, results were obtained after choosing different mesh sizes for mesh dependency analysis. The mesh size is one of the main factors that affect the simulation results. Applying fine mesh size with respect to the size of the defect will give better results, but of course, that will affect the simulation time a lot because the simulation will take more time and more CPU memory. The mesh type used for this model is the on-selection skin depth-based since it gave better simulation results when it comes to a very small size defect compared to the on-selection length-based one. The surface triangle length is 0.2 mm. Sweep over frequency is done over a big range of frequencies (10 KHz - 500 KHz) to find out the best frequency value that will give better results for the designed probe. The frequency value chosen for the designed probe is 28 KHz. For the AC current used in the simulation, it was produced using a circuit that was created using ANSYS circuit, which was attached to the coil terminal and the winding. It is a small RL circuit which is shown in Fig. 4.3. Building this circuit and attaching it to the winding of the coil helped in measuring the impedance of the coil.

To evaluate the change in the current density under the coil, three different cases were considered for simulation as shown in Fig. 4.4. The probe used for the simulation model



(a) (b) (c)

Figure 4.4: The magnitude of the eddy currents distribution, where (a) shows eddy current distribution in case there is no defect, (b) shows eddy current distribution if the defect is aligned with the center of the coil, and (c) shows eddy current distribution if the defect is aligned with the coil winding.

is the designed absolute probe. The probe has only one cylindrical coil with 8 mm outer radius, 3.5 mm inner radius and a length of 9.345 mm. The plate made of stainless steel 316L material. The frequency used is 28 KHz which allows for 3 mm depth of penetration inside the stainless steel plate. The mesh size used for the model is 0.3 mm. The mesh type used for the model is on selection, skin depth based. The defect shape in Fig. 4.4 (b) and Fig. 4.4 (c) is a subsurface notch that has a 0.4 mm width and 5 mm length. The defect is 1.5 mm from the surface of the plate and the plate has 4 mm thickness.

The first case is where there is no defect added to the stainless steel plate, the maximum value for the current density is $40.8469 A/m^2$. For the second case, a defect was added to the center of the plate where it is aligned with the center of the coil to see the effect of the defect on the current density value. The current density value for this case was $40.7993 A/m^2$ which is less than the case where there is no defect added to the plate. The third case considered was adding the defect to the plate in a way that it will be aligned with the coil winding to see if the maximum current density value will be different from case two, where the defect is aligned with the center of the coil. The maximum value of the current density is $42.6772 A/m^2$ which is higher than the other two cases.

When the center of the coil is aligned with the defect center, the magnetic field is the minimum, almost close to zero and there is almost no change in the coil impedance. When the winding of the coil is centered over the defect, the magnetic field is at it's maximum

and there is a big change in the impedance of the coil. In case the defect located under the coil winding, the change in the eddy current density inside the plate will be higher compared to the case where the defect is aligned with the center of the coil. Any change in the current density will be reflected on the secondary magnetic field that is created by the flow of the eddy currents inside the material. The change in the secondary magnetic field will affect the primary magnetic field created in the coil which will affect the coil inductance and as result it will cause a change in the coil impedance. At the points where the notch is centered with the winding of the coil, the notch has to be perpendicular to the electric field. If the notch is parallel to the electric field, there won't be much perturbation to the field and in turn no change to the coil impedance.

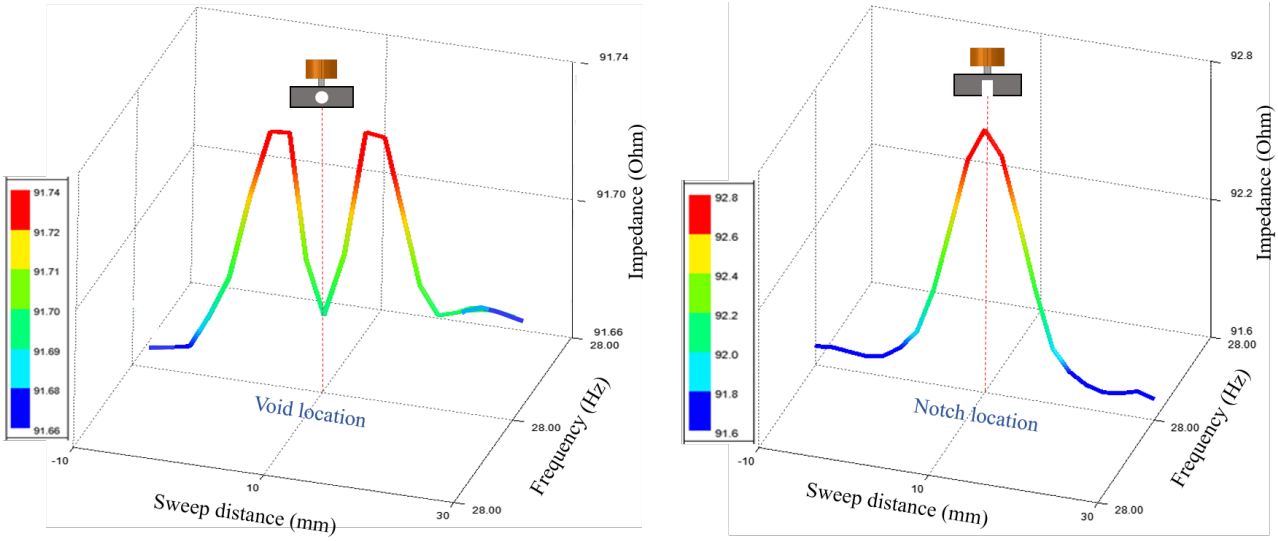
4.3 Simulation for notches and voids

There are two cases considered for simulation to show the difference of the probe response in case of a notch and in case of a void. The parameters for the simulation model shown in table 4.2. The sweep direction of the coil is in the Y direction and the defect is located at 10 mm position as shown in Fig. 4.5. The step size used for the parametric sweep in 2 mm. The probe gives a different response in case of a notch compared to the void. There are different mesh types that are supported by ANSYS Maxwell, eddy current solution such as inside selection (length based) and on selection (length based or skin depth). The mesh type used during simulation is on selection, skin depth based, number of layers of elements is 2. The surface triangle length is 0.2 mm.

In Fig. 4.5, the types of defects detected are a sphere that simulates a subsurface void and a notch that simulates a subsurface crack. Simulation done using same input values and dimensions of the designed absolute coil shown in chapter 3. The sweep distance is 40 mm, and it starts from 10 mm before the zero position to 30 mm after the zero position. In Fig. 4.5.a and Fig. 4.5.b, the magnetic field will be the minimum when center of the coil is aligned with the center of the defect and there won't be much change in the coil impedance. The magnetic field will reach its maximum when the coil winding is centered over the defect causing a big change in the coil impedance. In case of a sphere, the defect will still give maximum change in the field in as the sphere largest cross-section will intersect with the field at all orientations. In case of a notch, the changes in the coil impedance will only happen if the notch is perpendicular to the electric field. In Fig. 4.5.a, the void diameter is 3 mm, which is big, and that will cause generating two different peaks when the edges of the coils are aligned with the edges of the void during a sweep motion.

Plate thickness	8 mm
Plate length	50 mm
Material	Stainless steel (316)
Notch length	15 mm
Notch width	0.4 mm
Void radius	1.5 mm
lift-off distance	0.2 mm
Defect location	10 mm in Y direction
Mesh type	On selection, skin depth, 2 layers

Table 4.2: Parameters used for both simulation cases.



(a) (b)

Figure 4.5: Shows simulation results of the probe impedance change on top of a plate with a defect at 10 mm, where (a) defect type is a sphere, (b) defect type is a notch.

4.4 Methods for modeling sensitivity analysis simulations

In this section different scenarios are considered for sensitivity analysis in simulation. The first case is to detect defects that are close to an edge. The second case is to detect defects

where the probe is placed at different lift-off distance from the top surface of the test piece. The third case is to detect multiple defects that are located in the same region or at a close distance from each other.

4.4.1 Testing close to an edge

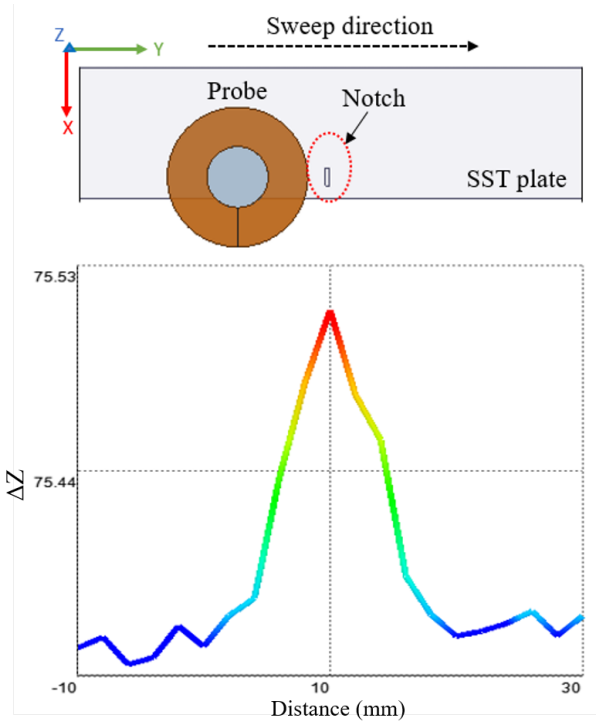


Figure 4.6: Subsurface notch close to an edge.

In this section the possibility of detecting subsurface defect that are close to an edge are explored by doing two different simulation models that have subsurface notch and subsurface void. Moving the probe parallel to the edge of the plate helps detecting the defect without getting a false signal of a flaw that represents the edge of the sample. The subsurface void radius is 0.4 mm since it is the smallest void size that can be put detected through simulation in case of locating the void close to an edge. The subsurface notch length is 2mm and 0.3 mm width since it is the smallest notch size that can be through simulation in case of locating the notch close to an edge. Plate thickness is 4 mm and the defects are located at 1.5 mm under the surface. The probe used for the simulation model

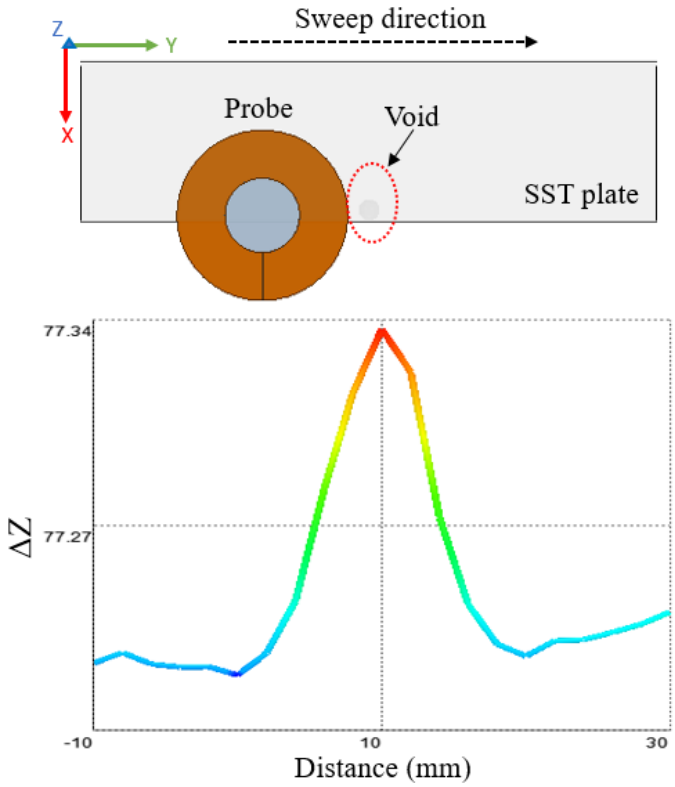


Figure 4.7: Subsurface void close to an edge.

is the designed absolute probe. The probe has only one cylindrical coil with 8 mm outer radius, 3.5 mm inner radius and a length of 9.345 mm. The plate made of stainless steel 316L material. The frequency used is 28 KHz. The mesh type used for the model is on selection, skin depth based with 0.2 mm size. Simulation results shown in Fig. 4.6 and Fig. 4.7. The defects are 1 mm away from the edge of the plate.

4.4.2 Effect of lift-off distance

The Second case is to explore the effect of different lift-off distances on the accuracy of defect detection. The reason behind adding layers of non-conductive material between the probe and the part under test is to test the effect of material coating on the measured defect signal. Two different case were considered for testing the effect of lift-off by adding a layer made of plastic with 1 mm thickness and 2 mm thickness. The probe used for

the simulation model is the designed absolute probe. The probe has only one cylindrical coil with 8 mm outer radius, 3.5 mm inner radius and a length of 9.345 mm. The plate made of stainless steel 316L material with conductivity 1.35×10^6 siemens/m and relative permeability 1.005. The frequency used is 28 KHz. The mesh type used for the model is on selection, skin depth based with 0.2 mm size.

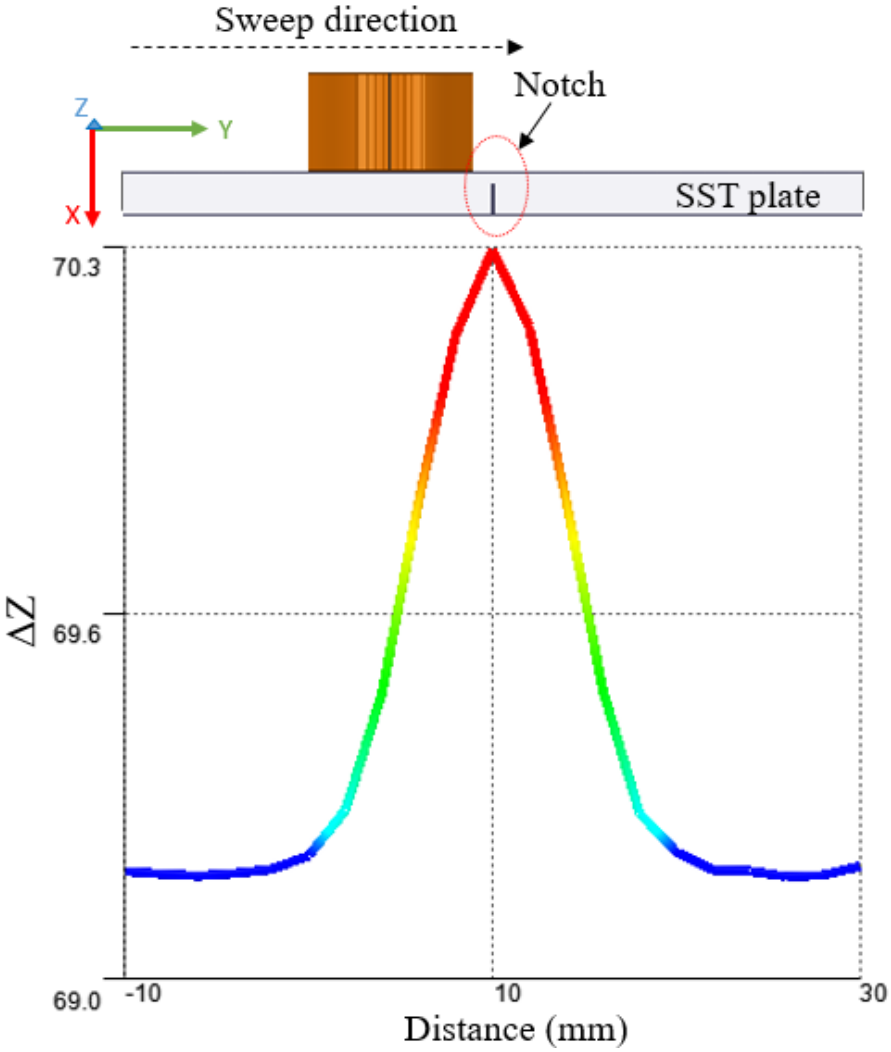


Figure 4.8: No lift-off distance.

In Fig4.8, it shows the probe on top of a plate without lift-off distance between the probe and the plate. The plate is made of stainless steel and the probe is moved in the Y

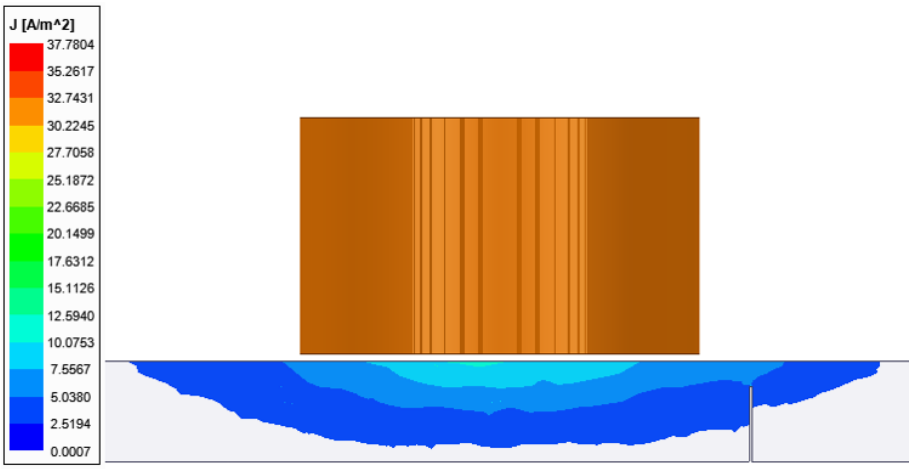


Figure 4.9: No lift-off distance current density.

direction. The eddy currents and the current density is shown in Fig.4.9.

In Fig4.10, it shows the probe on top of a plate with 1 mm lift-off distance between the probe and the plate. The plate is made of stainless steel and the probe is moved in the Y direction. The eddy currents and the current density is shown in Fig.4.11. The 1 mm sheet between the probe and the stainless steel plate is made of plastic.

In Fig**??**, it shows the probe on top of a plate with 2 mm lift-off distance between the probe and the plate. The plate is made of stainless steel and the probe is moved in the Y direction. The eddy currents and the current density is shown in Fig.**??**. The 2 mm sheet between the probe and the stainless steel plate is made of plastic.

As shown in Fig. 4.8, 4.10, and **??**, the higher the lift-off distance the smaller the change on the probe impedance value. Also; the current density values for each case shown in Fig. 4.9, Fig. 4.11, and **??** are decreasing in case of having higher lift-off distance between the probe and the stainless steel plate which means less standard depth of penetration.

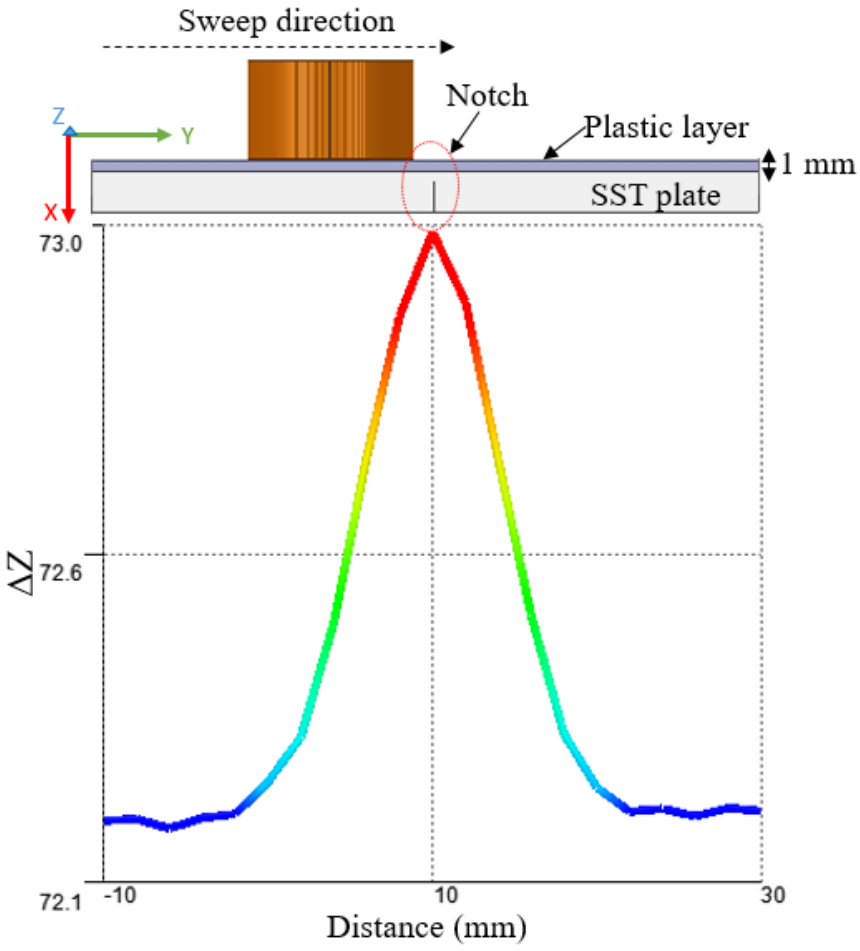


Figure 4.10: 1 mm lift-off distance.

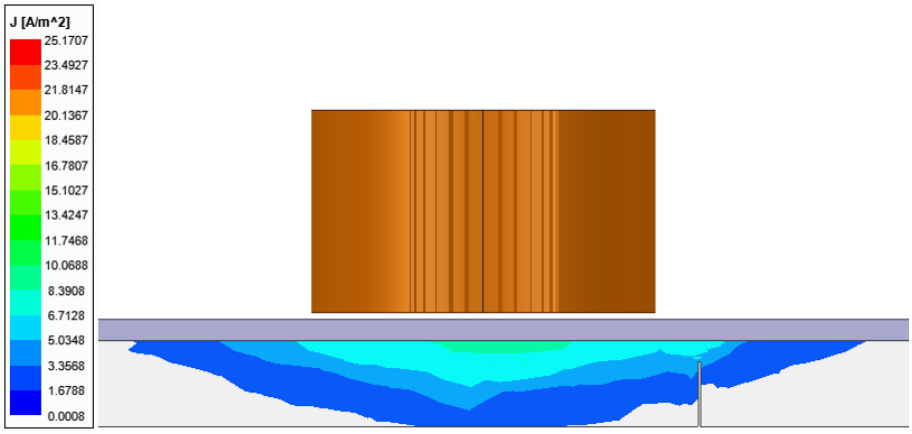


Figure 4.11: 1 mm lift-off distance current density.

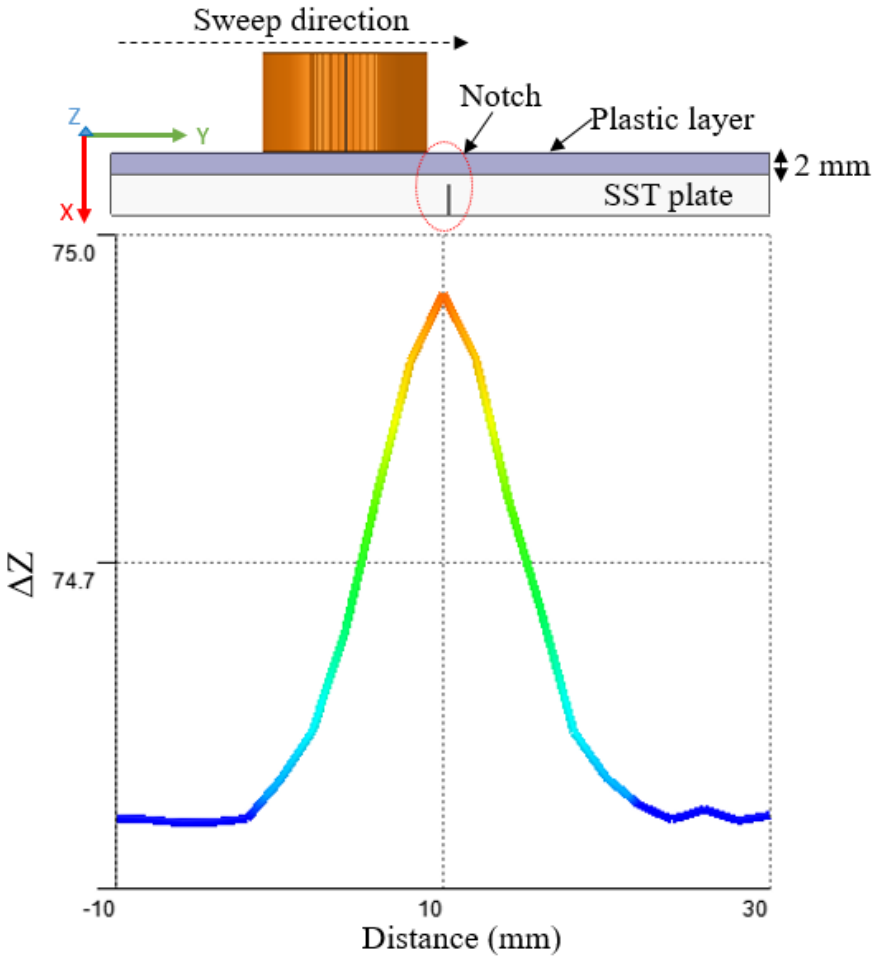


Figure 4.12: 2 mm lift-off distance.

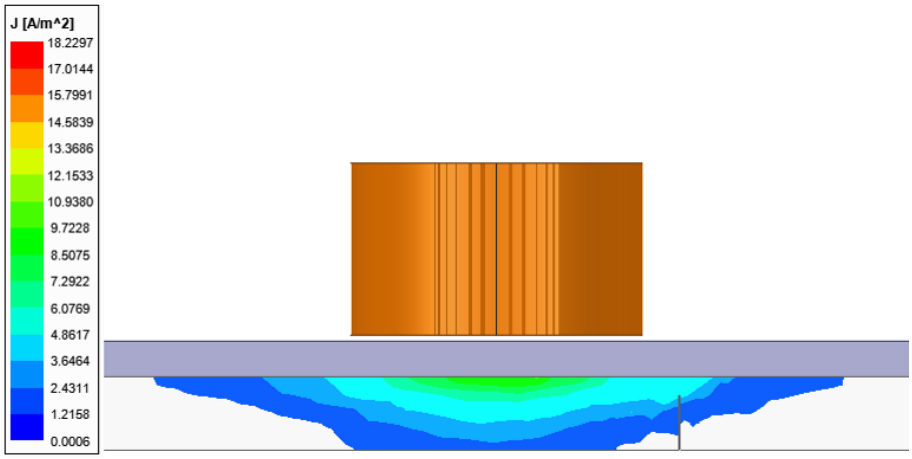


Figure 4.13: 2 mm lift-off distance current density.

4.4.3 Multiple defects in the same region

The third case is to explore detecting multiple defects that exists in the same region or defects that are separated by small distance in between. There are two different cases considered here. The first case is having two voids parallel to each others and the second case is having two voids on top of each others. The probe used for the simulation model is the designed absolute probe. The probe has only one cylindrical coil with 8 mm outer radius, 3.5 mm inner radius and a length of 9.345 mm. The plate made of stainless steel 316L material with conductivity 1.35×10^6 siemens/m and relative permeability 1.005. The frequency used is 28 KHz. The mesh type used for the model is on selection, skin depth based with 0.2 mm size. In case of a plate with two parallel defects, both defects has the same size of 0.3 mm radius. In case of a plate with two defects above each other, the smallest defect has 0.3 mm radius and the bigger one has 0.8 mm radius. The reason behind chosing 0.3 mm radius size is that, this is the smallest size that can be detected in case of running the FEM model with multiple defects.

As shown in Fig. 4.14, there is a sharp edge peak value in case of moving the probe on top of a plate with only one void.

In the first case, there are two voids that are almost the same size which are located close to each others in the same region, Fig. 4.16.

In the second case, there are two voids where one of them is slightly bigger than the other. The voids are located on top of each others in the same region, Fig. 4.18. As shown in Fig. 4.18, the peak value of the impedance change is affected by both defects and gives one peak value change in case of moving the probe on top of a plate instead of showing two different peaks for each void. The peak is a more representation of the bigger size void not the smaller one.

In the case, where there are two voids with different sizes that are located on top of each other in the same region, the peak value of the impedance change is affected by both defects. This configuration gives one peak value change in case of moving the probe on the top of the plate instead of showing two different peaks for each void. The peak normally represents equivalence of both the bigger size void and the smaller one. In Fig. 4.16, there is only one peak shown in case of two voids parallel to each other because the space between them is too small. In case the space between both voids (in the Y direction) is big enough which depends on the coil geometry and the eddy current flow under it, it will show two different peaks for each void. In 4.18, there is only one peak shown in case of two voids on top of each other because both voids center are aligned regardless of spaces between them. The current density is shown for each case in Fig. 4.15, Fig. 4.17, and 4.19.

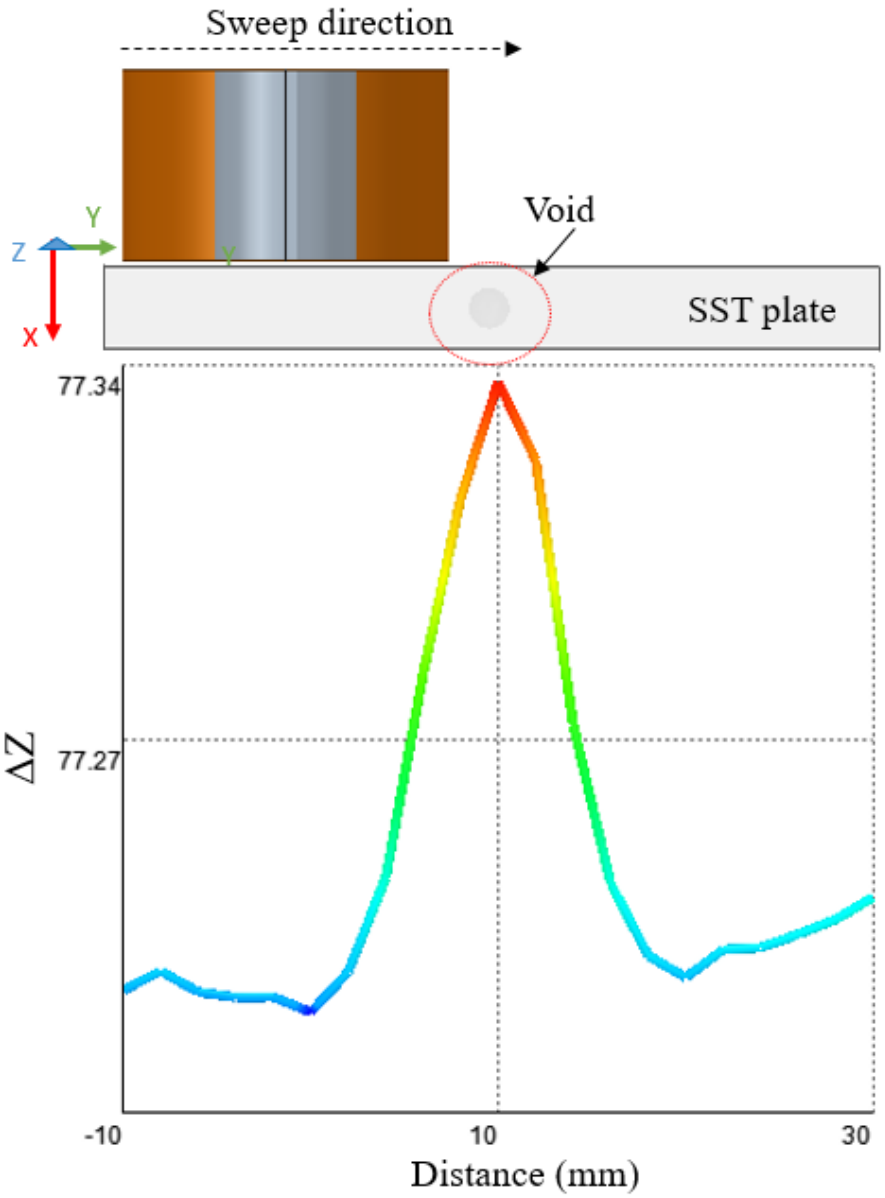


Figure 4.14: Sweep over the position on top of a plate with one void defect type.

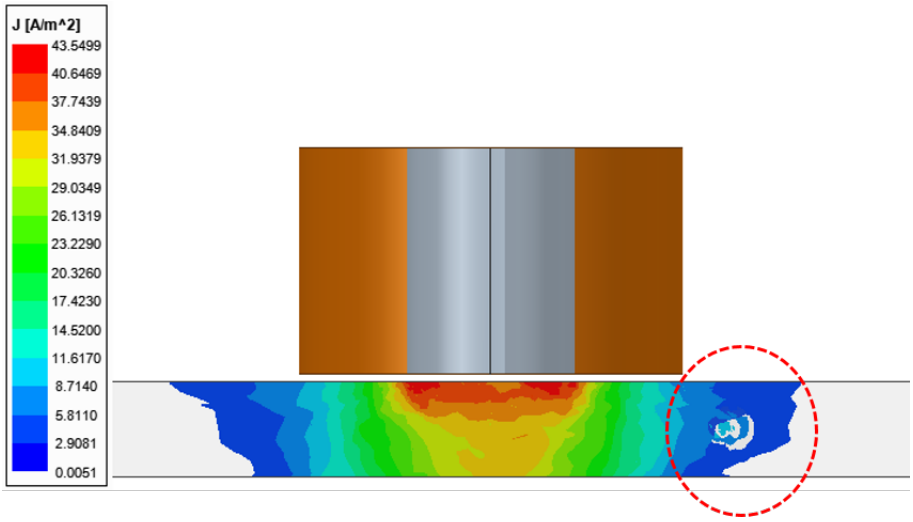


Figure 4.15: Current density under a probe on top of a plate with one void defect type.

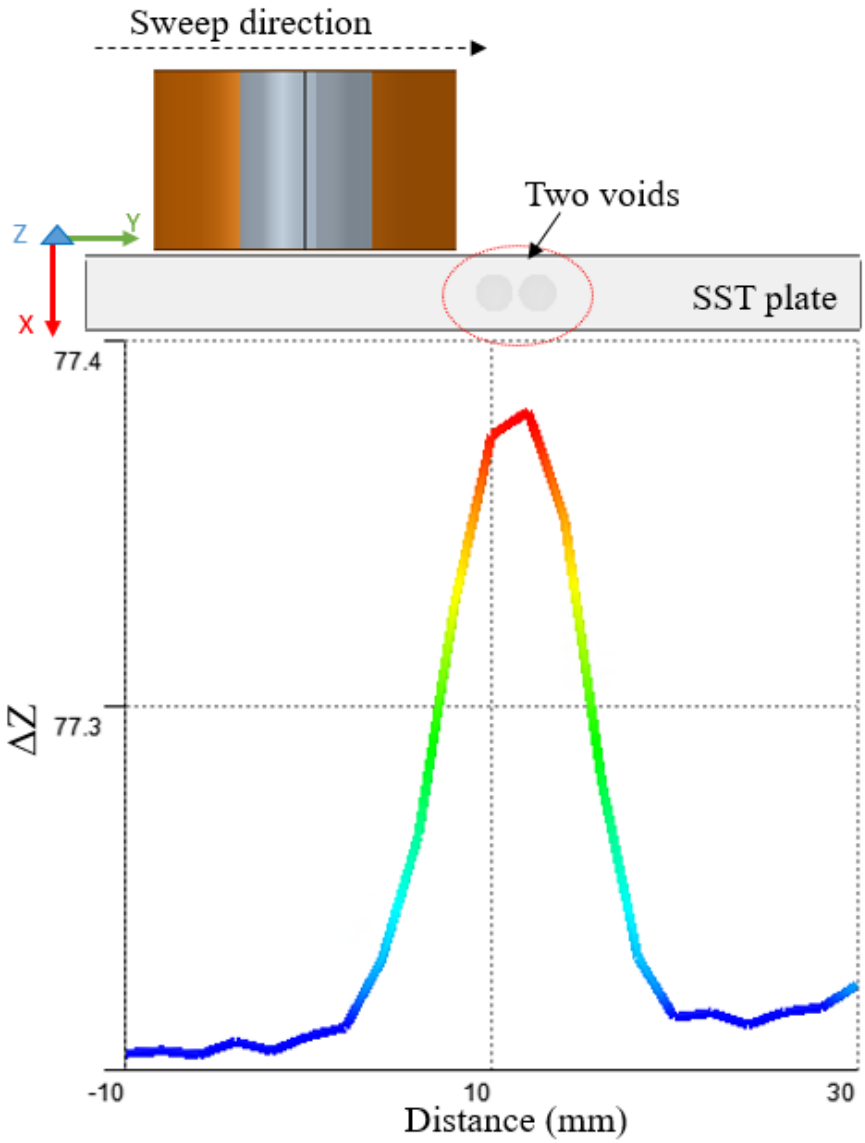


Figure 4.16: Sweep over the position on top of a plate with two voids besides each others in the same region.

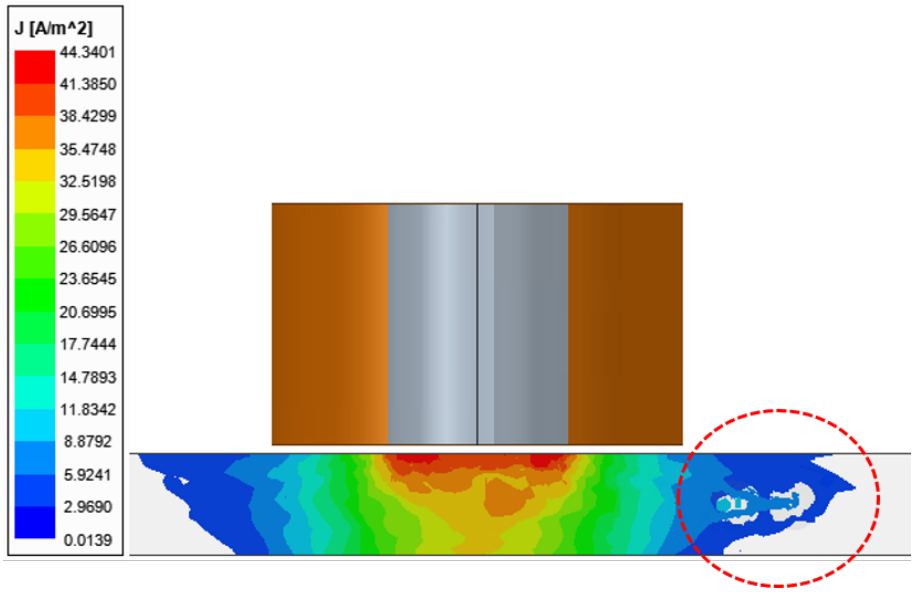


Figure 4.17: Current density under a probe on top of a plate with two parallel voids in the same region.

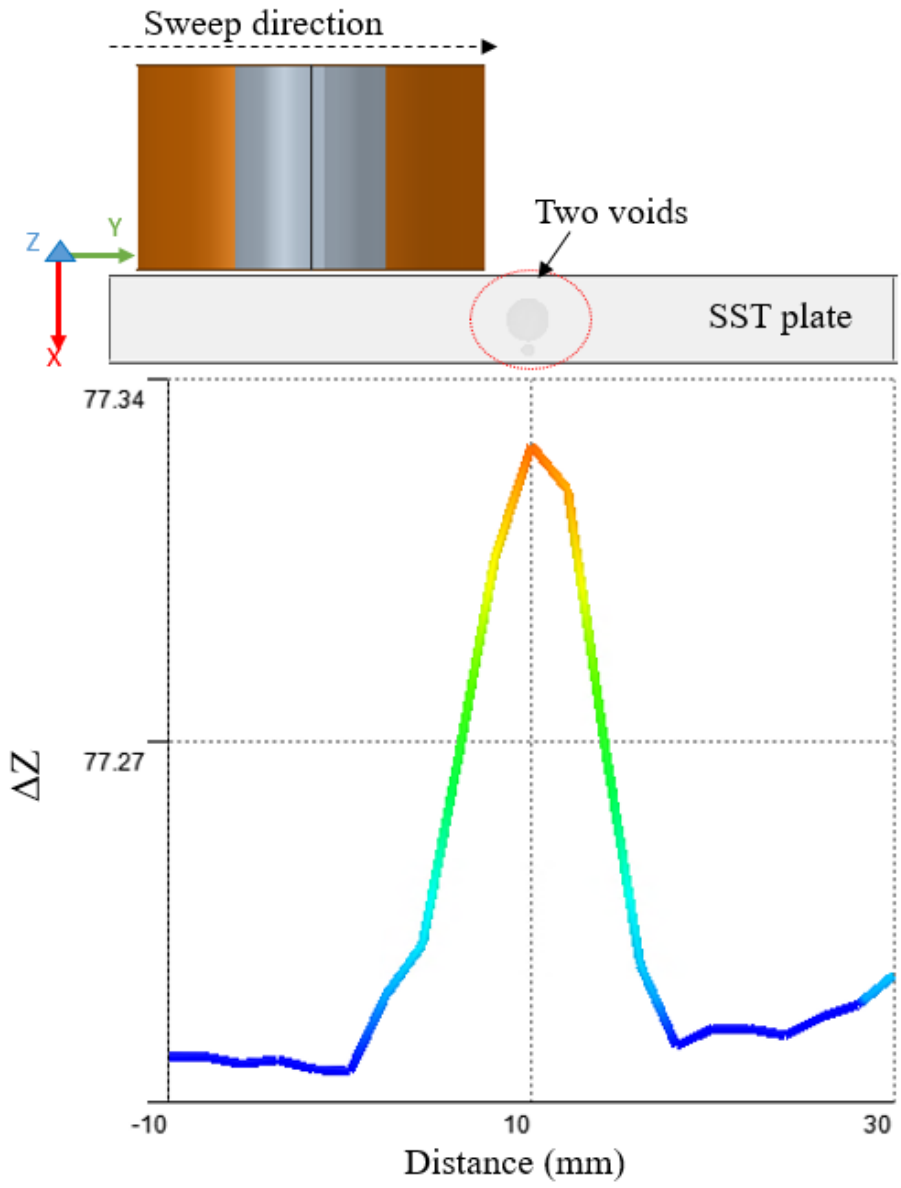


Figure 4.18: Sweep over the position on top of a plate with two voids above each others in the same region.

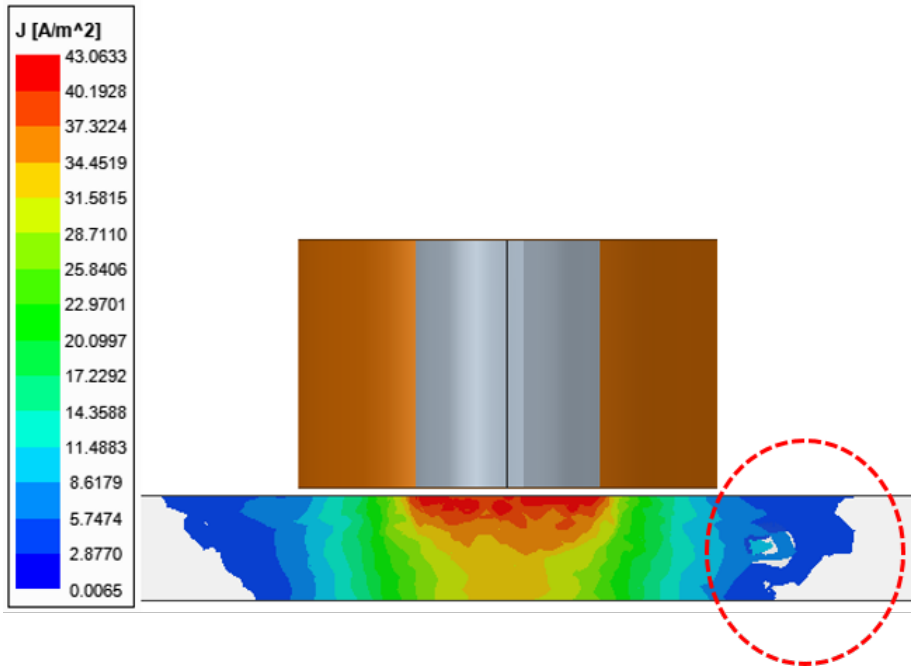


Figure 4.19: Current density under a probe on top of a plate with two voids above each others in the same region.

4.4.4 Effect of temperature

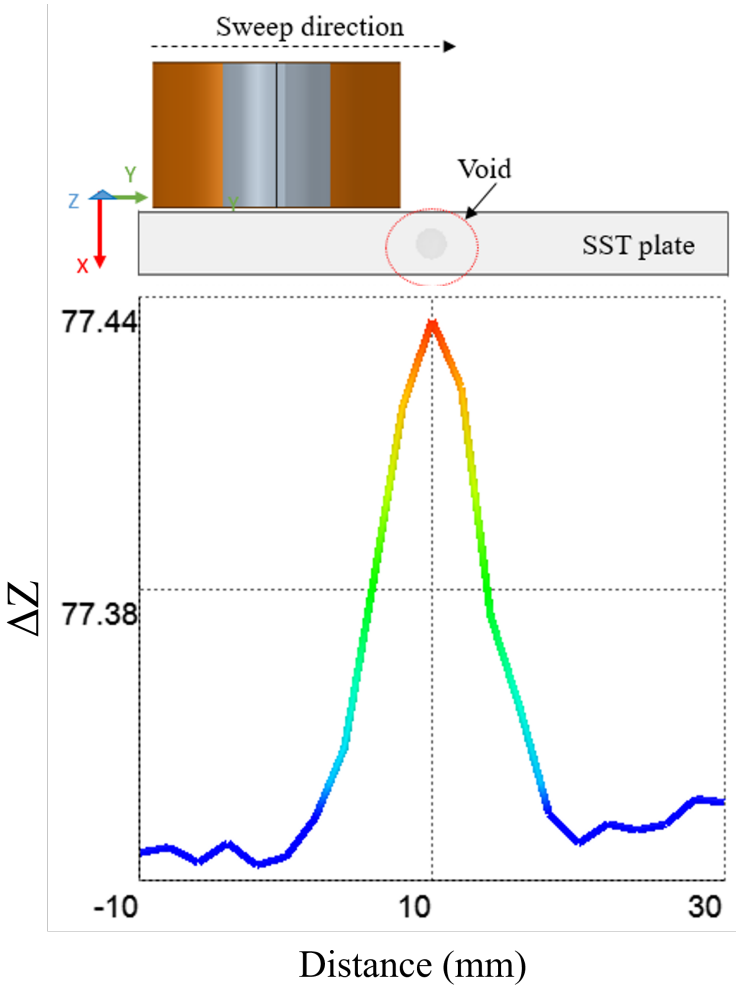


Figure 4.20: Sweep over position on top of a plate with one void defect type at high temperature for conductivity analysis.

One of the cases considered for sensitivity analysis is to test the effect of temperature on the coil impedance change during the testing process. During building the parts by LPBF process, the temperature is very high. It is well known that the electric conductivity of the material decreases when the temperature increases. The electrical conductivity of stainless steel 316 at room temperature is 1.35×10^6 siemens/m. The electrical conductivity of stainless steel at high temperature around 673 K is 1.26×10^6 siemens/m. Same model

shown in Fig. 4.14 that has a stainless steel 316 plate with a conductivity of 1.35 $\times 10^6$ siemens/m was run at different conductivity value of 1.26 $\times$ 10^6 siemens/m [45]. The impedance change of the coil in case of increasing the temperature of the part under test is shown in Fig. 4.20. Comparing both models shown in Fig. 4.14 where the stainless steel plate is tested at room temperature and the results of the model in Fig. 4.20, the impedance of the coil increased when increasing the temperature.

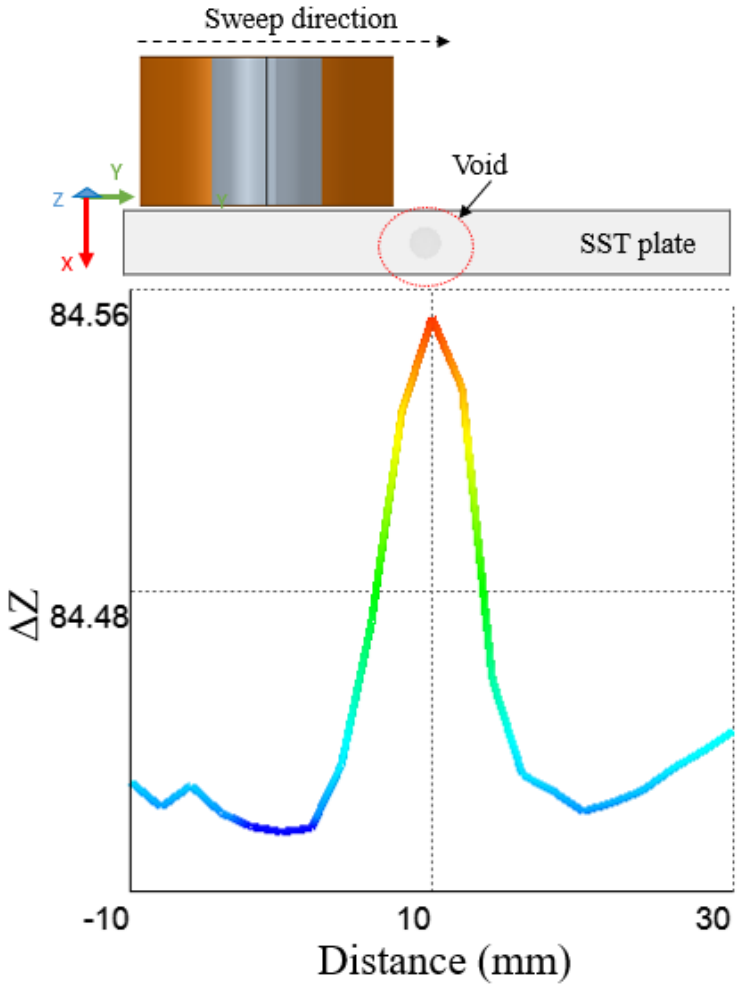


Figure 4.21: Sweep over the position on top of a plate with one void defect type at room temperature for permeability analysis.

Another case was considered to evaluate the effect of temperature on the impedance of the probe from the point view of permeability. For simulation purposes SST 304 is used

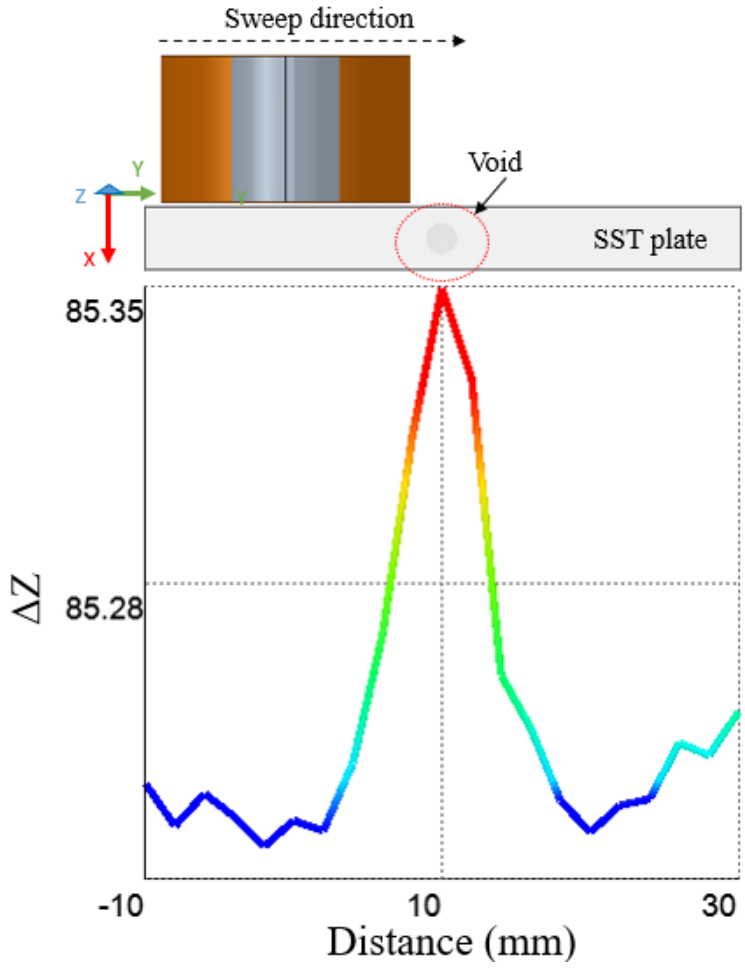


Figure 4.22: Sweep over the position on top of a plate with one void defect type at high temperature for permeability analysis.

as the material properties are available in literature [46]. The electrical conductivity of stainless steel 304 is 1.38×10^6 siemens/m. Two different FEM models were created in ANSYS Maxwell to compare the impedance of the probe in case of permeability value of 3.5 at room temperature and in case of permeability value of 4 at high temperature of 673 K [47]. Results obtained for the model where the impedance of the probe on top of a plate made of SST 304 measured at room temperature with permeability value of 3.5 are shown in Fig. 4.21. Results obtained for the model where the impedance of the probe on top of a plate made of SST 304 measured at high temperature with permeability value of 4 are

shown in Fig. 4.22. As shown in [47], the permeability of SST 304 increases in case of high temperature. Comparing both models shown in Fig. 4.21 and Fig. 4.22 where the stainless steel plate is tested at room temperature and high temperature, the impedance of the coil increased by increasing the temperature.

4.5 Sensitivity analysis for new designs

In this section different scenarios are considered for sensitivity analysis of probe design to specify the most sensitive parameter to increase the probe sensitivity to detect small size defects. Mesh type used for all the FEM models is on selection, skin depth based with 0.2 mm size. There are certain parameters that affect the sensitivity of the probe to detect small size subsurface defects such as the coil length, number of turns, inner and outer diameter. Some of these parameters are explored through several FEM models done in ANSYS Maxwell. New probes are designed after considering different cases where the inner diameter and the outer diameter of the coils have been selected for different values to evaluate the sensitivity of the probe at each case. The procedures done to design the probes are the same procedures used to design the absolute probe. Different probe operating modes were considered for the design sensitivity analysis. Fabry factor formula was used to chose the best lengths of the coils. Four probes are designed to operate in the absolute mode and another three probes are designed to operate in the reflection mode. Several simulation results are shown below for different models where a sweep over the inner radius and the outer radius of the coils is done. Also, different shield radius were considered for the designs and the results are shown later in this chapter Fig. 4.31. As shown in Fig. 4.23, Fig. 4.24, Fig. 4.25, and Fig. 4.26 the inner radius of the coil has the highest effect on the probe sensitivity. In Fig. 4.23, a sweep over outer radius of the coil in the range of (4.5 mm-7 mm) and a sweep of the position of the coil on top of a plate with a 0.1 mm notch width are done to find the best radius value of the coil to detect the notch. Same model created in ANSYS Maxwell to detect a blind hole with a 0.2 mm radius and the results are shown in Fig. 4.24. Exploring adding multiple coils to the probe was done to find their effect on the sensitivity of the probe to detect small size defects, some of the results are shown in Fig. 4.25 and Fig. 4.26. The best values of the inner radius, outer radius, length of the coil, number of turns, and the wire gauge used for the new design are shown in table 4.3 and table 4.4.

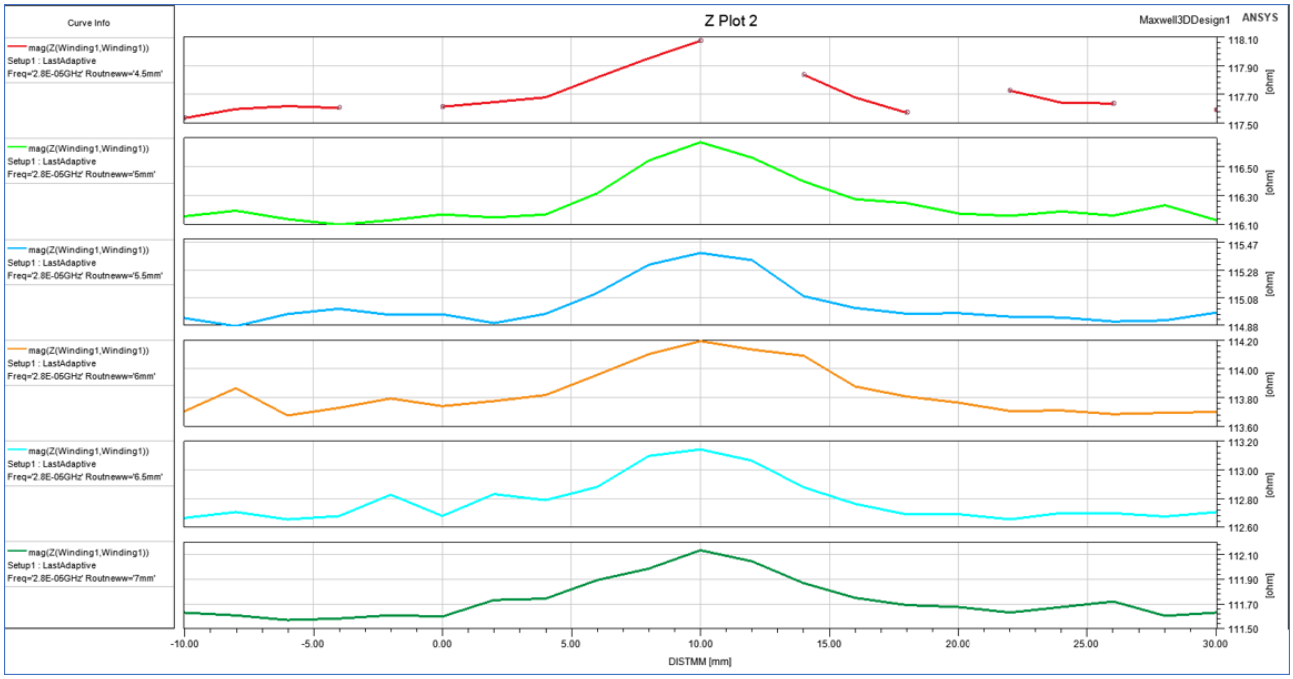


Figure 4.23: Sweep over the outer radius(4.5mm-7mm) and position on top of a plate with a 0.1 mm notch width.

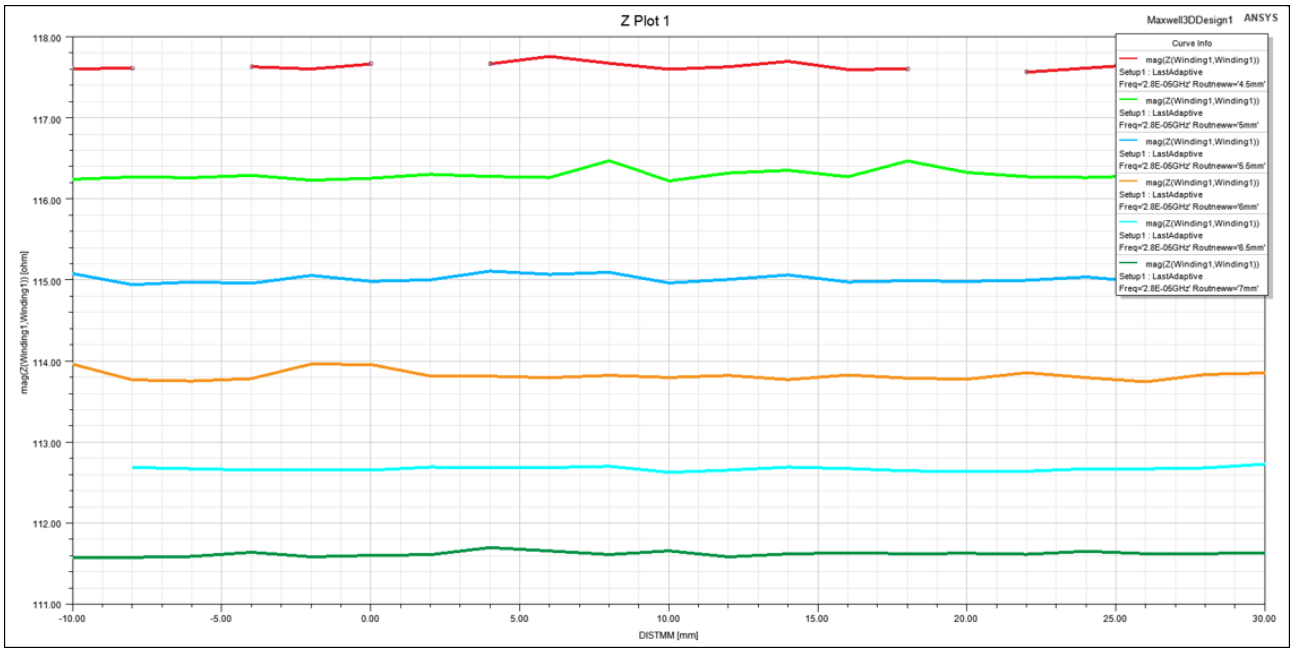


Figure 4.24: Sweep over the outer radius(4.5 mm-7 mm) and position on top of a plate with a 0.2 mm blind hole radius.

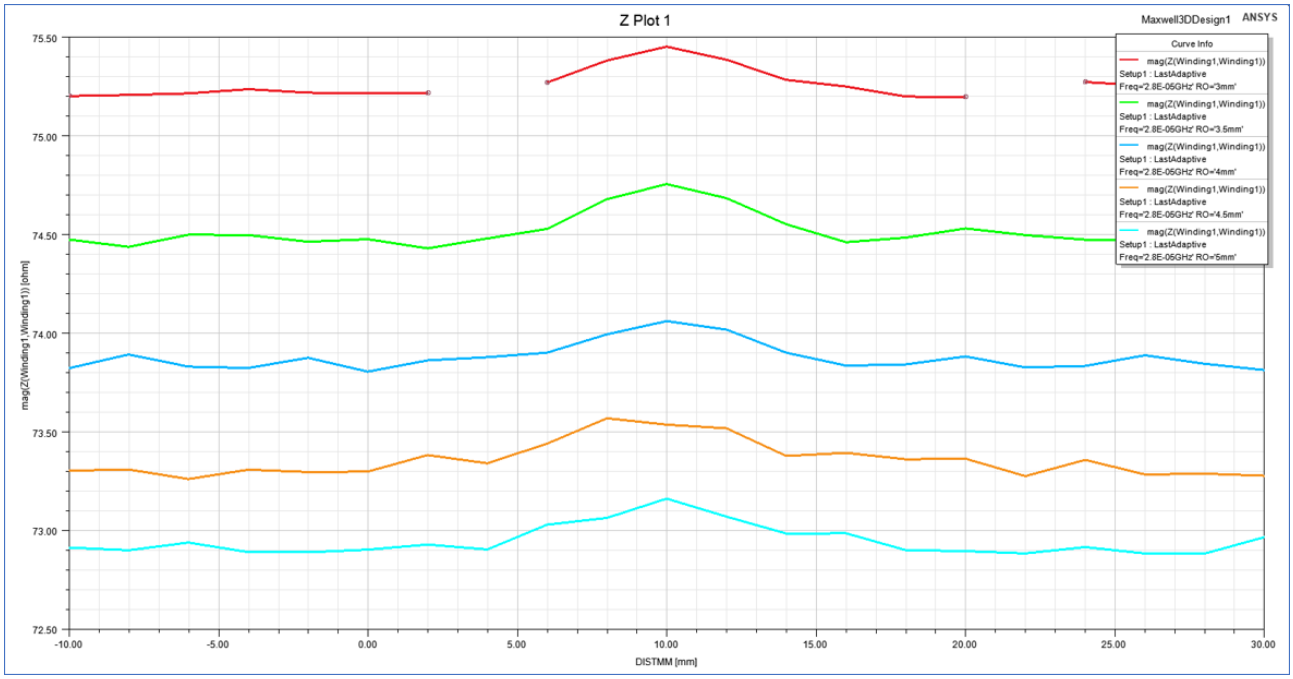


Figure 4.25: Transmit/receive probe sweep over the outer radius of the transmitter 3 mm to 5 mm.

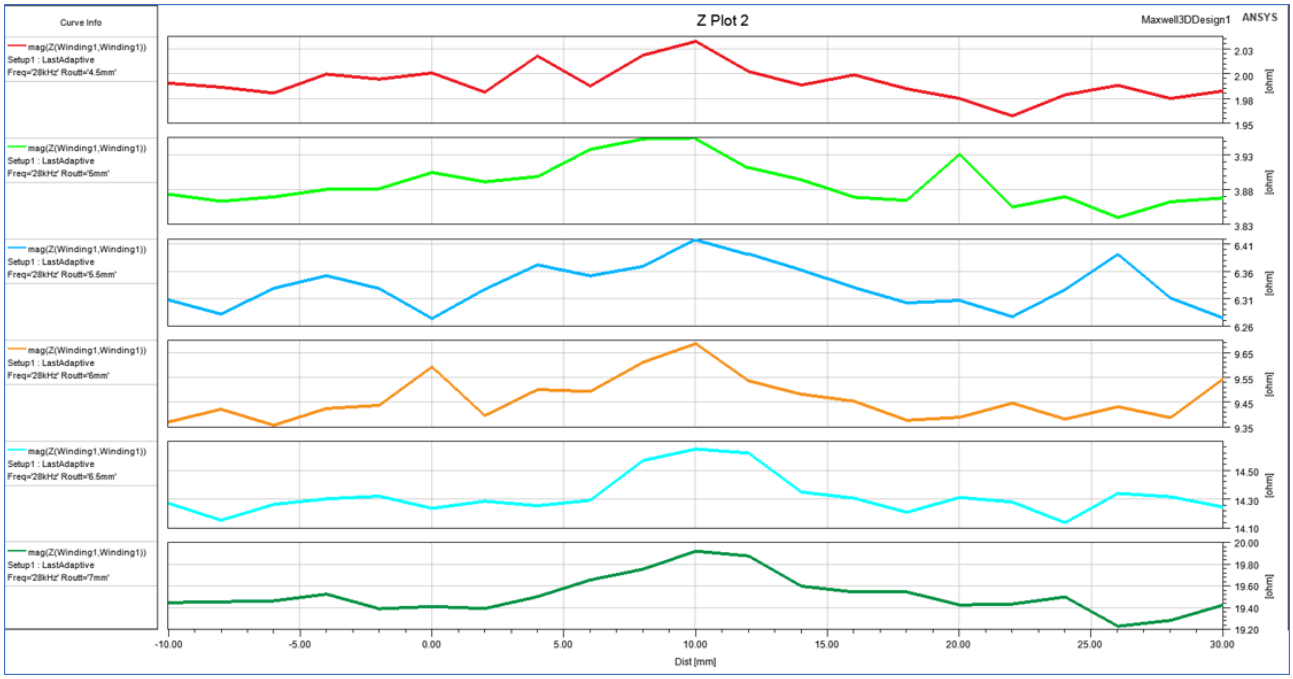


Figure 4.26: Transmit/receive probe sweep over the outer radius of the receiver 4.5 mm to 7 mm.

Based on the simulation results, new eddy current probes designs are shown in the tables below. In Fig. 4.27 The top view of the probe coils are shown according to their numbering in table 4.3 and table 4.4. The probes that are numbered form 1 to 4 work in the absolute mode and the probes that are numbered from 5 to 7 work in the reflection mode with different coils orientations.

In table 4.3 and table 4.4, W is the shield thickness, L is the coil length, Rin is the coil inner radius, Rout is the coil outer radius, AWG is the American wire gauge, and D is the diameter. The probes that are numbered form 5 to 7 work in the reflection mode. As mentioned before probes that operates in the reflection mode have two coil. One coil to induce the eddy currents inside the material and the other coil detects the defect signal. probes that operates in the absolute mode has only one coil to induce the eddy currents inside the material and sense the defect signal. The coil arrangements of the probes number 5 and 7 are different from the coil arrangements of probe number 6. Other parameters to be explored such as the American wire gauge diameter, number of turns and adding a ferrite shield around the coils are considered for the new designs. The American wire gauge used for the designs number 1 and 2 is AWG-25. The American wire gauge used for the designs number 3, 4, and 7 is AWG-28. The American wire gauge used for the designs number 5 and 6 is AWG-26.

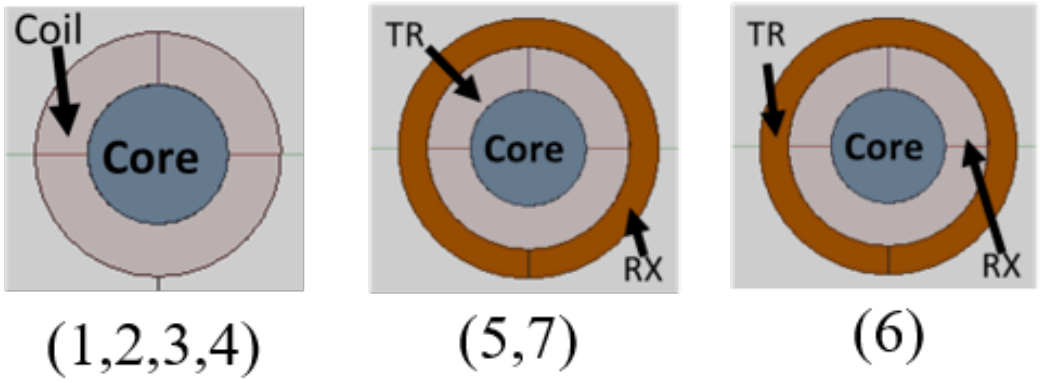


Figure 4.27: Different coil geometry for new probes designs.

#	Coil Dimensions	turns	layers	turns per layer	Core	Shield
1	Rin=2.3mm, Rout=5mm,L=22mm	229	5	48	D=4.6mm, L=22mm	W=1 mm, L=20mm
2	Rin=2.3mm, Rout=5mm,L=22mm	229	5	48	D=4.6mm, L=20mm	W=1 mm, L=20mm
3	Rin=2.3mm, Rout=5mm,L=22mm	463	7	68	D=4.6mm, L=22mm	W=1 mm, L=20mm
4	Rin=2.3mm, Rout=5mm,L=22mm	463	7	68	D=4.6mm, L=22mm	W=1 mm, L=20mm

Table 4.3: Specs of the new designed absolute probes.

#	Coil Dimensions		Turns(T)		Layer		T/Layer		Core	Shield	
5	TX Rin=1mm Rout=3.5mm L=15mm	RX 3.5mm 6.5mm 15mm	TX 183	RX 220	5	6	37	37	D=2mm L=15mm	TX W=0.1mm L=15mm	RX 1 mm 15mm
6	Rin=3.5mm Rout=6.5mm L=15mm	1mm 3.5mm 15 mm	220	183	6	5	37	37	D=2mm L=15mm	W=1 mm L=15mm	0.1mm 15mm
7	Rin=1.5mm Rout=5mm L=20mm	5mm 7mm 20mm	546	312	9	5	62	62	D=3mm L=20 mm	W=0.1mm L=20 mm	1 mm 20mm

Table 4.4: Specs of the new designed reflection probes.

4.5.1 Shield effect

For the new designs, adding a shield around the coil is considered. It helps to focus the eddy currents under the coils and reducing magnetic field leakage. One of the important factors that affects the sensitivity of the eddy current probe to detect a small size defects is to induce enough and confined eddy currents inside the material.

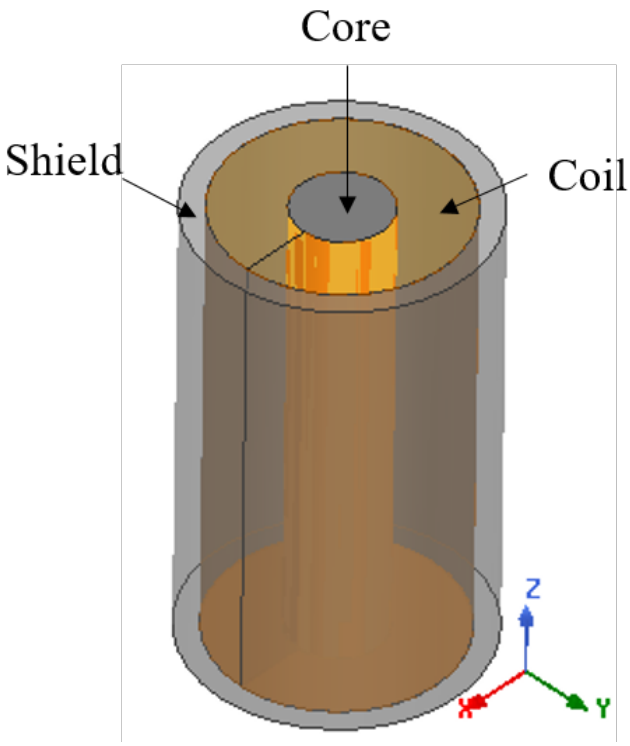
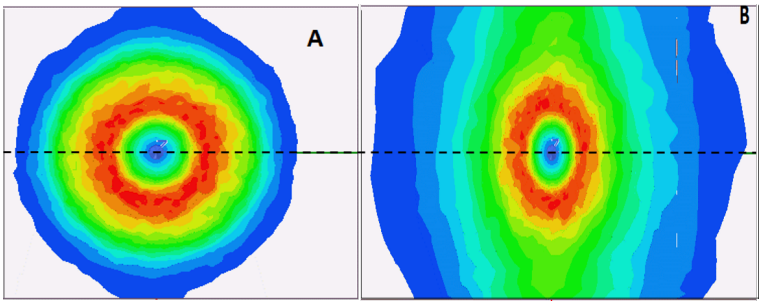


Figure 4.28: A shield surrounding the coil of the absolute probe .

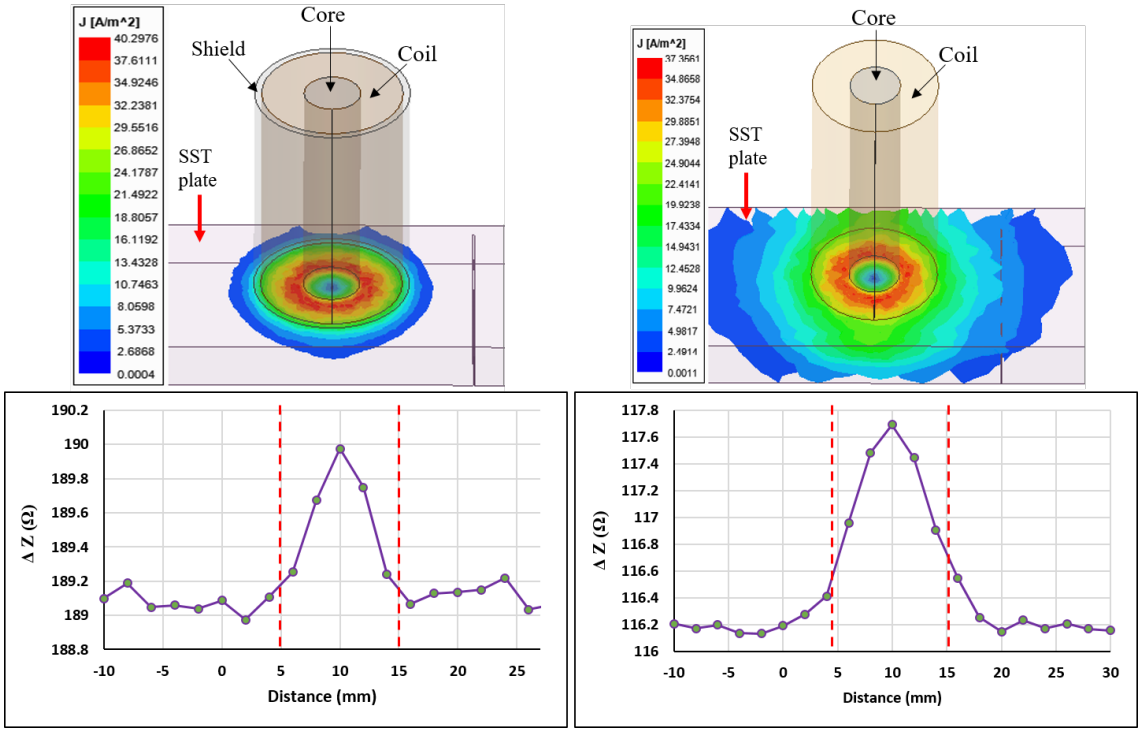
Adding a shield around the coil will focus the primary magnetic field created within the coil winding which results in strengthening the flow of the eddy currents in the region of interest inside the material. Also adding the shield will concentrate the magnetic field near the coil which will limit the spread of the eddy currents and as a result reduce the possibility of the probe to pick any non-relevant signal as shown in Fig. 4.28 and Fig. 4.29.

In Fig. 4.30 it shows that the distribution of the eddy currents in case of a shield around the coil are more focused and confined. Also, the eddy current density (J) increased from 37.36 A/m^2 in case of no shield to 40.29 A/m^2 in case of shield.



(a) (b)

Figure 4.29: Top view of the shield effect on the distribution of the eddy currents under the coil where(a) is eddy current distribution under the coil in case of a shield around the coil and (b) is eddy current distribution under the coil in case there is no shield.



(a) (b)

Figure 4.30: Eddy current density and impedance change in case of a shield around the coil.

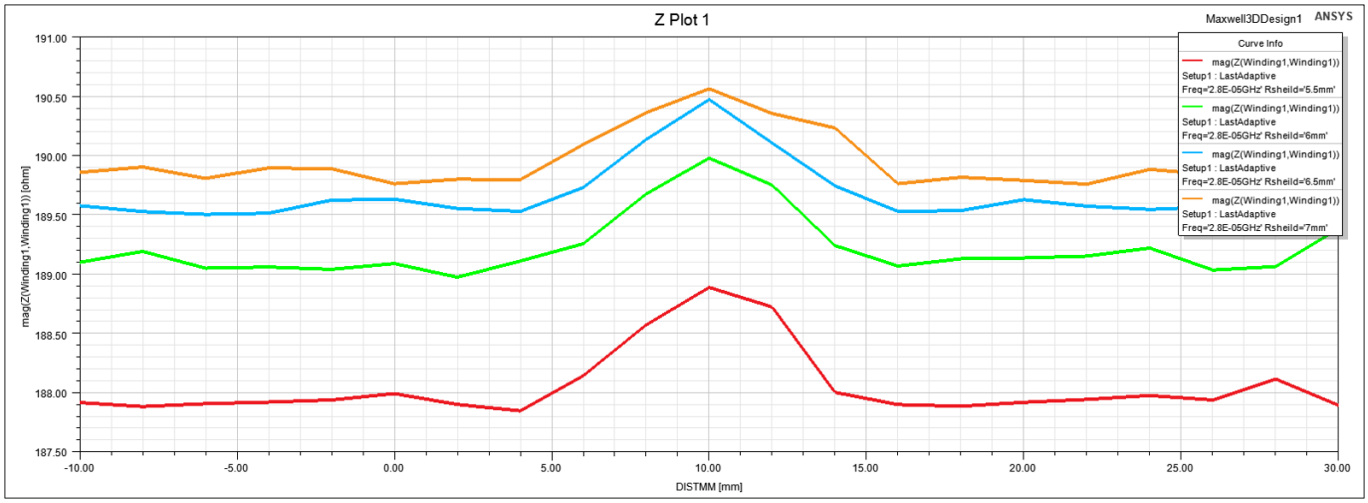


Figure 4.31: Sweep over shield thickness.

As shown in Fig. 4.31 different shield thickness were explored to find the best shield thickness that will improve the sensitivity of the probe to detect small size defects and concentrate the eddy current distribution under the coil. The effect of adding a shield is also shown in the probe impedance change (Z) on top of a plate with a 0.1 mm notch width and 15 mm length. The plate is made of stainless steel SS316L with conductivity 1.35×10^6 siemens/m and relative permeability 1.005. Both core and shield are made of ferrite.

Different shield thicknesses were considered for the new designs. A comparison of the probe with different shield thicknesses are shown in Fig. 4.31. By doing a sweep over position of the probe on top of 0.1 mm width notch, it shows that the shield with 1 mm thickness gave a better detection results. Simulation is done using ANSYS Maxwell software tool. The probe coil inner radius is 2.3 mm and the outer radius is 5 mm. Two different parametric sweep were done during the simulation. A sweep over position along the stainless steel plate and starting at 10 mm before zero position to 30 mm after zero position across a notch with 0.1 mm width. The second sweep is done over the shield thickness starting from 0.5 mm to 2 mm thickness. The material chosen for the shield is ferrite since it has high permeability.

4.6 Summary

In this chapter, the main steps to design an eddy current probe using FEM modelling are explored. Several models were created in ANSYS Maxwell software to evaluate the performance of the probe. The main purpose of creating the FEM models is to measure the probe impedance in case of the existence of porosities and cracks inside the material of the parts made by AM. All models contain a plate made of stainless steel and titanium materials, and a probe that has the same specifications as the designed one. Subsurface notches were created inside the plates to represent subsurface cracks inside parts made by AM. Subsurface spherical shape defects were created inside the plates to represent subsurface voids inside parts made by AM.

Different scenarios are considered for sensitivity analysis. These cases are to detect defects that are close to an edge, detection of multiple defects in the same region or at a close distance from each other, detection of defects at different depths by increasing the lift-off distance between the probe and the part under test. Another case were considered for sensitivity analysis to evaluate the effect of temperature on the electrical conductivity and magnetic permeability of the part under test and it's effect on the change of impedance of the probe.

To be able to determine the most sensitive parameter that affects the sensitivity of the probe to detect small size defects, several models were created in ANSYS Maxwell. The main parameters that affect the sensitivity of the probe to small size defects are the coil dimensions such as the inner radius, outer radius, the length of the coil, number of turns, the diameter of the wire gauge, and the number of the coils in the probe. Several models were created in ANSYS Maxwell where a sweep over the coil inner radius, outer radius and coil length were done. A sweep over position of the probe on top of plates that have small sizes of notches and voids were considered to find the best values for the inner radius, outer radius, and length of the coil. Also, adding a shield to the coil is considered to increase the sensitivity of the coil to small size defects. Different shield thicknesses and different shield materials were considered. Both absolute mode and reflection mode were considered to explore the effect of increasing the number of the coils on the detection of small size defects.

In [55] eddy current NDT technique is used to detect subsurface defects for additive/subtractive hybrid manufacturing. Models were created in ANSYS Maxwell to detect subsurface defects in parts made of titanium Ti6Al4V. Several simulation models were created to explore the effect of temperature, lift-off distance and effect of edges on the detected defect signal. In the FEM model, specimen size was set to 18 mm $\times$ 17 mm

$\times$ 7.6 mm, a defect was 1.2 mm below the detection surface and had dimensions of 0.8 mm in width and 15 mm in length. The effect of specimen temperatures on the output signals was investigated in terms of the normalized inductive reactance. The temperature range was set to be 20 C to 270 C. As the temperature increases, the reactance of the probe also increases which increases the total impedance of the probe since the reactance is the imaginary part of the impedance. Below a certain temperature, permeability is only slightly varied with the change in temperature compared to the electrical conductivity of the material.

Another scenario considered was to explore the effect of lift-off distance by changing the distance between the probe and the part under test from 0.08 mm to 1.4 mm. In case of increasing the lift-off distance, the standard depth of penetration of the eddy currents inside the material will decrease.

Chapter 5

Characterisation and experiments

5.1 Introduction

In this chapter, the designed absolute probe is tested on parts made by AM. Several cases were considered during experiment. A comparison between the designed absolute probe and a commercial reflection probe was done to compare the performance of both probes. The main tools used during the testing process are the probe and the data acquisition system. The experimental setup is very simple which is considered as one of the advantages of using EC testing technique since the portable EC devices allow for outdoor inspection compared to other NDT techniques. The data acquisition system has a portable size that can be easily carried for outdoor defect detection [48-54]. The results for several cases were discussed later in this chapter including cases considered for sensitivity analysis.

5.2 Methods, materials, and instrumentation

The experimental setup used during the testing process is shown in Fig. 5.15. Different data acquisition instruments and eddy current probes that are available in the market were tested to chose the most suitable equipment for our type of work. Both instruments are shown below:

- The first data acquisition system used for the testing process is NORTEC 600 from Olympus company and a surface/subsurface reflection Probe. The standard reflection detachable surface probe has a diameter of 0.25 in (6.3 mm) and an operating

frequency range of 2 KHz - 200 KHz that is connected to the NORTEC 600 data acquisition system through a triax fischer/LEMO connector.

- The second data acquisition system used during the testing process is MIZ-21C and a detachable spot probe with reflection (driver pick-up coils). The probe diameter is 0.400 in (10.2 mm) with operating frequency range 1 KHz - 100 KHz.

The chosen data acquisition system for the experimental setup is MIZ-21C and the spot reflection probe from Zetec company. A comparison done between the spot reflection probe and the designed absolute probe later in this chapter. The are certain procedures that are usually followed during the testing process, some of these procedures are shown below:

- If the system allows for multiple modes of coil drive operation such as absolute, differential, or driver/pick-up (reflection) then it is important to select the mode of operation based on the used probe and based on the location of defect either surface or sub-surface one.
- Select a frequency that is within the specified range of the coil operating range. Lower frequencies less than 50 KHz are preferred for higher depth of penetration and for defects that are far from the surface. High frequencies that are higher than 100 KHz should be considered for detecting surface defects.
- Move the probe slightly from side to side to create a "lift-off" signal. The probe doesn't have to be completely removed from contact with the surface.
- Rotate the phase adjustment on the data acquisition system so that the lift-off response leaves the screen directly to the left.
- Keeping the probe in a vertical position, move it slowly over the range of notches and blind holes on the plate.
- If the defect is close to an edge, instead of moving the probe across the defect and across the edge, it is better to move the probe parallel to the edge to avoid the edge effect.
- Choosing the right type of filter that should be applied to the measured signal and the speed to move the probe over the test piece should be determined based on the size of the part under test, the length of the flaw and the noise source. Applying a filter helps to remove the background drift from the eddy current signal [56-64].

- The overlay method can be used to gauge the size of defects. This is where a known defect size signal is taken and superimposed on the screen so that when another defect is scanned, it will give an idea of the defect size.

More details about the experimental setup and the values selected tor the experimental tools are shown in section (5.8)

5.2.1 Limitation with eddy current in experiment

One of the challenges to detect flaws in additive manufactured parts is the surface roughness. Surface roughness can be caused by either the solidification of the melt pool or by adhered powder particles. Some factors such as alloy uniformity and surface roughness can affect the detected eddy current signal. When testing metallic components, the bad surface condition is a concern because it limits the possibility to detect surface or subsurface flaws. This is because rough surfaces produce very similar signals to the ones detected from shallow surface defects of the part under test. Any changes in electrical conductivity or magnetic properties of the material will affect the eddy current response which is another limitation in detecting defects in parts made by AM.

Another factor that affects the accuracy of the detected defect signal is the noise level. Since the measured EC signal is low, noise is always a concern. It is important to figure out the noise source and determine if the noise is coming from outside sources or within the EC testing system itself. The design of the grounding and shielding scheme is very important as this significantly affects the noise levels of the system. The signal-to-noise ratio (SNR) should be kept high.

Defects that are located close to the edge of the sample are another concern since the edge will produce a signal that is similar to the flaw signal.

5.2.2 Testing done on machined parts using absolute probe

The steps to design an eddy current probe that operates in the absolute mode are shown in chapter 3 and the main probe specs are shown in table 5.1. To test the designed absolute probe, different cases were considered for experiment on machined parts that have a smooth surface and parts made by Laser Powder Bed Fusion process with a surface roughness size in the range of 8 μm-11 μm which are shown later in this chapter. For all cases experimental results are compared to the simulation model done on ANSYS Maxwell

Coil outer radius (r_2)	8 mm
Coil inner radius (r_1)	3.5 mm
Coil length (h)	9.435 mm
Core diameter	7 mm
Core length	13.435 mm
Input current	0.0148 RMS AMP
Wire gauge	AWG-25
Diameter of the wire	0.45466 mm
Frequency (f)	28 KHz
Voltage	5 V
Plain core type	Ferrite
Coil inductance	444.942 H
Number of turns (w)	164

Table 5.1: Coil and core parameters of the absolute probe.

and the analytical modelling that solves the vector potential using the Truncated Region Eigenfunction Expansion method (TREE).

The samples used for testing the absolute probe have different types of artificial defects with different sizes that are machined in plates made of stainless steel (SS316L) material. The machined test pieces have a smooth surface. The samples dimensions and the defects locations and types are shown in Fig. 5.1, Fig. 5.4, and Fig. 5.7.

To test the designed absolute probe, different cases were considered. The cases are to test machined stainless steel plates with defects to mock-up parts with defects made by additive manufacturing. The cases are to detect notches with the same width, different lengths, notches with different widths same length, and finally blind holes with different sizes. Comparison done between the response of the designed probe in the experiment to the analytical and simulation results. The types of defects considered for all the above cases are subsurface blind holes which simulate porosities, and subsurface notches which simulate cracks created between the layers of the additive manufactured parts. The blind holes sizes are 0.17 mm, 0.2 mm, 0.27 mm, and 0.3 mm radius. The sizes of the notches are 0.437 mm, 0.47 mm, and 0.57 mm width, with lengths of 5 mm, 15 mm, and 25.2 mm. All tests are done from the opposite side of the defect to simulate subsurface defects.

5.2.3 Three notches same width different lengths

One of the cases considered for testing the designed absolute probe is to detect three notches in machined parts with 0.43 mm width and lengths of 5 mm, 15 mm, and 25.2 mm. Notches are 0.5 mm from the surface of the plate since this is the deepest distance the blades can go under the surface, and the thickness of the plate is 2 mm as shown in Fig. 5.1. the probe is moved across the notches in the (Y) direction without leaving an air gap between the probe and the sample. Samples are made of stainless steel (SS316L) with a conductivity of 1.35×10^6 siemens/m and a relative permeability of 1.005.

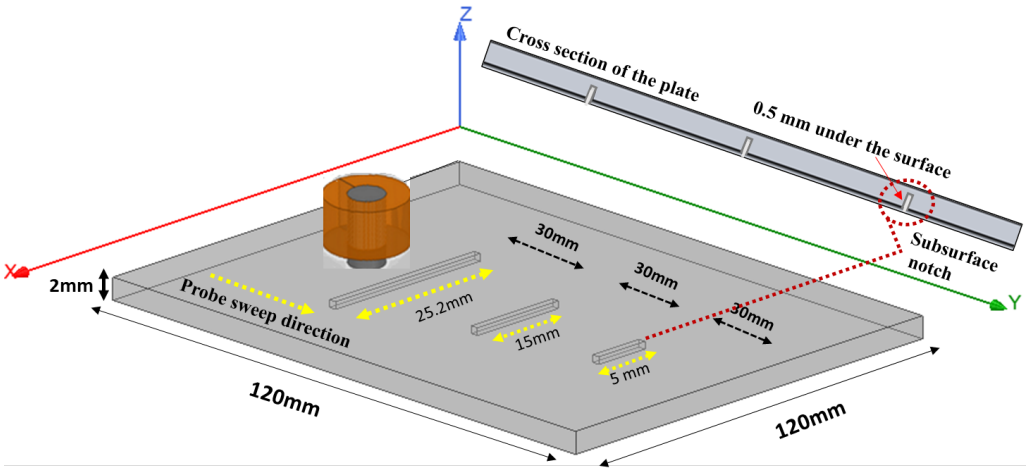


Figure 5.1: Plate with three notches same width and different length.

Fig. 5.2 shows the measured peak-to-peak voltage value for each defect. To get better and more accurate results, multiple readings were taken for each defect. The standard deviation and the average of all readings are calculated. During the experiment, it is noticed that the best way to get accurate results for each defect is not to change the lift-off distance between the probe and the specimen. To do so, it is better to sweep the probe back and forth on top of the defect without lifting the probe up to get multiple readings of the defect with the same phase, which helped improve the standard deviation values for each defect. The RMS value of the average measured peak-to-peak voltage of each defect is the one used in Fig. 5.3 after representing it in terms of impedance (ΔZ).

The higher the length of the defect, the higher the change in the coil impedance. At defect length 25.2 mm, it shows a higher value of the coil impedance change compared to the values obtained at defect lengths of 15 mm and 5 mm. For defect lengths 15 mm and

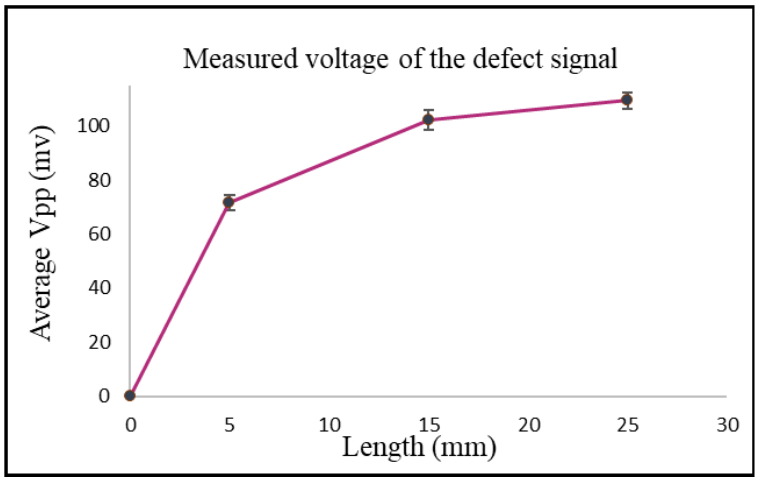


Figure 5.2: The average and standard deviation values of the defect for each length.

25 mm, the simulation results are more accurate since the mesh size used for simulation is suitable with respect to the defect size. There is a difference between the simulation, analytical, and experimental results for each length as shown in Fig 5.3. The reason is the results obtained from experiment will always be higher compared to the ones obtained from simulation since the mesh size affects the accuracy of the simulation results.

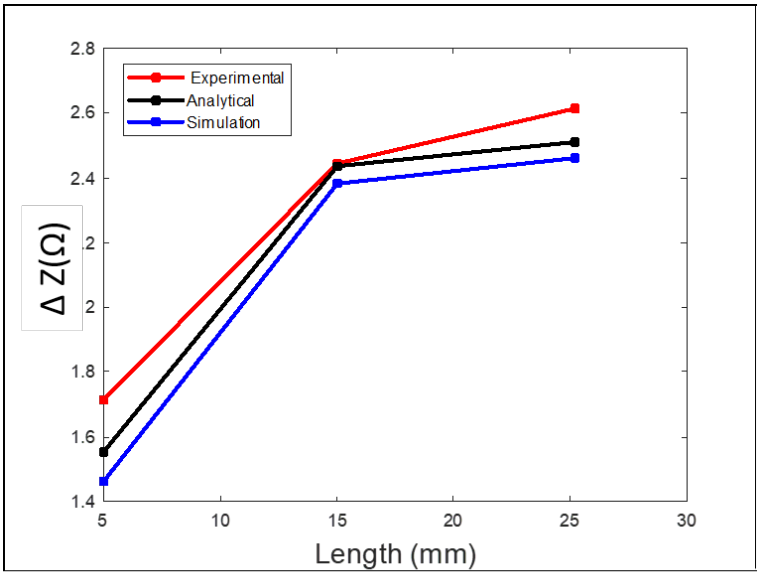


Figure 5.3: Comparison between the experimental, analytical, and simulation results for the three notches same width different length case.

5.2.4 Three notches same length different width

Another case considered for testing the designed absolute probe is to detect three notches with 0.57 mm, 0.47 mm, and 0.437 mm width. The three notches have the same length of 25.2 mm as shown in Fig. 5.4. The widths of the notches were chosen to be close in size to study the effect on the measured defect signal if the difference between the width sizes are small (less than 0.1 mm). Notches are 0.5 mm from the surface of the plate, and the thickness of the plate is 2 mm. Detection is done from the opposite side of the notches to simulate subsurface cracks. Scanning is done across the notches in the (Y) direction. Results are compared to the simulation model done on ANSYS Maxwell and analytical modelling. There is a difference between the simulation, analytical, and experimental results for each length as shown in Fig 5.6. The reason is that the results obtained from experiment will always be higher compared to the ones obtained from simulation since the mesh size affects the accuracy of the simulation results.

Fig. 5.5 shows the measured peak-to-peak voltage value for each defect. To get better and more accurate results, multiple readings were taken for each defect. The standard deviation and the average of all readings are calculated. The RMS value of the average measured peak-to-peak voltage of each defect is the one used in Fig. 5.6 after representing

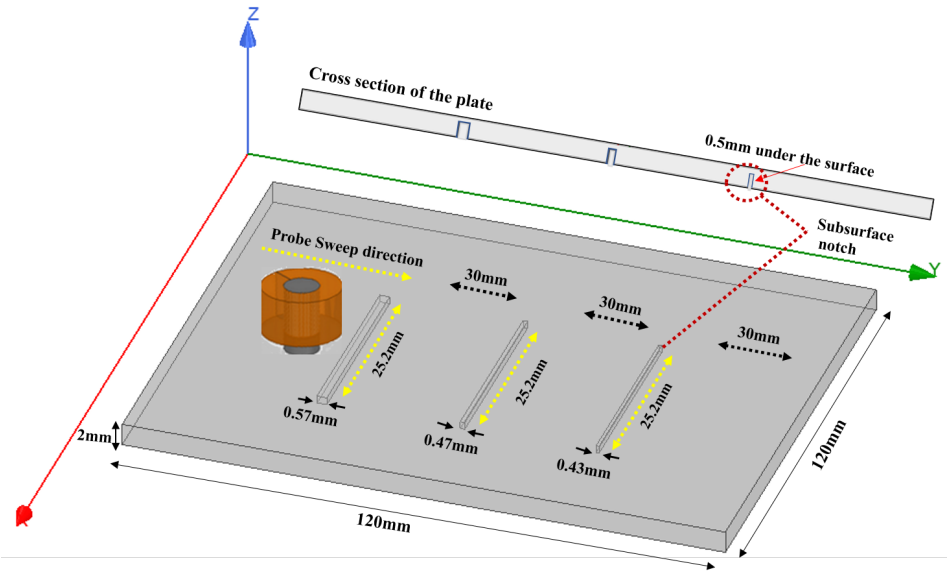


Figure 5.4: Plate with three notches same length and different width.

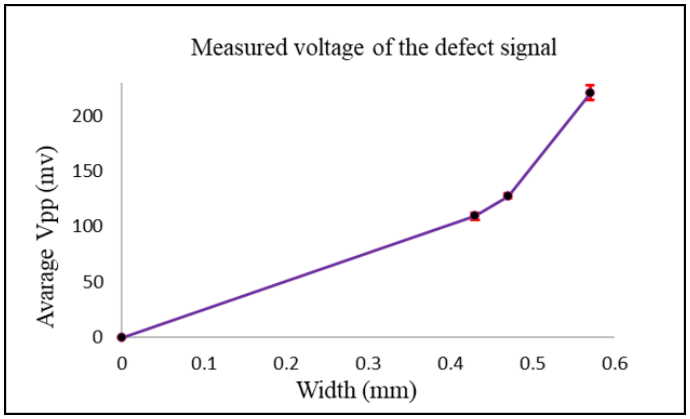


Figure 5.5: The average and standard deviation values of the defect for each width.

it in terms of impedance (ΔZ).

The higher the width of the defect, the higher the change in the coil impedance. At a defect width 0.57 mm, it shows a higher value of the coil impedance change compared to the values obtained from the defects with width 0.47 mm and 0.43 mm. Also, there is not much difference in the values obtained from 0.47 mm defect width compared to the ones obtained from 0.43 mm defect width since there is not much difference between both

widths.

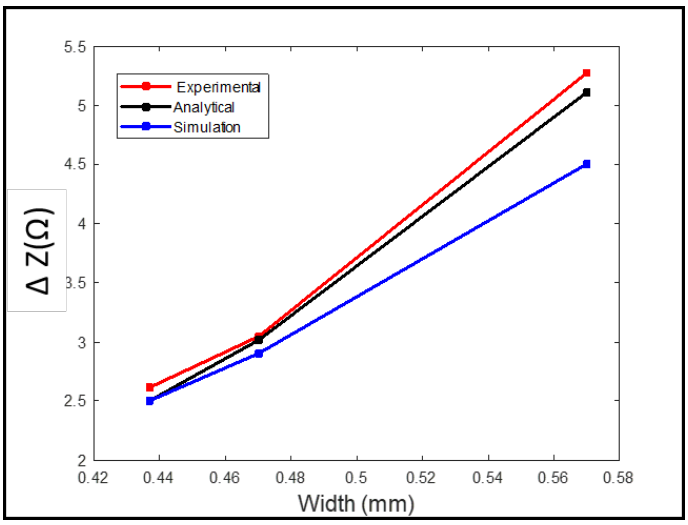


Figure 5.6: Comparison between the experimental, analytical, and simulation results for the three notches same length different width.

5.2.5 Blind holes with different diameters

Both of the previous cases used to test the designed absolute probe were to detect subsurface notches that represent subsurface cracks inside parts made by AM. This case is considered for testing the designed probe to detect four blind holes with the radius of 0.17 mm, 0.2 mm, 0.27 mm, and 0.3 mm in a plate made of stainless steel (SS316L). The four blind holes are 0.5 mm from the surface of the plate and have a depth of 1.5 mm. The plate thickness is 2 mm as shown in Fig. 5.7. Detection is done from the opposite side of the blind holes to simulate subsurface porosities inside the material. The probe can be moved either in the (X) direction or the (Y) direction the measure the impedance of the probe. Results are compared to the simulation model done on ANSYS Maxwell and analytical modelling.

Fig. 5.8 shows the measured peak-to-peak voltage value for each void. To get better and more accurate results, multiple readings were taken for each defect. The standard deviation and the average of all readings are calculated. The RMS value of the average measured peak-to-peak voltage of each defect is the one used in Fig. 5.9 after representing it in terms of impedance (ΔZ).

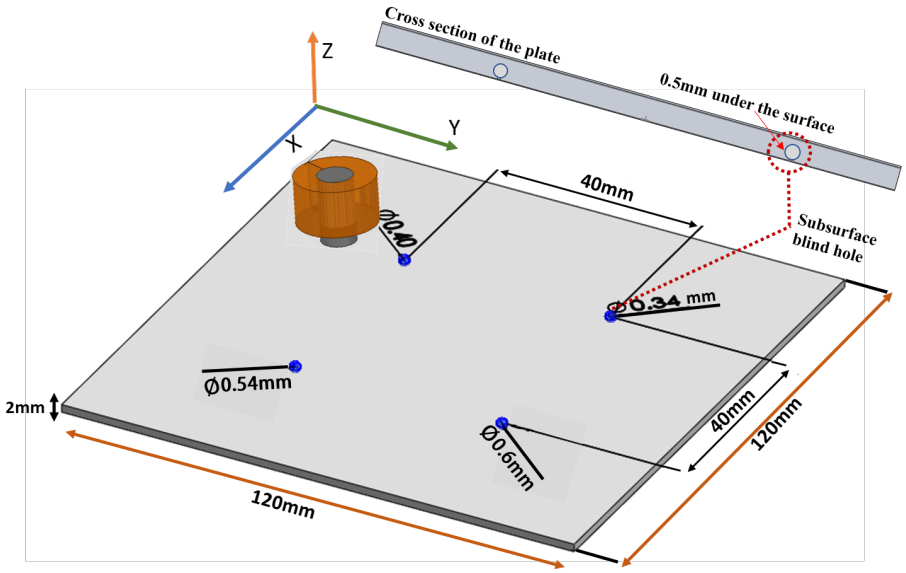


Figure 5.7: Plate with blind holes with different diameters.

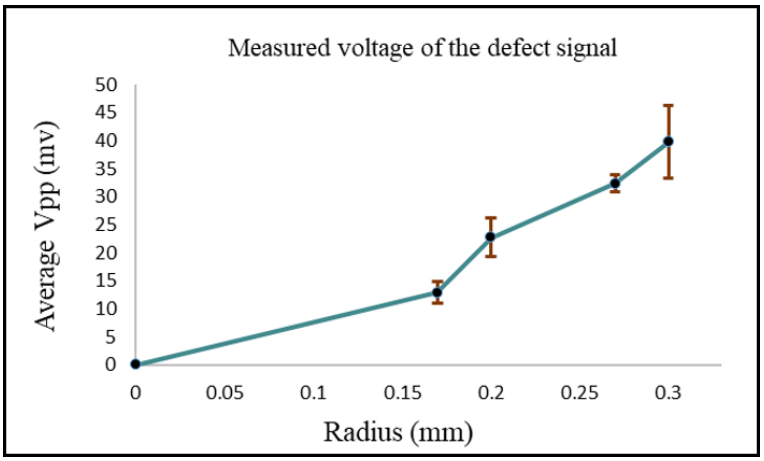


Figure 5.8: The average and standard deviation values of the defect for each void radius.

In Fig. 5.9 values obtained from the finite element modelling are low compared to values obtained from analytical modelling and experiment. The mesh size used for simulation is big compared to the blind hole diameter, which plays a big role in the accuracy of the results. The smaller the diameter of the blind hole, the smaller the probe response to it. There is a difference between the simulation, analytical, and experimental results for each

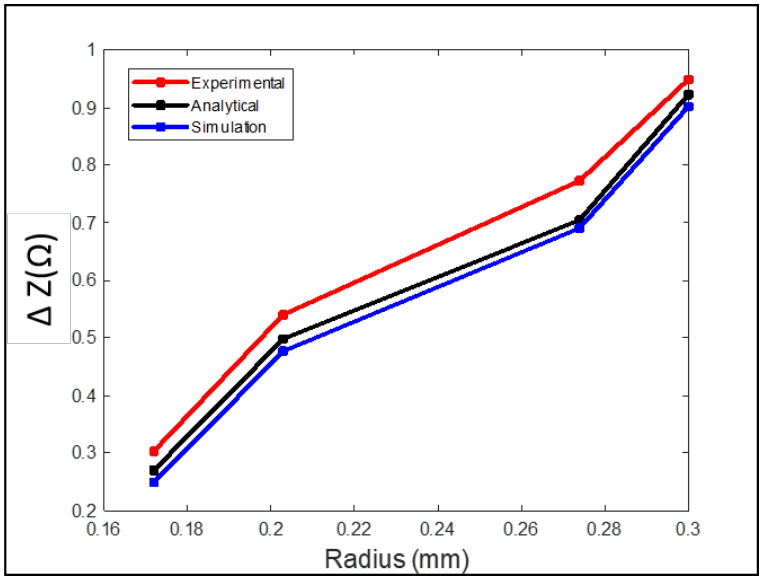


Figure 5.9: Comparison between the experimental, analytical, and simulation results for each subsurface void.

length as shown in Fig 5.9. The reason is that the results obtained from experiment will always be higher compared to the ones obtained from simulation since the mesh size affects the accuracy of the simulation results.

5.3 Testing done on parts made by AM using absolute and reflection probes

The main tool used in eddy current testing for defect detection is the probe. Eddy current probes are responsible for inducing the eddy current inside the material and in the meantime detecting the defect signal. Most of the available probes either has one coil which works in the absolute mode or two coils which work in the reflection or differential mode. Fig. 1.5. shows the difference in the geometry between absolute and reflection probes.

One of the probes used for comparison is an absolute type that has one coil to induce the eddy currents inside the material and detect the defect signal. The designed absolute probe dimensions are listed in table 5.1. The other probe used for comparison is a commercial probe that works in the reflection mode. The reflection probe has two coils, one coil

transmits eddy currents inside the material and the other coil receives the detected defect signal.

Frequency used for the commercial probe which works in reflection mode is 2 KHz. The peak-to-peak voltage value supplied to the probe is 12 V. Its diameter is around 9 mm which is almost half the diameter of the absolute probe. Using a current probe, the measured RMS input current value is 0.0205 AMP. The length of the probe is around 35 mm.

In the following sections, a comparison will be done between the response of an absolute designed probe and a reflection commercial probe for subsurface defects in parts made by laser powder bed fusion process. Comparison between different eddy current probes with different coil specs helped understanding the effect of each parameter such as coil length, inner diameter, outer diameter, number of turns, and the different operating modes on the probe sensitivity to detect subsurface cracks with width less than 0.4 mm and voids with diameter less than 0.4 mm.

Exploring both probes performance towards some of the limitations and challenges they face using eddy current testing technique in additive manufacturing such as surface roughness is done by testing different samples with different surface roughness sizes in the range of $8\mu m$ to $11\mu m$.

5.3.1 Samples used for experiment

Samples used for experiment to test both probes are made of stainless steel and titanium. The stainless steel (SS316L) samples were printed using a (Renishaw AM400 machine, Multi-Scale Additive Manufacturing lab, Waterloo) and the titanium (TI64) samples were printed using (EOS M290 machine, Multi Scale Additive Manufacturing lab, Waterloo). The process parameters used during printing the stainless steel samples are hatch power 190 W, hatch distance 60 μm, borders power 140 W, borders distance 30 μm, fill hatch distance 0.110 mm, and repetition limit 20. The process parameters used during printing the titanium samples are stripes distance 0.09 mm, stripes speed 1250.0 mm/s, stripes power 195.0 W, beam offset 0.015 mm, stripe width 5 mm, and stripes overlap 0.12 mm. All samples have subsurface artificial defects and are designed using Solidworks software.

To be able to check the accuracy of the defect width, depth and length sizes, CT has been used as a way to check each defect dimensions. All stainless steel and titanium samples inspected using CT. In Fig. 5.10 it shows one of the stainless steel samples used for experiment which has a subsurface notch with 25 mm length and 0.3 mm width. The notch is 1.5 mm below the surface to detect defects at higher depth. The XYZ plane is

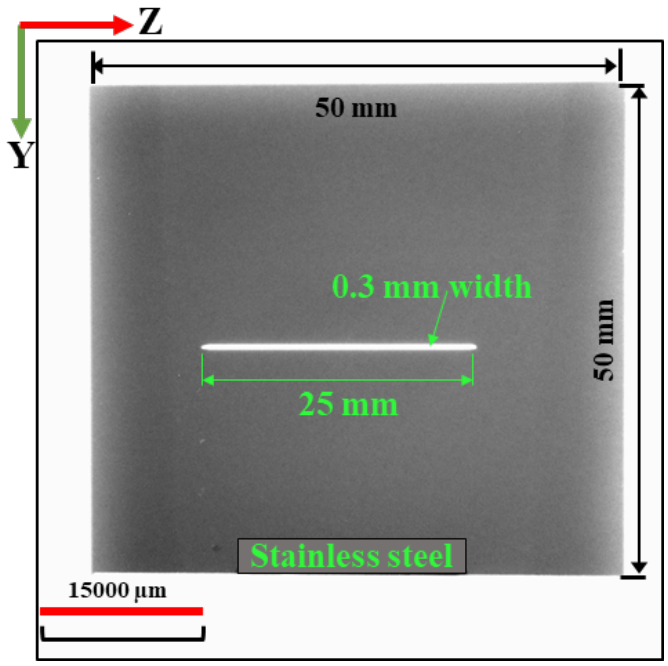


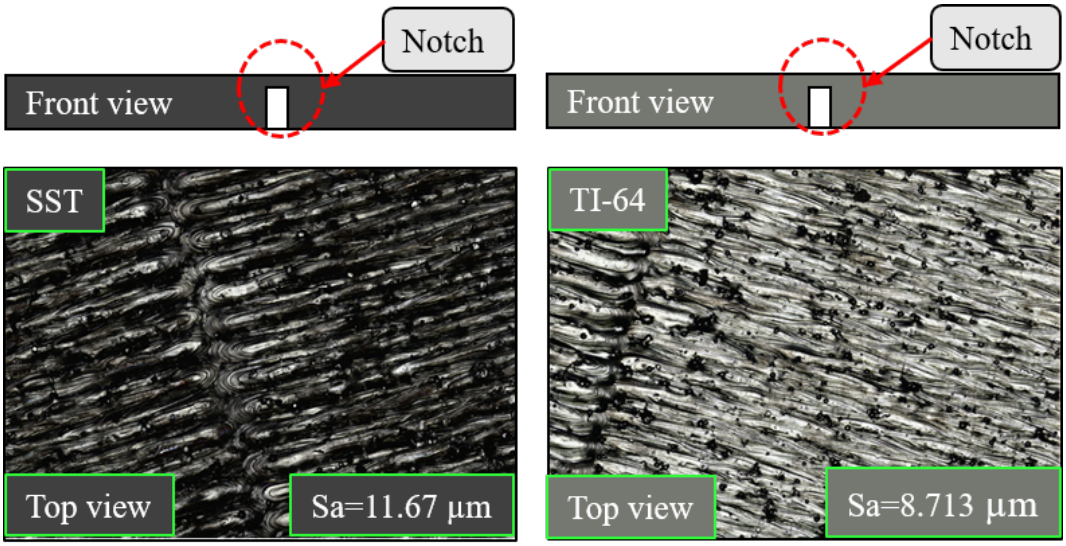
Figure 5.10: CT results of a stainless steel sample.

the CT plane. Images were taken using a (ZEISS Xradia Versa 520, Multi Scale Additive Manufacturing lab, Waterloo) at the following settings:

- Voltage: 140kV.
- Power: 10 kW.
- Exposure Time: 2.0 seconds.
- Source Distance: 110.2702 mm.
- Detector Distance: 27.0012 mm.
- Voxel Size: 55.1493 um.
- Optical Magnification: 0.39328.

All stainless steel and titanium samples has rough surface because of the laser hatch pattern and the random distribution of the powder.

Surface roughness is one of the challenges that makes it difficult to interpret the measured signal. The surface roughness and finish of the test piece will cause disturbance



(a) (b)

Figure 5.11: The measured surface roughness size of the samples where (a) stainless steel (SS316L) sample, (b) Titanium sample (TI-64).

to the flow of the eddy currents inside the material which produces unwanted signal in addition to the actual defect signal. Detecting small size defects in parts with high surface roughness will be difficult and requires applying different filters to the measured signal. An example of the different surface roughness in stainless steel and titanium parts made by additive manufacturing shown in Fig. 5.11. The surface roughness size of all samples was measured using the microscope. Fig. 5.11 shows the front view and the top view of the samples. The images were taken using a (Keyence VK-X250 Laser Con-focal Microscope, Multi-Scale Additive Manufacturing lab, Waterloo) with the following settings:

- 20X Magnification Lens.
- 0.5um Z-pitch.
- 693.630 um X-Y calibration per pixel.

All samples size are 50 mm× 50 mm. The defects are located at the center of each sample to be able to move the probe easily and to avoid edge effect, or perturbing the eddy currents.

5.3.2 Intermittent measurements, sensing and circuitry

A schematic diagram of the intermittent defect detection while the parts are printed using LPBF technology shown in Fig. 5.12. The intermittent defect detection can be done after the melt pool in the 3D printed part solidifies for fast defect detection process. In the proposed schematic diagram, the system has a current generator and a low pas filter, and A/D converter. Most of the data acquisition systems that exist in the market have these features. An alternating current or an alternating voltage is required to drive the probe coils to produce the magnetic field inside the coil. The supplied AC voltage to the absolute probe has a peak-to-peak value of 5 V and frequency of 28 KHz. The supplied peak-to-peak voltage value to the reflection probe is 12 V and the frequency used is 2 KHz. Based on the used frequency and both stainless steel and titanium conductivity and permeability, the eddy currents SDP is around 3 mm inside the material. The SDP formula were used to get the eddy currents depth inside the material.

Applying a filter is necessary to reduce any noise in the measured signal and to differentiate between the actual defect signal and the noise. Applying a filter to the measured signal helps to remove the background drift from the eddy current signal. Different types of filters can be applied to the measured signal such as low pas filter, high pass filter, band-pass filter, and median filter. Choosing which filter should be applied to the measured signal depends on the length of the flaw and the noise source. The length of the filter should be at least twice the length of the defect otherwise the defect signal will be attenuated. The filter type that is used during measuring the defects signals is a low pass filter with a cutoff frequency of 30 Hz. The low pass filter passes only signals with low frequencies and cuts off high frequency signal such as electrical noise. The PC is used to control the whole system and the detection process.

The data acquisition system used during the detection process is MIZ-12C. To move the probe on top of the samples in different direction, a 3D printer XYZ Motorized Linear Stage could be used which will help keeping the lift-off distance between the probe and the sample constant.

An illustration of the circuit attached to the probe for the experimental setup is shown in Fig. 5.13. To drive the absolute probe coil, a simple RL circuit was attached to it. The coil winding is attached to the voltmeter to be able to measure the flaw signal and attached to an AC voltage source to be able to drive the coil and induce eddy currents inside the part under test. The peak-to-peak voltage value supplied to the probe's coil is 5 V with a frequency value of 28 KHz. The coil winding is attached to a resistor (R1) with a value 27 ohm. An operational amplifier used to amplify the measured signal since the measured signal value is in millivolts. The op-amp type used is LM358 and 5 volt

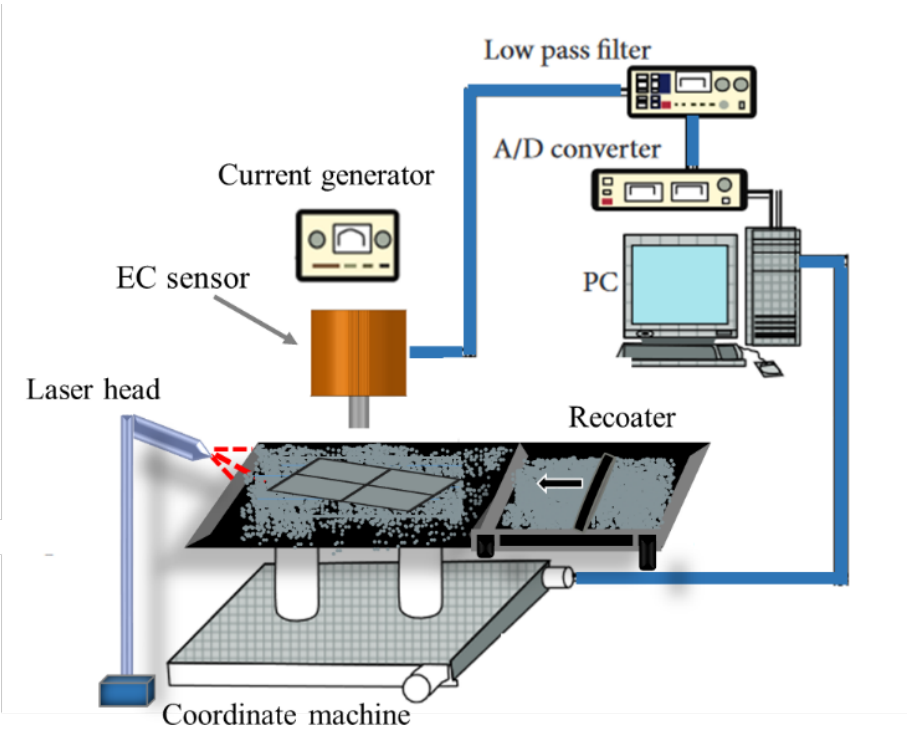


Figure 5.12: Schematic diagram of a proposed intermittent defect detection.

is supplied to the operational amplifier. The non-inverting amplifier used has an input resistance (R2) with a value of 1000 ohm and an output resistance (R3) with a value of 10000 ohm. The calculated gain of the op amp is 11. The circuit provided in 5.13 is the one provided to the simulation model created in ANSYS Simplorer to be able to validate the experimental results. In ANSYS simplorer, the whole model should be imported to do a co-simulation between the model created in ANSYS Maxwell and the circuit created in ANSYS Simplorer. The winding sink should be connected to the ground and the winding source is connected to the rest of the circuit.

The circuit attached to the reflection probe is shown in Fig. 5.14 It consists of two parts, the transmitter part that is attached to the transmitter coil and the receiver part that is attached to the receiver coil. The peak-to-peak voltage value supplied to the transmitter coil is 12 V with frequency of 2 KHz. The receiver coil is attached to a voltmeter to measure the defect signal. The measured inductance value of the transmitter coil is 10.9 mH and the measured inductance value of the receiver coil is 8.2 mH. Both absolute and reflection probes are connected to the data acquisition equipment using a Triax cable and

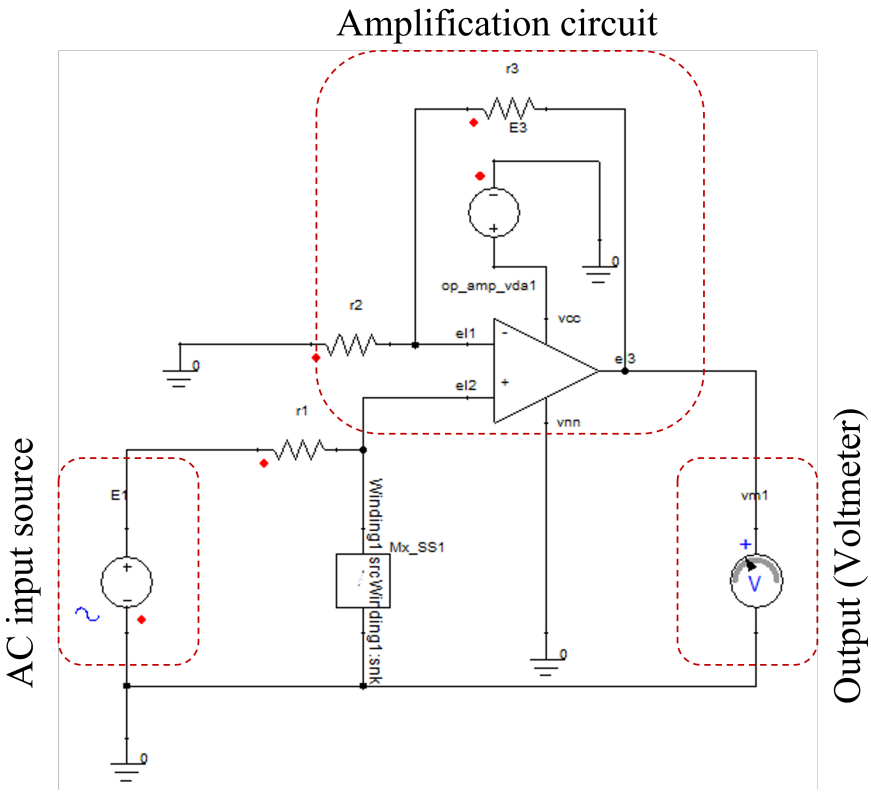


Figure 5.13: Circuit attached to the absolute probe.

a LEMO connector type. An illustration of the reflection probe circuit and the LEMO connector attached to it is shown in Fig. 5.14.

To be able to compare between both probes, samples made of stainless steel SST-316 and titanium TI-64 were used during the detection process. Multiple readings taken for each defect using both probes. Since both probes have different dimensions and different input values, the measured signals were normalized for comparison. Each defect has six readings, and the normalized value was calculated by dividing each voltage of the six reading by the maximum voltage value (Vpp) of all the six readings [15]. The defects are located at the center of each sample. The samples dimensions, defect size and location are shown in Fig. 5.10.

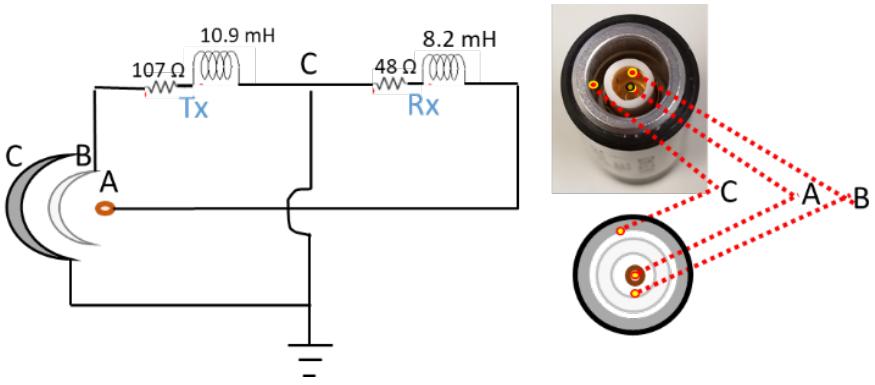


Figure 5.14: An illustration of the reflection probe circuit.

5.3.3 The experimental setup used during the detection process.

The experimental setup used in this work is shown in Fig. 5.15. The measured peak-to-peak voltage at the probe terminal on top of a stainless steel sample is 3.4 volt using the oscilloscope. The data acquisition system can only measure the raw voltage of the defect signal where there is a difference in the probe impedance between defect and non-defect area. The RMS input current value is 0.0148 Amp. The input Vpp to the coil is 5 V and the resistance connected in series with it is 27 ohms. The measured value of the probe impedance (Z) on top of a stainless steel plate and titanium plate using the absolute probe can be calculated using equation (5.1).

$$Z = \sqrt{R^2 + x_l^2} = \frac{V}{I} \tag{5.1}$$

where V is the measured Vpp value of the probe on top of the stainless steel or the titanium plates. The RMS value of the measured Vpp is 1.202 V. Using Equation (5.1), the measured coil impedance is $\frac{1.202}{0.0148}$ =81.2 .

5.3.4 Detecting defects in stainless steel samples

Different defect types can be formed in parts made by AM technology such as cracks and porosities due to lack of fusion. The size of porosities is usually around 5 μm-200 μm. Cracks with the range between 200 μm-700 μm are formed in different alloys (e.g., superalloys) due to the great residual thermal stress combined with the high temperature gradient [20, 21, 22]. Several cases were considered for testing both probes on parts made

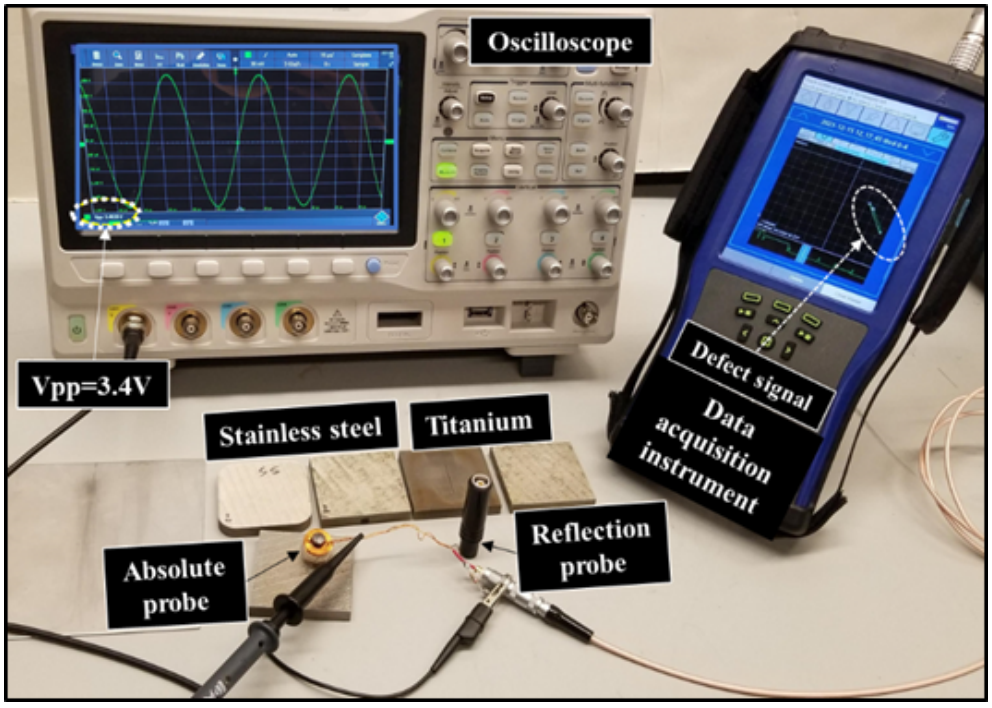


Figure 5.15: Experimental setup showing both probes used to test titanium and stainless steel samples.

by AM. The first case is to detect 0.07 mm, 0.1 mm, 0.2 mm, 0.3 mm and 0.4 mm notches width. All notches have a length of 25 mm and located at 1.5 mm from the sample surface. All samples thickness is 8 mm. Samples are made of stainless steel (SS316L) with conductivity 1.35×10^6 siemens/m and relative permeability 1.005. To simulate subsurface cracks, the detection process is done form the opposite side of the notches.

Second case considered for testing both probes is to detect blind holes which are located at 0.5 mm from the surface with different diameters. The diameters are 0.34 mm, 0.4 mm, 0.54 mm, and 0.6 mm. The samples thickness is 2 mm. Values shown in Fig. 5.16 and Fig. 5.17 are the ones obtained experimentally. An example of the samples used for experiment shown in Fig. 5.10. The probe is moved across each defect in the Y direction. In Fig. 5.16 both probes are used to test the stainless steel plate with notches and the measured signal is the raw peak to peak voltage measured at the probe terminals in millivolts. Values shown in Fig. 5.16 are the normalized value. The actual peak to peak voltage of the defect signal using both probes are shown in Fig. 5.19 and Fig. 5.20. As shown in Fig. 5.16 the absolute probe shows a better response detecting the notches compared to the reflection

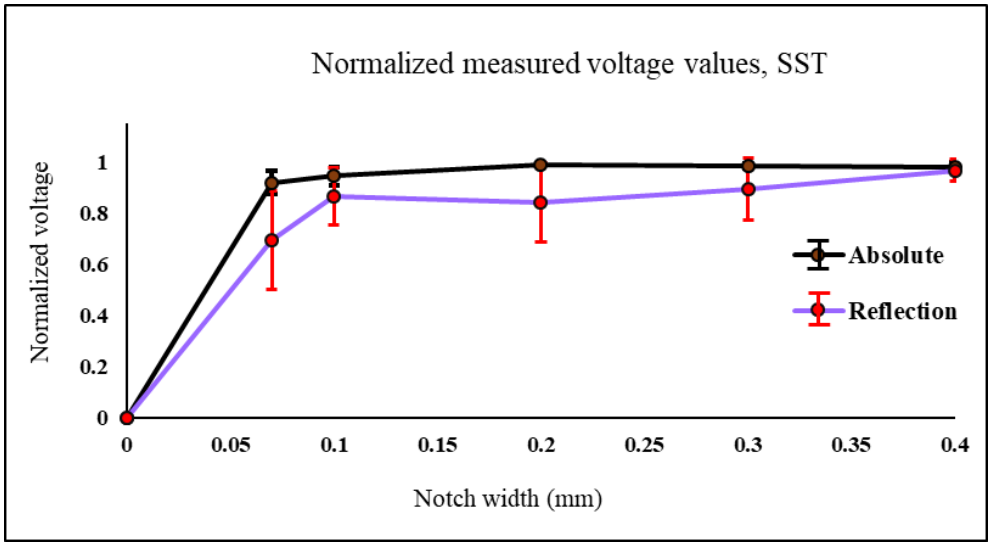


Figure 5.16: Normalized values of the measured voltage for both probes on top of plates made of stainless steel with notches with different widths made by AM.

probe. There is a relationship between the size of the detected defect and the diameter of the probe coil. The smaller the diameter of the coil the smaller the defect that can be detected.

In Fig. 5.17. the reflection probe gives a better response detecting the blind holes compared to the absolute probe since the diameter of the reflection probe is almost have of the absolute one which improved its detectability to smaller defect sizes. The average of all normalized values for each defect and the standard deviation error bars are the one shown in Fig. 5.16 and Fig. 5.17.

5.3.5 Detecting defects in titanium samples made by AM

Third case considered for testing both probes is to detect notches with different widths and same lengths. The samples are made of titanium and the notches are located at the center of each sample. All samples in this section were made by AM. An example of the samples is shown in Fig. 5.10.

The AM parts are made of titanium (TI-64) with conductivity 0.56×10^6 siemens/m and relative permeability 1.05. Both probes were used to test them. The measured peak to peak voltage of the defect signal was normalized and plotted as shown in Fig. 5.18. The

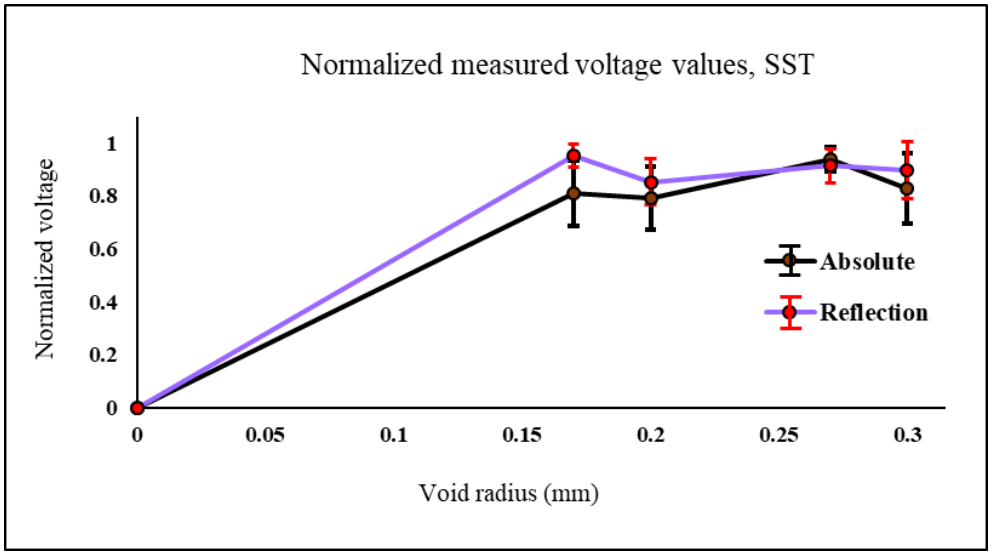


Figure 5.17: Normalized values of the measured voltage for both probes on top of machined plates made of stainless steel with different radius blind holes.

titanium plates have notches with the same length of 25 mm and each notch is located at the center of the plate as shown in Fig. 5.10. The absolute probe gives a higher and better response to each notch compared to the reflection probe. The repeatability of the measured voltage values of each notch using the absolute probe is also better and the average values are the ones used in Fig. 5.18. All the samples made by AM had a rough surface and the effect of the rough surface was neglected because of the coating layer that was added to the designed absolute probe. Also, the commercial probe is encapsulated inside a case that helped overcoming the effect of the surface roughness.

5.3.6 Material conductivity comparison for both probes

Another comparison conducted using both probes, shown in Fig. 5.19 and Fig.5.20, exhibits how much the detected defect signal will be affected in case of testing different materials with different conductivity. The comparison done based on the measured defect signals obtained from the samples used in the first and third cases. Materials with higher conductivity will cause higher amount of eddy currents to be induced inside the material. Therefore, the existence of any crack inside the material with the higher conductivity will perturb these eddy currents causing a higher probe response and a higher measured voltage value.

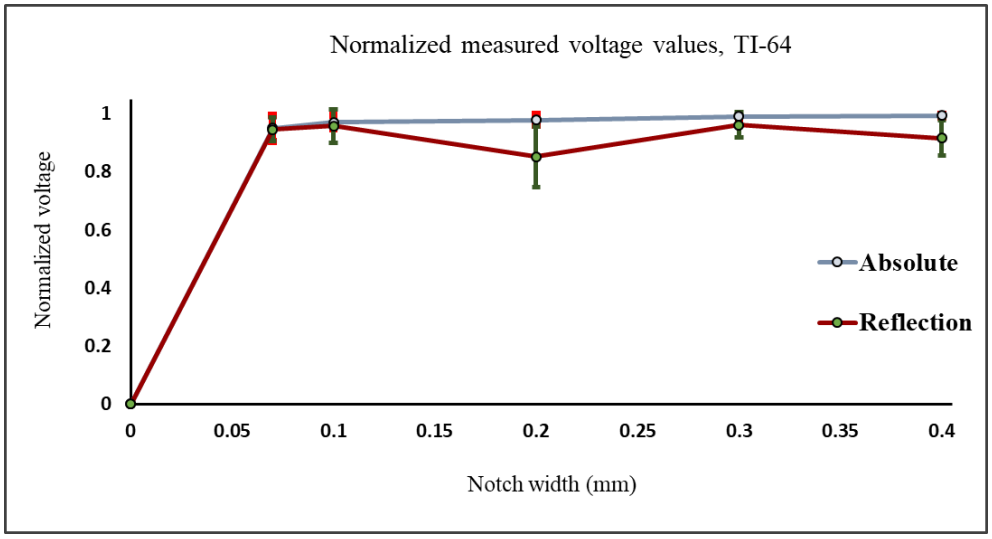


Figure 5.18: Normalized values of the measured voltage for both probes on top of plates made of titanium with notches with different widths.

In Fig. 5.19 a comparison on the absolute probe detection response to notches on stainless steel and titanium samples is done. The measured Vpp values at the probe terminal in case of stainless steel is higher than the measured ones in case of titanium since stainless steel (SS316L) has a higher conductivity than titanium (TI-64).

Same behavior found using the reflection probe during testing both materials in Fig. 5.20. The probe is moved across each defect multiple times keeping the lift-off distance constant all the time. Looking at Fig. 5.19 and Fig. 5.20 the error bars shown for each defect represent the repeatability of the measured peak-to-peak voltage values for all six readings for each defect. In Fig. 5.19 the six readings of the measured peak-to-peak voltage for each defect show more repeatability which means that the results are more accurate and reliable compared to the results shown in Fig. 5.20. Based on the previous explanation, the absolute probe shows better results to detect notches compared to the reflection probe.

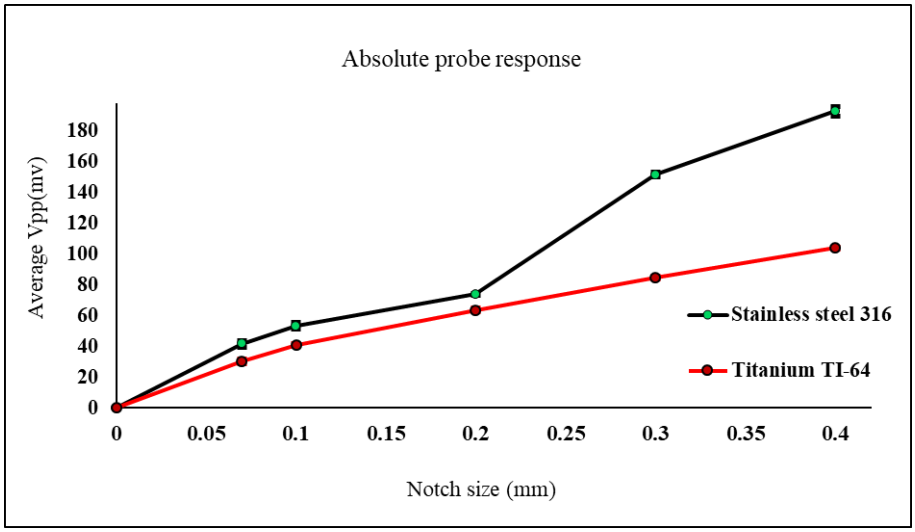


Figure 5.19: Measured Vpp values using absolute eddy current sensor on top of titanium and stainless steel samples with notches.

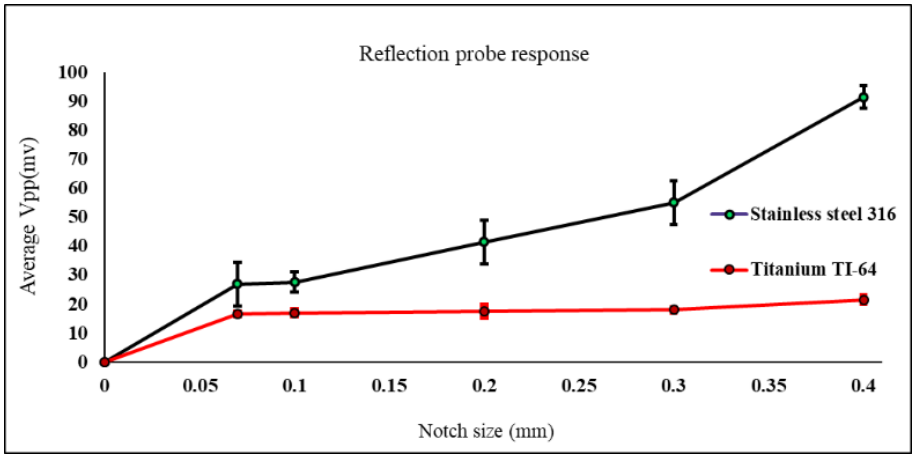


Figure 5.20: Measured Vpp values using reflection eddy current sensor on top of titanium and stainless steel samples with notches.

5.4 Methods for sensitivity analysis experiments

In this section different cases are considered for sensitivity analysis during running experiment. All parts in this section were made by AM. The cases are:

Testing samples made by AM with defects close to the edge of it to find out the best way to detect those defects without getting a false signal produced by the samples edges that represents a crack. Second case is to explore the effect of different lift-off distances on the accuracy of defect detection. Third case is to explore detecting multiple defects that exists in the same region or defects that are separated by small distance in between. All testing done from the opposite side of the defects.

5.4.1 Testing close to an edge

The edge effect is one of the challenges when it comes to detecting flaws in small samples. The edges of the samples will produce a false signal that looks like a signal produced by a crack.

The best way to avoid the effect of edges is to move the probe parallel to the edge. In Fig. 5.21 it shows the dimensions of a stainless steel sample that has two notches close to an edge. Instead of moving the probe in the X direction to detect the defect, it is better to move it in the Y direction parallel to the edge of the sample, that way the effect of edges will be eliminated. The probe is moved on top of the stainless steel (SS316L) sample from the opposite direction of the defect to simulate subsurface defects. The plate used during experiment has 0.1 mm notch width. The average measured voltage at the probe terminal is 54.11 mv.

5.4.2 Effect of lift-off distance

The same sample used in Fig. 5.21 is used in that case as well to show the effect of having different lift-off distances between the probe and the samples. Two lift-off distances were considered during experiment. The fist lift-off distance considered is 1 mm and this is done by adding a sheet made of Plastic with 1 mm thickness between the probe and the stainless steel plate. The plastic sheet has zero conductivity. The second lift-off distance considered is 2 mm and this is done by adding a sheet made of Plastic with 2 mm thickness between the probe and the stainless steel plate.

The higher the lift-off distance between the probe and the part under test, the less the amount of the eddy currents that will be produced inside the material which leads to smaller standard depth of penetration. One more thing noticed during the experiment is that the The effect of surface roughness will be suppressed in case of adding a sheet made

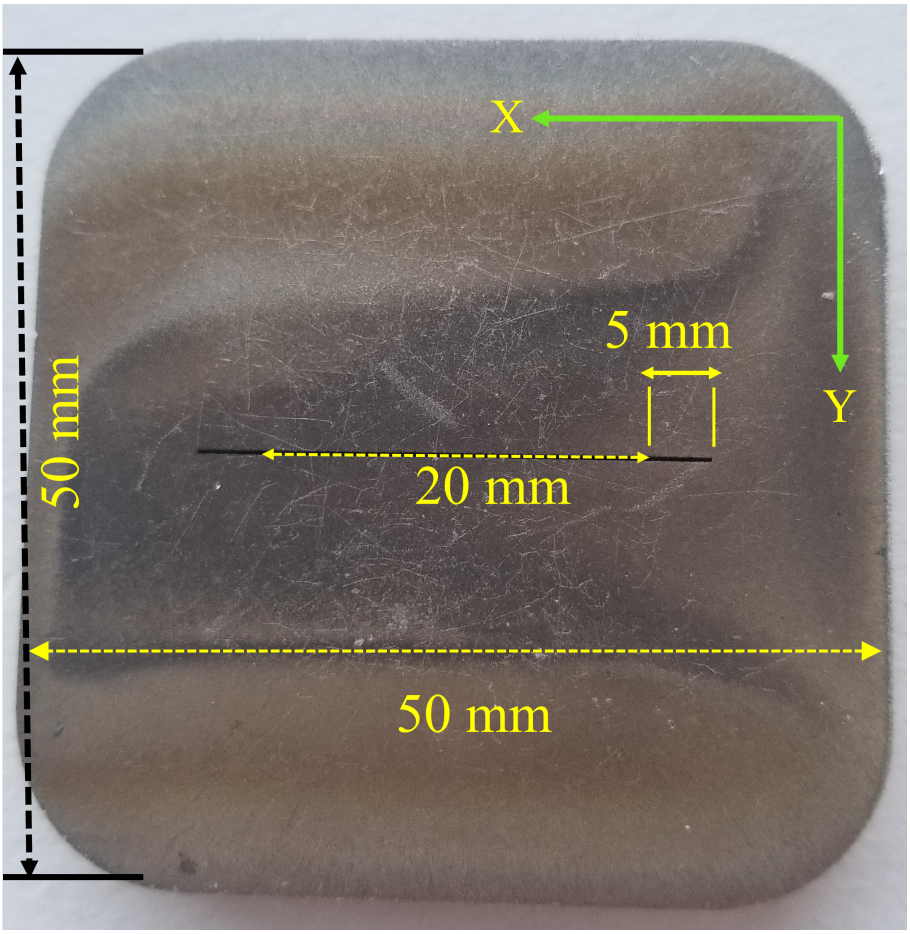


Figure 5.21: Notches close to edges in stainless steel samples.

of plastic or any other non-conductive material between the probe and the test piece. The plate used during experiment has 0.1 mm notch width. The average measured voltage at the probe terminal is 54.11 mv. In case of 1 mm lift-off distance, the measured peak-to-peak voltage value at the probe terminal is less which is around 42.7 mv. In case of 2 mm lift-off distance, the measured peak-to-peak voltage value at the probe terminal is very weak which is around 35.03 mv.

Defect size	lift-off distance	Measured voltage
0.1 mm	0 mm	54.11 mv
0.1 mm	1 mm	42.7 mv
0.1 mm	2 mm	35.03 mv

Table 5.2: Measured voltage of the probe at different lift-off distances.

5.4.3 Multiple defects in the same region

All previous testing done on samples that has only one defect inside the material. In this section other cases are considered where the detection done on samples that have multiple defects in the same region of defects that are separated by a very small distance to see the effect of it on the detected defect signal. Samples used during experiment are shown in Fig.5.22 and Fig. 5.23. Testing is done from the opposite side of the defects to represent a subsurface defects.

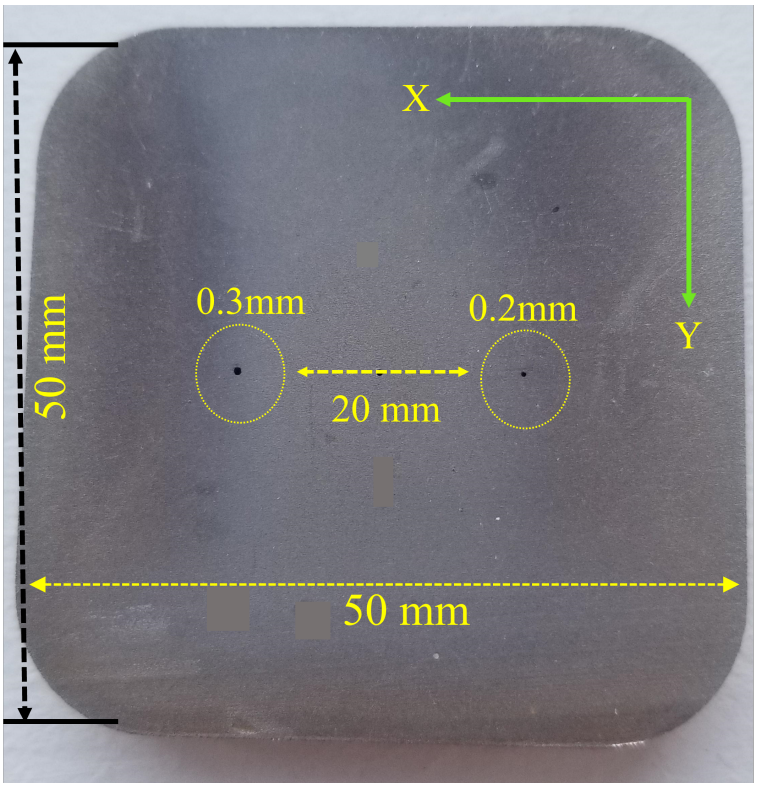


Figure 5.22: Two voids separated by a very small distance in a stainless steel sample

In Fig.5.22 it shows a stainless steel plate that has two defects separated by 20 mm distance. The diameter of the designed probe is 16 mm which almost as big as the distance between both voids. The Eddy currents created in the material under the probe is usually around twice the size of the probe diameter. The probe is moved in the X direction on top of the stainless steel sample. Since the probe diameter is around 16 mm, the eddy currents created under it will have around 30 mm diameter of a circular loop. The distance between the two voids, is too close compared to the size of the eddy currents circular loop diameter which will eventually show only one peak value of the measured voltage for both defects instead of showing two different peak value for each defect alone. The average measured peak-to-peak voltage value of both defects together is 782.22 mv. Moving the probe on top of the 0.2 mm defect only gives a value of 264.03 mv. Moving the probe on top of the 0.3 mm defect only gives a value of 314.6 mv.

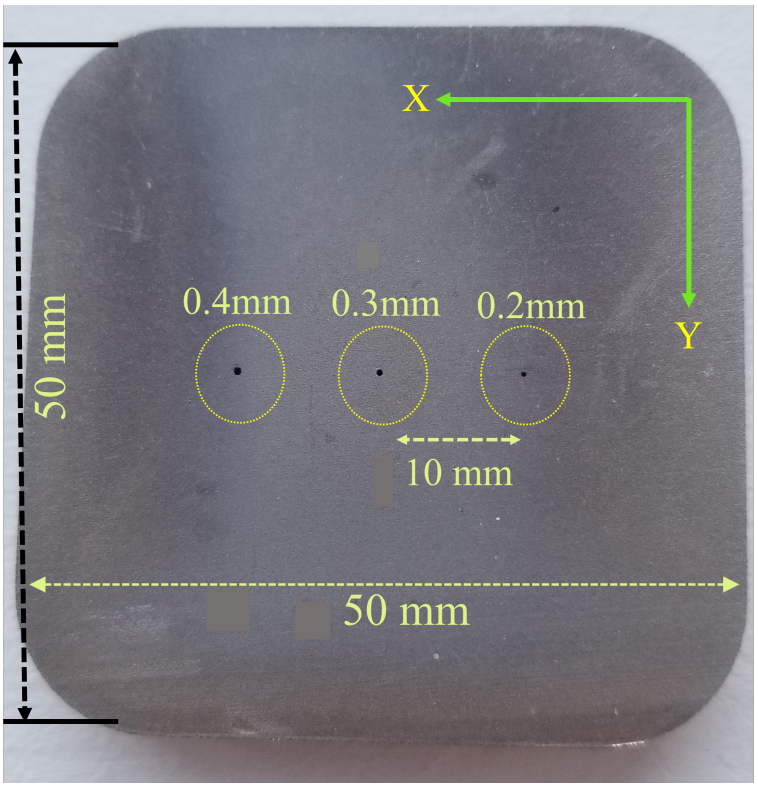


Figure 5.23: Three voids separated by a very small distance in a stainless steel sample.

In Fig.5.23 it shows a stainless steel plate that has three defects separated by 10 mm distance. Same scenario happens in this case as well. The short distance between the

Defect size	Path of travel	Measured voltage
0.2 mm	Y direction	264.03 mv
0.3 mm	Y direction	314.6 mv
0.4 mm	Y direction	410.28 mv.
Both defects (0.2 mm, 0.3 mm)	X direction	782.22 mv.
All defects (0.2 mm, 0.3 mm, 0.4 mm)	X direction	1175.74 mv

Table 5.3: Measured voltage of the probe for cases of multiple defects in the same region.

defects in case of moving the probe in the X direction will show only one peak change in the measured voltage of the probe instead of three different peaks, one for each defect. The average measured peak-to-peak voltage value of the three defects together is 1175.74 mv. Moving the probe on top of the 0.2 mm defect only gives a value of 264.03 mv. Moving the probe on top of the 0.3 mm defect only gives a value of 314.6 mv. Moving the probe on top of the 0.4 mm defect only gives a value of 410.28 mv.

5.5 Summary

In this chapter, different EC based probe designs (absolute and commercial reflection) are used to detect artificial defects with different sizes and at different depths. The comparison is carried out between the response of an absolute designed probe and a reflection commercial probe for the detection of subsurface defects in parts made of stainless steel (316) and titanium (TI-64) made by LPBF technology. Comparison between different EC probes with different coil specifications helps in understanding the effect of each parameter such as coil length, inner diameter, outer diameter, number of turns, and the different operating modes on the probe sensitivity to detect cracks with width less than 0.3 mm and voids with diameter less than 0.3 mm. Exploring both probes helped in evaluating their performance towards some of the limitations and challenges that face using eddy current testing technique in additive manufacturing such as surface roughness and edge effect. The comparison is carried out by testing different samples with different surface roughness sizes in the range of 8 μm to 11 μm.

In [55] eddy current NDT technique is used to detect subsurface defects for additive/subtractive hybrid manufacturing. In experiment several cases were considered to detect subsurface defects in parts made of Titanium Ti6Al4V. Exploring the effect of temperature, lift-off distance and effect of defect size on the detected defect signal were

considered. The specimen size was set to 18 mm × 17 mm × 7.6 mm, a defect was 1.2 mm below the detection surface and had dimensions of 0.8 mm in width and 15 mm in length. The effect of specimen temperatures on the output signals was investigated in terms of the normalized inductive reactance. A heating plate was placed under the specimen to mimic the temperature. Once the laser is powered off, the temperature dropped rapidly from the melting temperature to room temperature, that's why the experiment was done at temperature range from 20 C to 270 C. As the temperature increases, the reactance of the probe also increases which increases the total impedance of the probe. The change in the temperature causes changes in the electrical conductivity and the permeability of the material. The increment in the temperature cause the electrical conductivity of the material to decrease which increases the standard depth of penetration of the eddy currents inside the material.

Another case considered during experiment is to explore the effect of changing the lift-off distance between the probe and the part under test on detecting small size defects. The SDP of the eddy currents inside the material decreases in case of increasing the lift-off distance which has a negative impact on the detection of the defects. the lift-off distance was changed for values in the range of 0.08 mm to 1.4 mm. the normalized reactance values decrease in case of increasing the lift-off distance.

To find the relation between the defect size and the detected signal, several defects were embedded inside part made by AM. The defects are located at the same depth of 1.2 mm from the top surface of the sample which represent subsurface cracks in parts made by AM. All defect widths were measured to be approximately 0.8, 0.6, 0.4, and 0.2 mm, respectively. The higher the width of the crack, the higher the measured defect signal value. the signal intensity decreased with a decrease in the defect size. Linearity was observed in the signal magnitudes, which demonstrated the relationship between the signal intensity and defect size.

In this thesis, the measured defect signal value using the probes is in the range of (20–200) millivolts. Both probes can detect subsurface defects on stainless steel samples with average surface roughness of 11.6 μm and titanium samples with average surface roughness of 8.7 μm. It is found that the signal reading can be improved by adding a coating layer made of thin non-conductive material to the bottom of the absolute designed probe. The layer will decrease the surface roughness effect and smooth out the detected defect signal from any ripples. The smallest subsurface artificial defect size detected by both probes is an artificially made notch with 0.07 mm width and 25 mm length. In addition, both probes detected subsurface artificial blind holes in the range of 0.17 mm–0.3 mm radius. Results show that the absolute probe is more suitable to detect cracks and incomplete fusion holes, whereas the reflection probe is more suitable to detect small diameter

blind holes. The setup can be used for defect detection during the additive manufacturing process once the melt pool is solidified.

Chapter 6

Conclusions and Future work

6.1 Conclusions

The following conclusions can be drawn from this thesis:

1) The Work done in this thesis aims to answer three questions. The questions are if eddy current testing technique could be used in defect detection for parts made by additive manufacturing, what are the challenges that face using eddy current testing in additive manufacturing and how to design a probe that overcomes these challenges? The answers for these three questions are answered in previous chapters and will also summarize them in this chapter. Eddy current testing technique is one of the reliable non-destructive testing techniques that is used for defect detection in many industrial applications and fields. The technique is suitable for weld detection, corrosion detection, bolt Hole inspection, tubing inspection, surface inspection and conductivity measurements. Eddy current could be efficiently used for defect detection because the part under test doesn't require much preparation to be tested, as well as easy and cheap to use.

The first question to be answered is about the possibility of using eddy current testing technique to detect flaws in parts made by AM. There are several industries benefiting from additive manufacturing such as automotive, aerospace, energy, consumer products, infrastructure, medical and pharmaceutical edible goods. Like any other technology, parts made by additive manufacturing technology have to go through the stage of quality assurance to make sure that the quality requirements of the product have been fulfilled. Several non-destructive testing techniques such as ultrasonic, thermography, liquid and magnetic penetrate testing have been used to test parts made by additive manufacturing for the existence of defects. A comparison done between each one of these techniques in the literature

review chapter. The feasibility of using eddy current testing for defect detection in AM has been done by designing an eddy current probe that is used later to test parts made by laser powder bed fusion process. A comparison carried out between the responses of two different probes with different geometries which work in different modes to detect defects in samples made of titanium and stainless-steel. The samples are made by AM using laser powder bed fusion with artificial defects. In addition, different defect shapes were detected such as notches that simulates subsurface cracks and blind holes that simulates subsurface porosities [65-73]. Another comparison carried out using both probes to compare the effect on the defect signal from the point view of conductivity. The absolute probe gives a better response in case of detecting notches meanwhile the reflection probe gives a better response in case of detecting blind holes. The absolute probe is more suitable to detect cracks and incomplete fusion holes. The reflection probe is more suitable to detect small diameter blind holes with diameter less than 0.2 mm. It is easier to design and fabricate the absolute probe as well as cheaper to implement it. The minimum defect size that can be detected using the designed absolute probe applied to the experimental configuration used in this paper is 0.2 mm void radius and 0.07 notch width.

2) The main steps to design an eddy current probe are done, taking into consideration one of the challenges that face NDT for parts made by additive manufacturing, such as surface roughness which answers the second question regarding the challenges that face using eddy current testing in AM. The bottom surface of the probe has a layer of coating that helps smooth out the measured defect signal from any ripples. It is very important to design the EC probe in a way that will allow it to be sensitive enough to detect small size flaws. There is a relationship between the coil dimension and the size of the defect that could be detected. A smaller coil diameter is considered for better detection of small defect sizes. The current probe design can detect blind holes within the range of (0.3 mm - 0.6 mm) diameter. Also, it can detect cracks with different widths in the range of (0.07 mm - 0.6 mm) in stainless steel and titanium material. Having a cylindrical tip shape allowed focusing the magnetic field to the center of the coil which helps focusing the eddy currents in the region of interest. Using the coil tip, the probe was able to detect blind holes that are close to the edge of the samples with a radius of 0.17 mm and 0.3 mm. In case of using the probe to detect defects from the side that has no tip, both 0.17 mm and 0.2 mm blind holes were not detected because of the edge effect. The tip focuses the magnetic field and the eddy currents under the coil as well, which makes the small diameters blind holes big enough to disturb the flow of these eddy currents.

3) A comparison carried out between the responses of two different probes with different geometries which work in different modes to detect defects in samples made of titanium (TI-64) and stainless steel (SS316L). The samples are made by AM using laser powder bed

fusion with artificial defects. Also, different defect shapes were detected such as notches that simulates subsurface cracks and blind holes that simulates subsurface porosities. Another comparison carried out using both probes to compare the effect on the defect signal from the point view of conductivity. The absolute probe gives a better response in case of detecting notches meanwhile the reflection probe gives a better response in case of detecting blind holes. The absolute probe is more suitable to detect cracks and incomplete fusion holes. The reflection probe is more suitable to detect small diameter blind holes with diameter less than 0.3 mm.

The steps to design the eddy current probe involve analytical part and FEM simulation part. For FEM simulation the accuracy of the simulation results is affected by the mesh size and the boundary conditions. Since the size of the blind holes is very small, the mesh size must be very fine to get a better result which consumes a lot of time and computational resources. The simulation results for the notches cases are better since it is possible to increase the mesh size. The measured signal value during the experiment is always higher in all cases. For simulation and analytical modelling, the conditions are ideal compared to the experiment, which affect the accuracy of the results. The probe gives a better response on samples with smooth surfaces compared to the samples with high surface roughness. Machining could be done on samples with surface roughness higher than 11 µm to smooth its surface in order to suppress the noise signal of the rough surface for better defect detection. A rough surface may produce a signal that is similar to the signal obtained from small size defects, which makes the detection process difficult. By the end of this part, the answers regarding the feasibility of using eddy current testing for defect detection in additive manufacturing are provided.

6.2 Future work

In chapter 4 section 4.5, the main steps to design new probes that work in the absolute and reflection modes are explained. Based on the previous work done, there are certain parameters that have a big effect on the probe sensitivity to detect small size subsurface defects such as the coil length, number of turns, inner and outer diameter. Some of these parameters are explored through simulation. To design the new probe, several models were created in ANSYS Maxwell where different defects with different sizes are embedded inside stainless steel parts. Some factors considered for the new probe designs that affect the sensitivity of the probe to detect small size defects are shown below:

- An amplification circuit are considered and added to the new probes to amplify the measured signal.

- Multi-layer winding, adding more layers to the coil winding increase the inductance of the coil which means increasing the sensitivity of the coil to detect small size defects. The intended coil designs consists of multi-layer.

- It is important not to increase the current provided to the coil too much since it will cause over heating for the coil. Keeping the current through the coil is as low as possible is very important since too high current may produce a rise in magnetic hysteresis and temperature. The maximum current chosen for the intended designs is in the range of 0.0148 RMS AMP to 0.02 RMS AMP which is determined by the chosen American wire gauge for the designs.

- The eddy current loss is proportional to f^2. Which means at higher frequencies, the eddy current loss is very high. The optimum range of frequency used for the intended probe designs is in the range of (18-50) KHz.

- Adding a core to increase the focus of the magnetic field. A plain ferrite cores were considered for the potential probes designs.

- The minimal detectable flaw size is proportional to the diameter of the coil. As coil diameter increases, the minimum detectable flaw also increases. For notches, the rule of thumb is $\frac{1}{4}$ of a coil diameter. If the coil diameter is way bigger than the defect, the defect won't be detected since the eddy currents around the defect area are not disturbed. Small coil diameter are considered for all the probe designs.

- Adding a tip to the designed coil which helps focusing the magnetic field and making it more confined.

- Adding shields around the coils is considered to focus the magnetic field generated around the coil winding and as a result concentrate the distribution of the eddy currents under the coil and make it more confined which increases the coil sensitivity to detect small size defects.

The new probes parameters and dimensions are shown in table 4.3 and table 4.4. For future work random defects embedded inside parts made by AM with unknown sizes in the range of 0.01 mm to 0.5 mm width and different lengths in the range of 1 mm to 5 mm can be tested to get its approximate sizes and locations. Also, detection of defects with the same size at different depths in the range of 1 mm to 3.5 mm can be explored.

References

[1] Q. Y. Lu and C. H. Wong, "Additive manufacturing process monitoring and control by non-destructive testing techniques: challenges and in-process monitoring," *Virtual and physical prototyping*, vol. 13, no. 2, pp. 39–48, 2018.

[2] K. Taherkhani, E. Sheydaeian, C. Eischer, M. Otto, and E. Toyserkani, "Development of a defect-detection platform using photodiode signals collected from the melt pool of laser powder-bed fusion," *Additive Manufacturing*, vol. 46, p. 102152, 2021.

[3] Q. Qiu, "Imaging techniques for defect detection of fiber reinforced polymer-bonded civil infrastructures," *Structural Control and Health Monitoring*, vol. 27, no. 8, p. e2555, 2020.

[4] Q. Lu and C. Wong, "Applications of non-destructive testing techniques for post-process control of additively manufactured parts," *Virtual and Physical Prototyping*, vol. 12, no. 4, pp. 301–321, 2017.

[5] R. Hamia, C. Cordier, and C. Dolabdjian, "Eddy-current non-destructive testing system for the determination of crack orientation," *Ndt & E International*, vol. 61, pp. 24–28, 2014.

[6] J. A. Pelesko, M. Cesky, and S. Huertas, "Lenz's law and dimensional analysis," *American journal of physics*, vol. 73, no. 1, pp. 37–39, 2005.

[7] F. Förster, "Sensitive eddy-current testing of tubes for defects on the inner and outer surfaces," *Non-Destructive Testing*, vol. 7, no. 1, pp. 28–36, 1974.

[8] M. Pan, Y. He, G. Tian, D. Chen, and F. Luo, "Pec frequency band selection for locating defects in two-layer aircraft structures with air gap variations," *IEEE Transactions on Instrumentation and Measurement*, vol. 62, no. 10, pp. 2849–2856, 2013.

[9] P. J. Shull, *Nondestructive evaluation: theory, techniques, and applications*. CRC press, 2002.

[10] I. Scott and C. Scala, "A review of non-destructive testing of composite materials," *NDT international*, vol. 15, no. 2, pp. 75–86, 1982.

[11] X. Chen and Y. Lei, "Electrical conductivity measurement of ferromagnetic metallic materials using pulsed eddy current method," *Ndt & E International*, vol. 75, pp. 33–38, 2015.

[12] N. Bowler and Y. Huang, "Electrical conductivity measurement of metal plates using broadband eddy-current and four-point methods," *Measurement Science and Technology*, vol. 16, no. 11, p. 2193, 2005.

[13] H. Lemire, P. Underhill, T. Krause, M. Bunn, and D. Butcher, "Improving probability of detection of bolt hole eddy current inspection," *Research in Nondestructive Evaluation*, vol. 21, no. 3, pp. 141–156, 2010.

[14] L. Obrutsky, B. Lepine, J. Lu, R. Cassidy, and J. Carter, "Eddy current technology for heat exchanger and steam generator tube inspection," *Proc. 16th WCNDT, Montreal (Canada)*, vol. 30, 2004.

[15] J. B. Nestleroth and R. J. Davis, "Application of eddy currents induced by permanent magnets for pipeline inspection," *NDT & E International*, vol. 40, no. 1, pp. 77–84, 2007.

[16] E. Kriezis, T. D. Tsiboukis, S. M. Panas, and J. A. Tegopoulos, "Eddy currents: Theory and applications," *Proceedings of the IEEE*, vol. 80, no. 10, pp. 1559–1589, 1992.

[17] J. García-Martín, J. Gómez-Gil, and E. Vázquez-Sánchez, "Non-destructive techniques based on eddy current testing," *Sensors*, vol. 11, no. 3, pp. 2525–2565, 2011.

[18] R. Ghoni, M. Dollah, A. Sulaiman, and F. M. Ibrahim, "Defect characterization based on eddy current technique: Technical review," *Advances in Mechanical Engineering*, vol. 6, p. 182496, 2014.

[19] A. N. AbdAlla, M. A. Faraj, F. Samsuri, D. Rifai, K. Ali, and Y. Al-Douri, "Challenges in improving the performance of eddy current testing," *Measurement and Control*, vol. 52, no. 1-2, pp. 46–64, 2019.

[20] I. Abidin, M. Umar, M. Yusof, M. Ibrahim, A. Hamzah, and M. Salleh, "Advantages and applications of eddy current thermography testing for comprehensive and reliable defect assessment," in *Proceedings of 18th World Conference on Nondestructive Testing, Durban, South Africa*, vol. 1620, 2012.

[21] G. Van Drunen and V. Cecco, "Recognizing limitations in eddy-current testing," *NDT international*, vol. 17, no. 1, pp. 9–17, 1984.

[22] Y. Yating and G. Jia, "Investigation of signal features of pulsed eddy current testing technique by experiments," *Insight-Non-Destructive Testing and Condition Monitoring*, vol. 55, no. 9, pp. 487–491, 2013.

[23] S. Lai, D. Chen, H. Chen, and Y. Fu, "Pulsed eddy current testing of inner wall flaws in pipe under insulation," *Procedia Engineering*, vol. 130, pp. 1658–1664, 2015.

[24] E. Todorov, B. Nagy, S. Levesque, N. Ames, and J. Na, "Inspection of laser welds with array eddy current technique," in *AIP Conference Proceedings*, vol. 1511, no. 1. American Institute of Physics, 2013, pp. 1065–1072.

[25] R. P. Uhlig, M. Zec, H. Brauer, and A. Thess, "Lorentz force eddy current testing: a prototype model," *Journal of Nondestructive Evaluation*, vol. 31, no. 4, pp. 357–372, 2012.

[26] L. Zhang, R. Deng, N. Ning, J. Fan, W. Wang, and K. Song, "Study on remote field eddy current testing technology for crack-like defects in long truss structure of aircraft," *Materials*, vol. 15, no. 15, p. 5093, 2022.

[27] H. Brauer, K. Porzig, J. Mengelkamp, M. Carlstedt, M. Ziolkowski, and H. Toepfer, "Lorentz force eddy current testing: A novel nde-technique," *COMPEL: The International Journal for Computation and Mathematics in Electrical and Electronic Engineering*, 2014.

[28] G. Tian, J. Wilson, L. Cheng, D. P. Almond, E. Kostson, and B. Weekes, "Pulsed eddy current thermography and applications," in *New Developments in Sensing Technology for Structural Health Monitoring*. Springer, 2011, pp. 205–231.

[29] H. Xu, M. Lu, J. Avila, Q. Zhao, F. Zhou, X. Meng, and W. Yin, "Imaging a weld cross-section using a novel frequency feature in multi-frequency eddy current testing," *Insight-Non-Destructive Testing and Condition Monitoring*, vol. 61, no. 12, pp. 738–743, 2019.

[30] Q. Y. Lu and C. H. Wong, "Applications of non-destructive testing techniques for post-process control of additively manufactured parts," *Virtual and Physical Prototyping*, vol. 12, no. 4, pp. 301–321, 2017.

[31] I. Astm, "Astm52900-15 standard terminology for additive manufacturing—general principles—terminology," *ASTM International, West Conshohocken, PA*, vol. 3, no. 4, p. 5, 2015.

[32] R. Pohl, A. Erhard, H.-J. Montag, H.-M. Thomas, and H. Wüstenberg, "Ndt techniques for railroad wheel and gauge corner inspection," *NDT E International*, vol. 37, no. 2, pp. 89–94, 2004.

[33] R. Ippolito, L. Iuliano, and A. Gatto, "Benchmarking of rapid prototyping techniques in terms of dimensional accuracy and surface finish," *CIRP annals*, vol. 44, no. 1, pp. 157–160, 1995.

[34] I. G. Ian Gibson, "Additive manufacturing technologies 3d printing, rapid prototyping, and direct digital manufacturing," 2015.

[35] S. Jiao, X. Liu, and Z. Zeng, "Intensive study of skin effect in eddy current testing with pancake coil," *IEEE Transactions on Magnetics*, vol. 53, no. 7, pp. 1–8, 2017.

[36] S. Bennoud and M. Zergoug, "Modeling and simulation for 3d eddy current testing in conducting materials," *International Journal of Mechanical, Aerospace, Industrial and Mechatronics Engineering*, vol. 8, no. 4, pp. 749–752, 2014.

[37] E. Apostol, A. Nedelcu, D. V. Daniel, I. Chiriţă, and N. Tănase, "Mathematical modeling of eddy current non-destructive testing," in *2017 10th International Symposium on Advanced Topics in Electrical Engineering (ATEE)*, 2017.

[38] S. Gholizadeh, "A review of non-destructive testing methods of composite materials," *Procedia structural integrity*, vol. 1, pp. 50–57, 2016.

[39] H. Brauer, M. Ziolkowski, and H. Toepfer, "Defect detection in conducting materials using eddy current testing techniques," *SJEE*, vol. 11, no. 4, pp. 535–549, 2014.

[40] R. Falque, T. Vidal-Calleja, and J. V. Miro, "Defect detection and segmentation framework for remote field eddy current sensor data," *Sensors*, vol. 17, no. 10, p. 2276, 2017.

[41] M. Bowkett and K. Thanapalan, "Comparative analysis of failure detection methods of composites materials' systems," *Systems Science Control Engineering*, vol. 5, pp. 168–177, 01 2017.

[42] C. Dodd and W. Deeds, "Analytical solutions to eddy-current probe-coil problems," *Journal of applied physics*, vol. 39, no. 6, pp. 2829–2838, 1968.

[43] Y.-Z. Lei, "General series expression of eddy-current impedance for coil placed above multi-layer plate conductor," *Chinese Physics B*, vol. 27, no. 6, p. 060308, 2018.

[44] T. Theodoulidis and J. Bowler, "The truncated region eigenfunction expansion method for the solution of boundary value problems in eddy current nondestructive evaluation," *AIP Conference Proceedings*, vol. 760, pp. 403–408, 04 2005.

[45] S. Hadi, A. Indrawan, A. Kurniawan, and S. Suyitno, "Feasibility study of high-temperature resistivity measurement apparatus with four-point probe method: Designing, manufacturing, and validating process," 01 2017, p. 030135.

[46] S. Park, Y. J. Kang, and S. Majd, "A review of patterned organic bioelectronic materials and their biomedical applications," *Advanced Materials*, vol. 27, no. 46, pp. 7583–7619, 2015.

[47] A. Mitra, P. De, D. Bhattacharya, P. Srivastava, and D. Jiles, "Ferromagnetic properties of deformation-induced martensite transformation in aisi 304 stainless steel," *Metallurgical and Materials Transactions A*, vol. 35, pp. 599–605, 02 2004.

[48] C. Prindle and H. M. Feinman, "Eddy current flaw detector utilizing helical sensing coils surrounding the test path," 1969.

[49] M. Uesaka, K. Hakuta, K. Miya, K. Aoki, and A. Takahashi, "Eddy-current testing by flexible microloop magnetic sensor array," *IEEE transactions on magnetics*, vol. 34, no. 4, pp. 2287–2297, 1998.

[50] K. Stoddard, "Eddy current probe," 2014.

[51] C. Hellier, "Handbook of nondestructive evaluation," 2013.

[52] P. Langevin, "Procédé et appareils d'émission et de réception des ondes élastiques sous-marines à l'aide des propriétés piézo-électriques du quartz," 1918.

[53] H. Lester, "X-rays in the steel industry," *Journal of the Franklin Institute*, vol. 211, no. 5, pp. 567–579, 1931.

[54] H.H, "Radiographic testing," . *Proceedings-American Society for Testing and Materials*, vol. 211, no. 5, pp. 567–579, 1947.

[55] W. Du, Q. Bai, Y. Wang, and B. Zhang, "Eddy current detection of subsurface defects for additive/subtractive hybrid manufacturing," *The International Journal of Advanced Manufacturing Technology*, vol. 95, pp. 1–11, 04 2018.

[56] D. Fleisch, *A student's guide to Maxwell's equations*. Cambridge University Press, 2008.

[57] G. Mook, O. Hesse, and V. Uchanin, "Deep penetrating eddy currents and probes," *Materials Testing*, vol. 49, no. 5, pp. 258–264, 2007.

[58] M. Wright, *Eddy Current Testing Technology*. Eclipse Scientific Incorporated, 2015.

[59] "Specifications miz-85id." 2015 [cited 2015 10. November 2015]. [Online]. Available: http://www.zetec.com/products/eddycurrent/instrumentation/miz-85id/miz-85id-specifications/.

[60] "Ge sensing and inspection technologies," 2014. [Online]. Available: https://www.gemeasurement.com

[61] "Ectane," 2015. [Online]. Available: http://www.eddyfi.com/products/ectane-2-test-instrument/

[62] "Eddy current test instruments and systems product catalogue," 2008. [Online]. Available: http://www.Rohmann.com/products.

[63] "M., airport hangars and aircraft maintenence operations, in amity university dubai2015: Amity university dubai. p. 31." 2015.

[64] Q. Y. Lu and C. H. Wong, "Additive manufacturing process monitoring and control by non-destructive testing techniques: challenges and in-process monitoring," *Virtual and Physical Prototyping*, 2018.

[65] T. Theodoulidis and E. Kriezis, "Series expansions in eddy current nondestructive evaluation models," *Journal of materials processing technology*, vol. 161, no. 1-2, pp. 343–347, 2005.

[66] T. P. Theodoulidis and E. E. Kriezis, *Eddy current canonical problems (with applications to nondestructive evaluation)*. Tech Science Press, 2006.

[67] Y.-Z. Lei, "General series expression of eddy-current impedance for coil placed above multi-layer plate conductor," *Chinese Physics B*, vol. 27, no. 6, p. 060308, 2018.

[68] G. Tytko and Ł. Dawidowski, "Locating complex eigenvalues for analytical eddy-current models used to detect flaws," *COMPEL-The international journal for computation and mathematics in electrical and electronic engineering*, 2019.

[69] R. W. Erickson and D. Maksimovic, *Fundamentals of power electronics*. Springer Science & Business Media, 2007.

[70] "Eddy current testing (ect)," 2017. [Online]. Available: http://www.ndttechnologies.com/products/penetrant_testing.html

[71] M. Basharat, M. Ding, H. Cai, Y. Li, and J. Fang, "Design and analysis of multilayer solenoid coil for faraday modulator," in *MATEC Web of Conferences*, vol. 114. EDP Sciences, 2017, p. 04004.

[72] A. Cooke and S. Moylan, "Process intermittent measurement for powder-bed based additive manufacturing." 22nd International SFF Symposium - An Additive Manufacturing Conference, Austin, TX, 2011-08-31 2011.

[73] H. E. Farag, E. Toyserkani, and M. B. Khamesee, "Non-destructive testing using eddy current sensors for defect detection in additively manufactured titanium and stainless-steel parts," *Sensors*, vol. 22, no. 14, 2022. [Online]. Available: https://www.mdpi.com/1424-8220/22/14/5440

APPENDICES

Appendix A

Matlab Codes

Matlab Code for impedance change: (Comments are written between parentheses)

```
clear all ;
close all;
clc;
f=28000; (Frequency used)
W=164; (Number of turns)
r1=3.5e-3; r2=8.0e-3; h=9.435e-3; (Coil dimensions)
lo=0;
h1=1.0e-3; h2=1.0e-3; h3=1.0e-3;
sigma1=1.32e6;
sigma2=1.32e6;
sigma3=1.32e6; (Electrical conductivity)
mur1=1; mur2=1; mur3=1; (Permeability)
b=1.0;
M=300;
nden=W/h/(r2-r1);
i=complex(0,1);
```

mu0=4*pi*1e-7;
omega=2*pi*f;
a0=i*omega*mu0;
(Starting here, the first order and zero order Bessel functions calculations)
syms t
for j=1:1:M
y0=pi*(j+0.25);
yj=fzero(@(x)besselj(1,x),[y0-0.096,y0]);
x(j)=yj/b;
integral=double(int(t*besselj(1,t),t,x(j)*r1,x(j)*r2));
J0=besselj(0,yj);
C(j)=nden*(1-exp(-x(j)*h))*integral/(J0*yj^3.5);
end
c=complex(0,0);
for m=1:1:M
x2=x(m)*x(m);
alpha1=sqrt(x2+a0* mur1*sigma1);
alpha2=sqrt(x2+a0* mur2*sigma2);
alpha3=sqrt(x2+a0* mur3*sigma3);
q1=(1.0/mur1)*(alpha1/x(m));
q2=(mur1/mur2)*(alpha2/alpha1);
q3=(mur2/mur3)*(alpha3/alpha2);
q4=(mur3/1.0)*(x(m)/alpha3);
u3=q3*tanh(alpha3*h3+atanh(q4));
u2=q2*tanh(alpha2*h2+atanh(u3));
u1=q1*tanh(alpha1*h1+atanh(u2));
L3=tanh(0.5*log(u1));
c=c+L3*C(m)$^2 * exp(-2 * x(m) * lo)$;
end
deltaZ=-2*pi*b$^5 * a0 * c$; $(Results for the impedance)$

Finding values for Fabry factor

clear all

close all

clc

tic

inc=0.01;

alpha=1:inc:10;

beta=0:inc:10;

[alpha,beta] = meshgrid(alpha,beta);

(Calculation for fabry factor using the main formula)

G=(1/5).*(((2*pi.*beta)./(alpha.^{2} − 1)).^{0}.5). ∗ ...log((*alpha* + (*alpha*.^{2} + *beta*.^{2}).^{0}.5)./

(1+((beta.^{2}) + 1).^{0}.5));

figure(1)

contour(alpha,beta,G,'ShowText','on','LineWidth',1)

grid on

K$_m ax_G$ = $find(G == max(max(G)))$;

G$_o pt$ = $G(K_m ax_G)$

alpha$_o pt$ = $alpha(K_m ax_G)$

beta$_o pt$ = $beta(K_m ax_G)$

hold on

plot(alpha$_o pt, beta_o pt, ' r*')$

alpha=2.28;

rin=3.5;

rout=8.0;

(Starting here calculations for different formula)

Hight=[5.0; 9.435;20.76; 31.14; 41.52; 51.9; 62.28];

L=Hight./2;

beta=L./rin;

G=(1/5).*(((2*pi.*beta)./(alpha.^{2} − 1)).^{0}.5). ∗ ...$log((alpha + (alpha.^2 + beta.^2).^0.5)./$

(1+((beta.^{2}) + 1).^{0}.5));

D$_i n = ones(length(Hight), 1). * rin. * 2$;

D$_o ut = ones(length(Hight), 1). * rout. * 2$;

Alpha=ones(length(Hight),1).*alpha;

(Creating the table for all values) T=table(D$_i n, D_o ut, Hight, Alpha, beta, G$)

A= 'Number of G =

NormalizedG=G./max(G);

C=compose(A,G);

for z=1:length(C)

plot(Hight(z),NormalizedG(z),'')

hold on

end

legend(C)

hold on

grid on

toc